

Study of Desiccation Crack Patterns in Aqueous Clay Suspensions and The Role of Charge Distribution in Formation of Cracks Under Electric Field

By

Ankita Ghosh

(Index No.- 169/18/Inst. Sc./26)

Year- 2023


A Thesis submitted in fulfilment of the requirement for the degree of Doctor of Philosophy (Science)




Department of Instrumentation Science,
Jadavpur University,
India.

CERTIFICATE FROM THE
SUPERVISORS

This is to certify that the thesis entitled “*Study of Desiccation Crack Patterns in Aqueous Clay Suspensions and The Role of Charge Distribution in Formation of Cracks Under Electric Field*”, submitted by Smt. Ankita Ghosh, who got her name registered on 13.09.2018 for the award of Ph. D. (Science) degree of Jadavpur University, is absolutely based upon her own work under the supervision of Prof. Anup Kumar Ghosh and Dr. Tapati Dutta and that neither this thesis nor any part of it has been submitted for either any degree/diploma or any other academic award anywhere before.

 11/5/23

Prof. (Dr.) Anup Kr. Ghosh
Dept. of Instrumentation Science
Jadavpur University, Kol - 32

 11.5.23
Dean of Science
Arts & Science Dept.
St. Xavier's College
Kolkata

(Signature of the Supervisor(s) date with official seal)

DECLARATION

I hereby declare that the work reported in this thesis is entirely original. This thesis is composed independently by me at the Department of Instrumentation Science, Jadavpur University under the supervision of Prof. Anup Kumar Ghosh and Dr. Tapati Dutta. I further declare that the subject matter presented in this thesis has not previously formed the basis for the award of any degree, diploma, membership, associateship, fellowship or any other similar title of any university or institution.

Ankita Ghosh
12.05.2023

Ankita Ghosh

ACKNOWLEDGEMENT

“The pursuit of PhD is enduring daring adventure.”

— Lailah Gifty Akita.

The research work of this thesis entitled **“Study of Desiccation Crack Patterns in Aqueous Clay Suspensions and The Role of Charge Distribution in Formation of Cracks Under Electric Field”** was initiated in 2016 as my M.Sc. project and has been carried out at the Condensed Matter Physics Research Centre (CMPRC), department of Physics, Jadavpur University, Kolkata under the efficient guidance of Prof. Sujata Tarafdar and Dr. Tapati Dutta. Thereafter, I got my name registered for PhD on 13.09.2018 with **Index No.: 169/18/Inst. Sc./26** and continued my research under the supervision of Prof. Anup Kumar Ghosh and Dr. Tapati Dutta at Department of Instrumentation Science, Jadavpur University, Kolkata. As a sense of fulfilment at the completion of this phase of my academic career, I wish to express my gratitude to all those who made this thesis possible.

I would like to express my deepest appreciation to my Supervisor Prof. Anup Kumar Ghosh. These past few years, he has taught me a lot, both academically and otherwise. He has always been a continual source of motivation and inspiration for me, and I have always been in awe of his ideas, clear explanations of complex issues, and solutions. I have the utmost regard for him and would like to sincerely thank him for his enormous assistance with my work.

I am deeply indebted to Dr. Tapati Dutta for all of her help and support during the course of my work. I consider myself extremely fortunate to have had

her as my mentor over the past few years because her enthusiasm and excitement at work have always given me motivation. She has encouraged me to look for new approaches and use my imagination when tackling any issues. Her unwavering support and compassion have given me a great deal of courage and optimism throughout the challenging parts of my career.

I'm extremely grateful that Prof. Sujata Tarafdar gave me the chance to work under her supervision. Throughout my research at CMPRC, she was always cooperative and offered advice on both academic and non-academic concerns. Her unique perspectives on many issues and insistence on clarity have been extremely helpful and inspirational.

I would specially thank Prof. Tapas Ranjan Middy for his selfless support and guidance. I am truly grateful to him.

I want to express my sincere gratitude to my seniors as well as my co-authors Dr. Sudeshna Majumdar and Dr. Tajkera Khatun for helping me understand while closely collaborating with me on my study topic. They assisted me in developing the necessary laboratory techniques and methods for performing multiple tests. As they became like my elder sisters, I have never felt hesitation to ask for any aid or support when I have needed it. They have been a cherished friend and companion during my time working at the lab.

I would like to thank Dr. Sachindranath Das (HOD, Dept. of Instrumentation Science) for conducting the RAC Meetings and his constant cooperation and guidance for all academic matters throughout my research work. My sincere gratitude to all the office and laboratory staffs of the Department.

To my lab seniors and lab-mates, thanks for the fun and support. It goes without saying that my lab has an excellent academic and working environment, as well as a great deal of support and collaboration from the scholars and other

members. I've worked with Dr. Tania Basu, Dr. Moutushi Dutta Choudhury, Dr. Abhra Giri, Dr. Debabrata Das, Dr. Sourav Kumar, Dr. Somasri Hazra, Dr. Subir Kumar Patla, Biswajit Roy, Dr. Simantini Majumdar, Anamika Roy, Samiul Haque, Ruhul Amin Ibne Haque & Ammara Khatun and they provided their hands in whatever way they can when I needed assistance.

I would like to acknowledge Government of West Bengal for their financial support through SVMCM and RUSA 2.0 DOCTORAL fellowship.

To my friends, Aparna Deb, Sinjini Dhang, Poulami Roy, Ankita Sarkar, Subhamita Sengupta, Ratna Sarkar, Debjit Ghosh, Anupa Roy Chowdhury, Dr. Monali Das this would have been a much more difficult feat without you. Thank you all for your unwavering support and for reminding me to take breaks and have fun when I've been stressed out. I would specially like to acknowledge Dr. Somnath Roy, my dear friend, for being beside me at every turn of the way. I will always cherish our journey from being classmates to friends and then to fellow researchers and hope this journey continues through our lifetime.

Without the constant support and love of my parents, Subrata Paul and Karabi Paul, this endeavour would not be complete. I owe them a debt of gratitude that no words could ever adequately convey. My in-laws, Swapan Kumar Ghosh and Sulekha Ghosh, have always offered their continuous backing and best wishes for me, and I am appreciative of their acceptance and patience. I would also like to thank my brother for his support.

Finally, and most significantly, I want to thank my Husband Dr. Nilanjan Ghosh, who has been beside me through thick and thin. We both know I could not have done this without him. He is my knight in shining armour, and I cannot describe how grateful I am to him.

I can't leave without addressing the most important person in my life, my darling son, Mehan, who has been my greatest source of motivation in this journey. He is a blessing to us, and in the years to come, I hope to grow and learn with him.

LIST OF PUBLICATIONS

1. **Ghosh, A.**, Sircar, S., Khatun, T., Dutta, T. and Tarafdar, S., 2018. Tree-like crack patterns in clay dried in a uniform DC electric field. *Materials Research Express*, 6(2), p.026305.
2. **Ghosh, A.**, Dutta, T., Tarafdar, S. and Ghosh, A.K., 2020. Branched crack patterns in layers of Laponite® dried under electric fields: Evidence of power-laws and fractal scaling. *The European Physical Journal E*, 43, pp.1-6.
3. **Ghosh, A.**, Majumdar, S., Tarafdar, S., Ghosh, A.K. and Dutta, T., 2023. Effective Crack-prevention Strategy with composite of two clays of different sized particles. *Physica Scripta*, DOI :10.1088/1402-4896/acd22d.

FOREWORD

Nowadays ‘Fractures’ and ‘Pattern of Fractures’ bear enormous importance and significance due to their practical purposes in our day-to-day life. The main objective of studying this topic is to get an idea about crack prevention strategies and how to make cracks useful in improving our life and technology. Recently the method of controlling crack pattern has become as equipotent as the traditional objective of crack prevention. The formation of cracks and their unique characteristics depend on several external perturbations such as ambient condition, applications in stress fields, mechanical loading, addition of chemical components to the desiccating colloidal suspensions etc. According to the need in various field the cracks can be prevented or ‘designed’ by modifying these factors.

We report in this thesis the study of crack patterns on mainly two clay systems - Bentonite and Laponite[®] under such diverse environment. We have mainly studied how aqueous suspension of Laponite[®], a synthetic clay, reacts when it is under an external electric field enclosed in a particular geometry, and how the desiccation cracks modify when another clay, Bentonite, of same the class has been incorporated to it.

The brief layout of my thesis is as follows:

In [Chapter 1](#), I begin with the brief introduction of clay and cracks developed in it. I briefly review the earlier works done related to this topic. The chapter also includes discussions on the various clays involved in the experiments and theories that are useful to understand the behaviour of clay colloids in the presence of external electric fields.

In [Chapter 2](#), I have presented a study of unique crack patterns seen in Laponite® clay suspension when deposited in boxes of rectangular geometry and exposed to direct electric field. I also have included the model developed to give an explanation about the unique crack pattern formed in these circumstances.

In [Chapter 3](#), I have reported that the pattern of cracks formed in rectangular geometry is reminiscent of the Caley tree or Bethe Lattice which have fractal characteristics. Thus I establish that our fracture pattern is an example of an ideal scale-invariant system.

In [Chapter 4](#), the result in variation of crack patterns by using clay-clay composite in room ambient has been reported and discussed. The clay-clay composite is a Laponite-bentonite combination of various ratios. It is seen that for a critical ratio, cracks can be prevented by mixing two clays of same group.

In [Chapter 5](#), a brief summary and discussion of the results of each chapter are presented as the conclusion of the thesis and tentative plans of the future work are also projected.

Thesis-1

ORIGINALITY REPORT

6%

SIMILARITY INDEX

PRIMARY SOURCES

- | | | |
|----------|--|------------------|
| 1 | www.wattpad.com
<small>Internet</small> | 189 words — 1% |
| <hr/> | | |
| 2 | royalsocietypublishing.org
<small>Internet</small> | 124 words — < 1% |
| <hr/> | | |
| 3 | Xinmin Liu, Rui Tian, Wei Du, Rui Li, Wuquan Ding, Hang Li. "A theory to determine the surface potentials of clay particles in electrolyte solutions", Applied Clay Science, 2019
<small>Crossref</small> | 77 words — < 1% |
| <hr/> | | |
| 4 | Lucas Goehring, Akio Nakahara, Tapati Dutta, So Kitsunezaki, Sujata Tarafdar. "Desiccation Cracks and their Patterns", Wiley, 2015
<small>Crossref</small> | 68 words — < 1% |
| <hr/> | | |
| 5 | www.sydney.edu.au
<small>Internet</small> | 59 words — < 1% |
| <hr/> | | |
| 6 | hdl.handle.net
<small>Internet</small> | 56 words — < 1% |
| <hr/> | | |
| 7 | Sudeshna Sircar, Sujata Tarafdar, Tapati Dutta. "Crack formation in desiccating Laponite® films under AC field: Effect of varying frequency", Applied Clay Science, 2018
<small>Crossref</small> | 49 words — < 1% |

TABLE OF CONTENT

Chapter 1: Introduction (1 - 40)

1.1 Brief History and Applications of Cracks :.....	2
1.2. Introduction to Colloids :.....	4
1.2.1. Classification of Colloids :.....	5
1.2.2. Properties of Colloids :	5
1.3. Introduction to Clay :.....	6
1.3.1 Structure and Classification of Clays :	7
1.3.2. Charge of Clay :.....	9
1.3.3. Charge reversal of Clay :.....	10
1.4. Some Significant Phenomena in Clays and Colloids :	11
1.4.1 Electrophoresis :.....	11
1.4.2 Dielectrophoresis :	12
1.4.3. Electric Double Layer :.....	14
1.4.4 Electro-osmosis :	16
1.4.5 Sedimentation :.....	17
1.4.6 Coagulation :	17
1.4.7 Flocculation :	18
1.5. Brief Introduction to Laponite® and bentonite :.....	18
Laponite® :.....	19
Bentonite :.....	20
1.5. Mechanism for Cracking :.....	21
1.5.1 Formation of Desiccation Cracks :.....	21
Cracking by Evaporation :.....	21
Cracking due to Capillary Action :	22
1.5.2. Theory of Cracking: Griffith's Criterion:	23

1.5.3. Modes of Fracture :	25
1.5.4. Critical Cracking Thickness :	27
1.5.5. Some Significant Features of Desiccation Cracks :	28
1.6. Experimental Apparatus :	30
Optical Microscope :	30
FESEM :	31
1.7. List of References :	32

Chapter 2: Effect of Uniform Electric Field in Laponite[®] Clay: Formation of Branched Crack Pattern (43 - 76)

2.1. Introduction :	43
2.2. Overview of Previous Relevant Work :	44
2.3. Materials and Experimental Method :	49
2.4. Observations :	52
2.4.1. Experimental Findings :	52
2.4.2. SEM-images of various parts	53
2.4.3. An Additional Inspection	54
2.5. Analysis and Results :	55
2.6. Theory	59
2.6.1. Origin of Tree-like crack pattern	59
2.6.2. Role of Counter ion Charge density in crack formation	61
2.7. Discussion and Conclusion	69
2.8. List of References	72

Chapter 3: Study of tree-like Crack morphology: Existence of fractal laws (79 - 106)

3.1. Introduction.....	79
3.2. Overview of previous related work.....	79
3.3. Materials and Experimental Method	86
3.4. Observation : Formation of Crack Patterns.....	87
3.5. Analysis.....	90
3.5.1. Ped size distribution.....	92
3.5.2. Correlation of the dissipation of energy in the river network and the fracture system	96
3.6. Discussion and Conclusion	98
3.7. List of References	100

Chapter 4: Experimental Findings of Crack prevention using clay-clay composite. (109 - 142)

4.1. Introduction.....	109
4.2. Overview of previous related work.....	109
4.3. Materials and Method of Experiment.....	112
4.4. Observation	114
4.4.1. Effect of Addition of Laponite® into Bentonite Clay.....	114

4.4.2. Comparison of film thickness	116
4.5. Result Analysis.....	118
4.5.1. Image Processing and Quantitative Analysis.....	118
4.5.2. Roll of film thickness	121
4.5.3. Analysis of SEM images	123
4.6. Conclusions and Discussions	129
4.7. List of References	132

Chapter 5: Discussion and Future Plans (145-148)

1

Introduction

Cracks or fractures are too common in our daily lives. We've all seen different types of fractures in bones, cracks in glass windows, mud, or on walls of buildings. However, not everyone comprehends why and how cracks form. Cracks are defined as failures that split a whole into multiple pieces. It occurs when the system is deviated from its equilibrium conditions and develops stress. If the stress is elastic in nature, the system relieves the accumulated stress by the creation of fresh surface in the form of cracks. Natural fractures include those found in dried mud, bone fractures, dry skin in the winter, cracks in rocks and mountains due to earthquake or weather, and many others. Cracks can also be formed in an artificial manner. In both cases, cracks are caused by either desiccation, such as mud cracks or heel fissures, or external mechanical pressures, such as bone fractures, object breakage, and so on. Whatever the case may be, the study of cracks and their formation, mechanism, and prevention has garnered considerable attention in recent years, not only because of academic curiosity, but also because of practical applications in our everyday living [1].

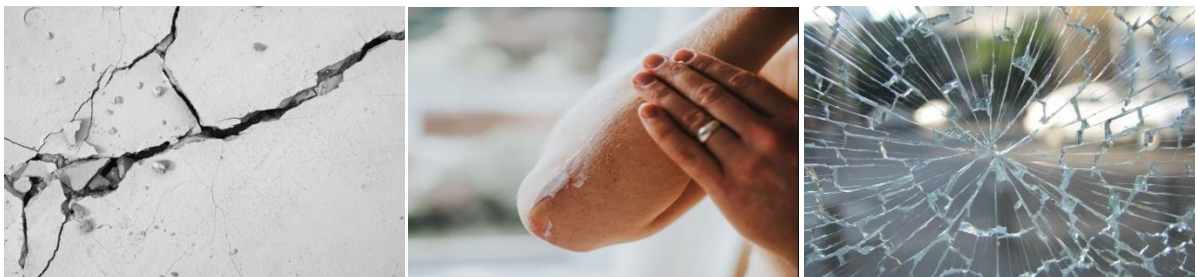


Figure 1.1: Examples of Cracks on the wall, in dry skin and on glass window (source: Internet)

1.1 Brief History and Applications of Cracks :

Fracture techniques were used in the age of the pyramids, according to El- Sehily's paper [2] which describes how the Egyptians used to cut and break giant rock structures during the process of building the pyramids and obelisks. The first written document of an explanation of the scaling law of fracture mechanics was discovered in one of Leonardo Da Vinci's notebooks [3, 4], after which Galileo Galilei formulated scaling laws regarding bars under tension and bending [5].

The hazard of forming fracture became a genuine issue as the field of architecture advanced and the usage of iron and steel as building components increased. A. A. Griffith is usually credited with laying the groundwork for current fracture theory in two fundamental publications on the fracture of glass, i.e. the brittle class of material [6, 7]. Brittle fracture research became even more important during World War II, when enormous welded constructions, particularly of steel, were only beginning to appear as a bridge-building technique. For the Allies, this method was also employed to build warships (Liberty ships). Orowan and Irwin expanded on Griffith's work by generalising it to less brittle materials [8] and calculating the fracture energy during cracking in terms of surface energy [9]. These investigations resulted in the creation of Linear Elastic Fracture Mechanics (LEFM), which is covered in more detail in the section that follows.

Several key uses of cracks have emerged in recent decades as a result of improved understanding of the process of cracking and the capacity to control its production [10, 11]. Cracks generate attractive patterns with an intrinsic aesthetic value that has been used for ornamental purposes in painting and texturing of surfaces [12]. Wax cracks when dried is used for creating unique motifs that are used to make batik-styled cloth [13]. The morphology of crack development in historical paintings [14] can provide a lot of information about the portrait's quality, the artist's painting skills, the conservation conditions, and so on. Fracture

formations have a wide range of applications in research, in addition to aesthetics. By examining fractures formed in human bone tissue, forensic medicine can reveal the nature and cause of injuries [15, 16]. Dried blood droplets exhibit distinct patterns based on their composition, which can be used to determine the existence of various medical anomalies [17]. Using spontaneously produced crack networks as templates to deposit conducting metal, transparent conducting electrodes can be made [18]. The formation of nano or micro fissures aids in the fabrication of templates for nanolithography, which is employed in electrical devices [19, 20], the growth of nanowires [21], and adjustable nano-channel arrays, among other things. Useful proteins can be selectively adsorbed on substrates with arrays of fractures [22] to generate reconfigurable arrays useful in cellular activities like as cell proliferation, motility, differentiation, and so on. Fruit cracking is directly related to the water

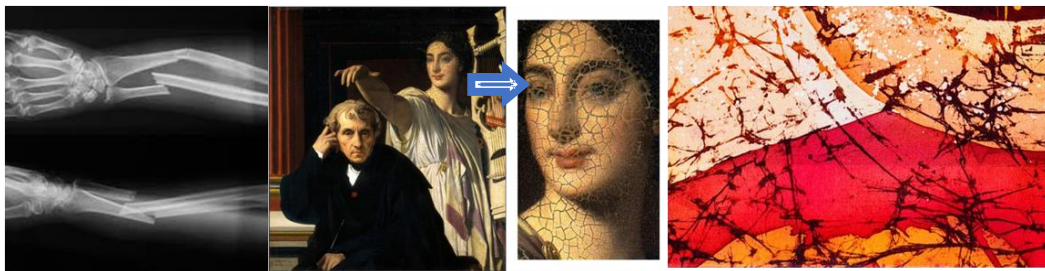


Figure 1.2. Images of Bone Fracture, Cracks in old paintings and Cracked batik print on cloths (Source: Internet)

content or irrigation of field in agriculture [23, 24]. The occurrence of desiccation fissures on the surface of Mars could indicate the presence of water on the planet at some point in the past [25]. Fractures on growing surfaces, such as tree barks, can reveal information about their age, climate conditions, growth patterns, and so on. Some examples are shown in figure 1.2. Overall, the field of fracture mechanics is a vast and expanding area of interest in modern science, with a wide range of academic and practical applications.

In this thesis we shall focus on two clays, Laponite[®] and bentonite which will be described in detail in the following parts. We will mainly report the results of experiments on how fracture patterns respond to various external perturbations on various clay systems.

1.2. Introduction to Colloids :

Systems with tiny particles of one material suspended in another are called colloids [50]. In a colloidal system, suspended particles size can range from 10^{-9}m to 10^{-6}m . The colloidal size range will be defined by linear dimensions rather than by particle weights or the number of atoms in a particle; still, alternate definitions might be found elsewhere. The suspended particles in a mixture must not settle if left undisturbed in order to be defined as a colloid. The fraction of the mixture that scatters or has a colloidal particle structure can be referred as the dispersed phase, and the medium in which the particles are scattered is known as the dispersion medium.

1.2.1. Classification of Colloids :

Dispersed Phase	Dispersing Medium	Name of Colloidal System	Common Examples
Liquid	Gas	Liquid Aerosol	Mist, clouds, fog
Solid	Gas	Aerosol	Dust, Smoke

Gas	Liquid	Foam	Suds, Whipped Cream
Liquid	Liquid	Emulsion	Cream, Mayo, Milk
Solid	Liquid	Sol	Paints, Jellies, Sewage
Gas	Solid	Solid Foam	Marshmallow
Liquid	Solid	Solid Emulsion	Butter, Cheese
Solid	Solid	Solid Sols	Opals, some alloys

1.2.2. Properties of Colloids :

1. Due to the presence of dispersed state and the dispersion medium, colloidal solution shows heterogeneous nature.
2. The Brownian movement of particles is caused by particle bombardment by the molecules of the dispersion medium. As a result, Brownian mobility prevents particle settling and promotes colloidal solution stability.
3. Colloidal solution particles pass through filter paper effortlessly but are trapped by animal membranes, ultra-filters, and cellophane paper (having <100 nm pore size). [51]
4. Colloids are known to possess Tyndall Effect in which the colloidal particles in the solution prevent a light beam from passing through a colloid entirely. The light is scattered when it collides with the colloidal particles, deviating from its typical path, which is a straight line.

Colloids can also be divided into another two types: simple colloids and network colloids. Simple colloids are those in which the dispersed phase and dispersion medium can be distinguished easily, such as fog, mist, and biological colloids such as blood, bone, and so on. Network colloids, on the other hand, are those in which the components are no longer independently

recognisable from one another, such as colloidal gels and two-phase glasses like opal [52]. Multiple colloids are colloids in which three or more phases coexist, such as polymer matrices, porous rocks containing the vapour and liquid state of some gases imbedded in them [26], multiple emulsions in which droplets of oil and other liquids coexist in some aqueous media, and so on [27]. Association colloids are another class of colloids whose dispersed particles may interact with one another to form small aggregates, such as soap, whose molecules come together to form micelles; liquid crystals, which have ordered aggregate structures.

1.3. Introduction to Clay :

Aqueous clay suspensions are examples of colloidal suspensions. Clays are natural fine-grained material found not only in different rocks and soil, but also suspended in natural bodies of water such as oceans, seas, rivers, atmospheric aerosols, naturally or industrially generated dust, etc. They are usually formed by erosion and weathering of rocks. It is chemically composed of hydrated phyllosilicates with minerals of planar or non-planar structure which gives it ductile and hardening properties. Beyond the clay minerals, they may also contain associated minerals, such as silicates, carbonates, metals hydroxide, as well as organic materials, amorphous substances etc.

1.3.1 Structure and Classification of Clays :

Tetrahedral layers of silica and octahedral layers of magnesia or alumina are the primary building components of any clay. Different types of clay structures are made by arranging the layers in different ways. The fundamental

structures of clay were described by H. Van Olphen [28]. In tetrahedral sheets four Oxygen atoms confine Silicon atoms. The four corners of a tetrahedron are made up of four oxygen atoms, whereas the centre is made up of silicon. Three of each tetrahedron's oxygen atoms are shared by three of its neighbours, while the fourth oxygen atom is shared by an octahedron in the octahedral sheet. (Fig. 1.3).

Six O atoms or OH groups situated at the corners of each octahedron coordinate aluminium (or magnesium) atoms in octahedral sheet [29]. Al or Mg atoms are sandwiched between two parallel planes formed by O atoms and OH groups. The two-dimensional representation of an octahedron and the octahedral structure of aluminium-oxygen are shown in the figure 1.3.

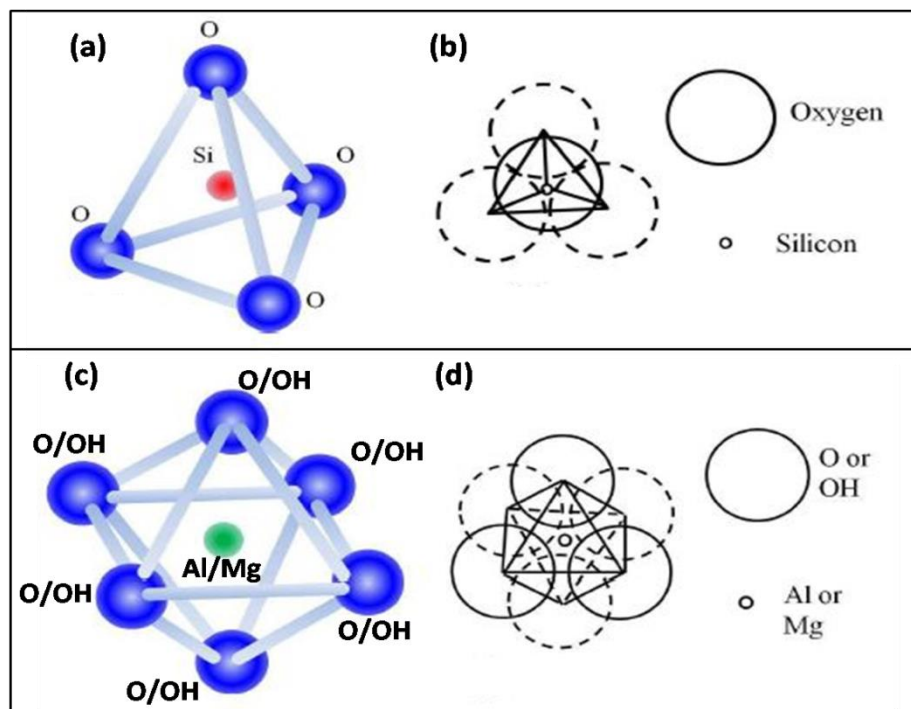


Figure 1.3: Schematic diagrams shows (a) Si and O atoms arranged in a tetrahedral structure [28], (b) tetrahedron projection on a sheet plane, (c) octahedral arrangement of Al/Mg atoms with O/OH atoms, (d) octahedron projection on plane of sheet.

There are **two types of clay** formations, based on the distribution of oxygen atoms between the tetrahedral and octahedral sheets:

- 1) **2 : 1 Clay** - A layer is formed by interposing an octahedral sheet between two tetrahedral sheets. Montmorillonite, illite, Laponite[®], and other minerals are examples. Figure 1.4 shows a schematic depiction of atomic groupings in a unit cell 2:1 layer clay. One unit cell has eight Si atoms, four Al atoms, four OH groups, and twenty O atoms. Thousands of such unit cells are combined to make a single layer of clay.

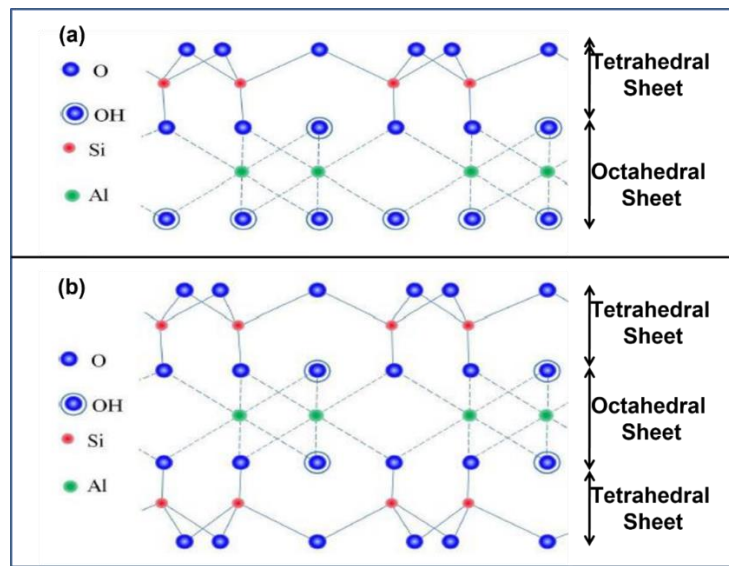


Figure. 1.4. Arrangement of atoms in the unit cell of (a) 1:1 layer clay and (b) 2:1 layer clay.

- 2) **1 : 1 Clay** - One tetrahedral sheet and one octahedral sheet combine to produce a layer. Kaolinite has a clay structure that is nearly ideal in terms of 1:1 layering. The schematic diagram of such clay structure is shown in figure 1.4.

1.3.2. Charge of Clay :

In aqueous suspension, a higher valence atom is replaced by a lower positive valence atom in most clay minerals, resulting in an increase in negative charge and a deficiency of positive charge within the structure. When these atoms having lower valency are substituted into the clay system in an isomorphous manner, it becomes negatively charged. In the clay structure (Fig. 1.3), some Si atoms are replaced by trivalent Al in the tetrahedral sheet, while many Al atoms are replaced by Mg, Cr, Zn, divalent Fe, Li, and other elements in the octahedral sheet. Because of modest size of these atoms, this form of substitution without adjusting the entire valency is quite simple.

The dried clay, on the other hand, is usually neutral and has no charge. To make up the net negative charge, some cations such as Na, K, Ca, and others are absorbed by clay layer during the production procedure or from the environment. The adsorbed cations cannot go into the core of the structure due to their huge size, therefore they remain on the outer surface of the interface of two clay layers. These cations which are adsorbed cause the dried clay to behave neutrally.

1.3.3. Charge reversal of Clay :

In general, clay has a negative charge. The negative charge of clay can be reversed by adding salt having multivalent cations (Al^{3+} , Th^{4+} , etc.) that can substitute the monovalent Na^+ ions of the clay. Then a substantial number of cations of higher valency can replace the monovalent cations, a charge reversal on the surface of clay particles occurs. Salt containing monovalent cations can sometimes also be used to invert the charge of the clay. Messina et al. [30] showed

the origin of this counter-intuitive phenomenon and explained that 'charge reversal' or 'overcharging' is the rule rather than the exception in the presence of multivalent cations.

1.4. Some Significant Phenomena in Clays and Colloids :

The interplay between macroscopic motion and diffuse electric charge give rise to Electrokinetic phenomena. When charged clay colloids are subjected to an electric field, electrokinetic events occur. Based on the character of the electrical field, i.e., direct or alternating, uniform or non-uniform, unique forces such as, electrophoresis, dielectrophoresis (DEP), electro-osmosis, etc. become activated.

1.4.1 Electrophoresis :

The mobility of charged colloidal particles in liquid media under an external electric field is known as electrophoresis. The balance between the applied electric field operating on the particles and the viscous resistance on the particles applied by the liquid is responsible for charged colloidal particles' steady rate of movement in steady state. It is essentially the Coulomb force, \vec{F}_{EP} , acting on a particle with a finite, fixed charge, q , in the presence of an electric field, \vec{E} .

$$\vec{F}_{EP} = q.\vec{E} \dots\dots(1a)$$

The velocity with which the particles move is known as the electrophoretic velocity, \vec{v}_e , and is given by,

$$\vec{v}_e = \frac{\epsilon\zeta\vec{E}}{4\pi\eta} \dots\dots(1b);$$

where, ϵ is the dielectric constant, η is viscosity of the medium and ζ is the zeta potential.

In a direct electric field, the particle movement due to this force is finite, however in an alternating electric field, the particle displacement is oscillatory in nature and equal to zero when averaged over time. Electrophoresis is a procedure that separates DNA, RNA, and protein molecules based on particle size and electrical charge.

1.4.2 Dielectrophoresis :

When a polarisable particle is placed in a non-uniform electric field, dielectrophoresis occurs [53]. The electric field polarises the particle, and the poles are then subjected to a force along the field lines that can be attractive or repulsive, depends on the dipole's orientation. Due to the non-uniformity of the field, the pole with the strongest electric field will dominate over the other, causing the particle to shift (Fig. 1.5).

The dielectrophoretic force, F_{DEP} , for a dipole, p , is given by,

$$\vec{F}_{DEP} = (\vec{p} \cdot \vec{\nabla}) E \dots\dots (1c)$$

In the case of an oscillating field, the DEP forces are affected not only by the strength but also by the frequency of the electric field. When the electric field is turned on, the charges cannot immediately orient themselves, but must take a few fractions of second. As a result, the free charges can catch up with the changing direction of the field in low frequency range. As a result, the force is

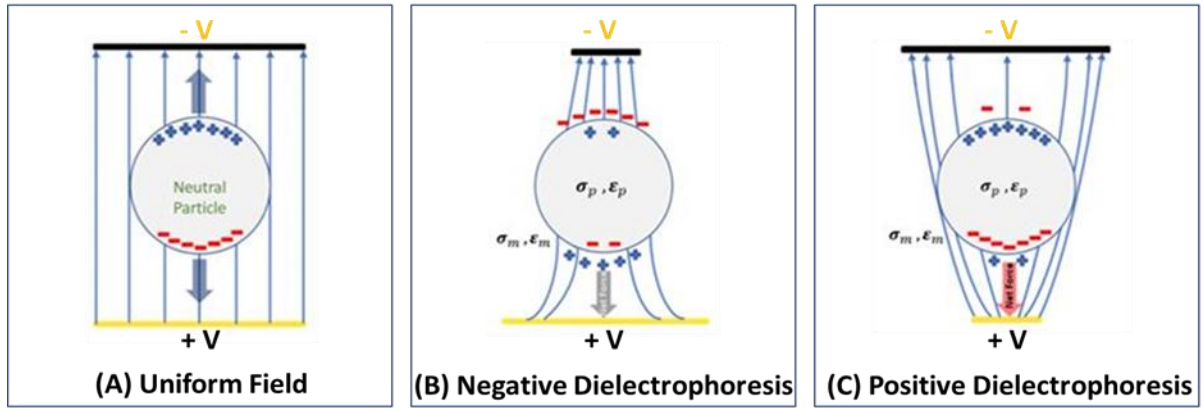


Figure. 1.5.(A) shows the distribution of field lines in the presence of a uniform field. (B) & (C) shows the same distribution but for a non-uniform field. DEP does not occur in case of a uniform field but is seen for (B) & (C). The direction of movement of the particle is indicated by arrows in (B) & (C).

unaltered. The free charges find it increasingly difficult to respond as the frequency increases. The force is constant once more, but this time the dipole may not be able to synchronize its oscillation to that of the alternating field. As a result, it is possible that the direction of the electric field and the oscillating dipole are opposite to each other and a shift from positive to negative DEP occurs in the middle frequency band. For an applied field, E , of frequency ν , the \vec{F}_{DEP} can be presented in the form of its time-averaged value.

$$\langle \vec{F}_{DEP} \rangle = \frac{1}{4} \nu \text{Re}[\alpha] \nabla |E^2| \dots\dots (1d)$$

Since the field is sufficiently spatially nonuniform (relative to the particle's size) to cause significant quadrupole and higher-order moments in the object, Eq. 1c is the simplest approximation to the DEP force and does not account for higher order components. Furthermore, since the dipole moment at field nulls is zero due to its proportionality to E , the dipole approximation to the DEP force (Eq. 1) will likewise be zero. Equation (1d) is the more clearly rewritten form for the time-averaged force as follows in order to calculate higher order DEP force.

1.4.3. Electric Double Layer :

Clay particles when dispersed in water form colloidal suspension. The primary cause of this is the discontinuity that forms at the interface when the dispersion medium and colloidal particle are combined. The particles may also attain charge as a result of isomorphous substitutions, selective ion adsorption, partial ion solution of a sparingly soluble colloidal particle, or ionisation of surface groups. Whatever the source of the charge, an equal and opposite amount of charges in the solution preserve the colloid's charge neutrality. The Electrical Double Layer (EDL) is formed when these balancing charges, also known as counter ions, aligning themselves next to the surfaces of charged colloidal particles.

The double layer as its name suggests mainly consist of two layers –

- 1) The first layer, the surface charge (either positive or negative), is formed of ions that are adsorbed onto the object as a result of chemical reactions.
- 2) The second layer is made up of ions that are attracted to the surface charge by the Coulomb force, electrically screening the first layer. The object is only tangentially related to this second layer. It is composed of loose ions, not firmly anchored, that move in the fluid due to thermal motion and electric attraction. Hence, the term "diffuse layer"

The counter-ions that surround the colloidal particle are dispersed across space and consist of two layers: an inner layer, also called as the Stern layer, with relatively stationary charges in close proximity to the charged surface, and an

outer diffuse layer, also known as the Guoy-Chapman layer, that is also accessible to exchange with other cations present in the medium (Fig. 1.6) [54].

On the particle surface (Stern layer), the electrical potential inside that electric double layer reaches its highest value. The potential decreases as one gets farther away from the surface and zeros off near the edge of the electric double layer.

When a colloidal particle shifts within the dispersion medium, a layer of the encircling liquid stays linked to the particle. The the layer's perimeter is termed as slippy plane or shear plane. The value of the electrical potential of this slipping plane is known as the zeta potential, that is a vital parameter in theory of interaction of colloidal particles.

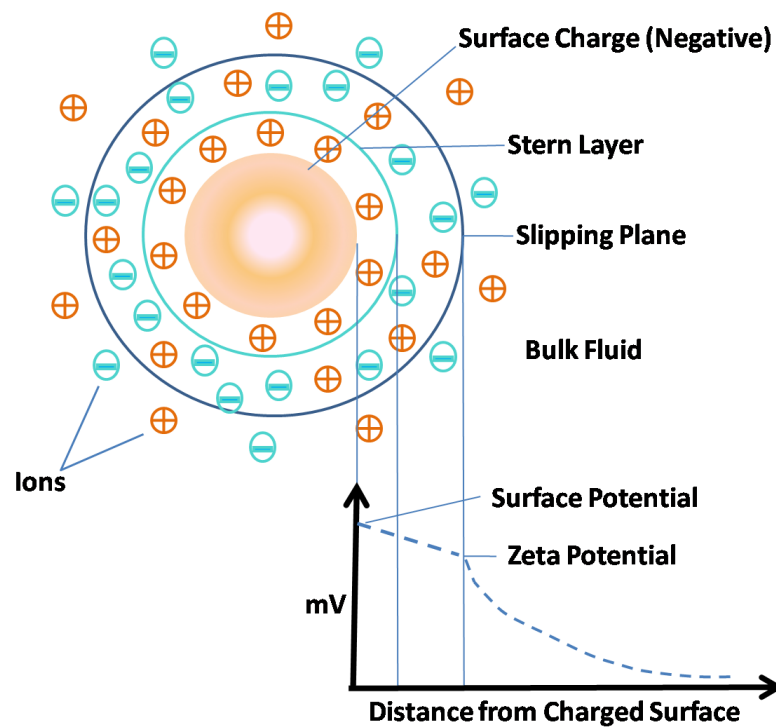


Figure. 1.6. A schematic representation of the electric double layer [54] formed at the interface of the charged surface and the electrolyte showing the Inner Helmholtz Plane (IHP), Outer Helmholtz Plane (OHP), Stern layer and diffuse layer. The variation in the electrical potential (ϕ) with distance y from the surface is also shown, where ϕ_d is the diffuse layer potential and the potential at the hydrodynamic slip plane i.e. the zeta potential, ζ is indicated.

The electric potential in the EDL falls off exponentially with distance from the charged surface as given below:

$$\psi = \psi_0 e^{-\kappa x}, \dots\dots (1e)$$

where,

$$\kappa = \sqrt{\frac{e^2 \sum c_i z_i^2}{\epsilon k T}} \dots\dots (1f)$$

$1/\kappa$ is the distance at which the potential falls off by $1/e$ of its initial value ψ_0 and is known as the Debye length or the thickness of double layer [29]. z_i , c_i are the charge and concentration of the ionic species, i , respectively.

1.4.4 Electro-osmosis :

The movement of a liquid when it comes into touch with a charged solid surface is known as electro-osmosis. As soon as an electric field is introduced, the charges in the double layer around the colloids begin to move. The charges drag the fluid medium along with them as they move, creating a tangential flow. This flow begins at zero near the charged surface and steadily increases with distance until it reaches a steady state.

In a static field, the velocity of the tangential electro-osmotic flow, u_t , is given by,

$$u_t = \frac{E_t \sigma}{\kappa \eta} \dots\dots (1g)$$

where, E_t is the tangential field and σ is the charge contained in the double layer.

u_t becomes frequency dependent in an alternating field. The potential across the medium is low at low frequencies, and the double layer is extremely thin. The induced charge as well as the potential between the two layers are both zero at high frequencies. As a result, there is no electro-osmotic flow at the two extremes of frequency, but it peaks at some intermediate frequency.

1.4.5 Sedimentation :

If the colloidal dispersion's particles are denser than the medium while the medium is less dense, a gravitational force will end up causing the particles to sink or sediment. If the particles become less dense than the medium, however, they will float to the top or form a layer of cream. In both situations, a particle concentration gradient that tends to re-establish a uniform concentration is created. Diffusion opposes the gravitational forces, and when these two processes are in equilibrium, a stable state is obtained (Jean Perrin's seminal experiments on sedimentation equilibrium).

1.4.6 Coagulation :

The colloid becomes unstable when Brownian motion-induced collisions between individual particles in a colloidal dispersion cause aggregation. Coagulation is the term for this process. The electrolyte concentration, surface charge density, and distance between the two edges of the particles all affect how energetically the edges interact.

1.4.7 Flocculation :

The act of causing fine particles to group together into a floc is known as flocculation in the field of colloid chemistry. The floc may then easily be filtered from the liquid or float to the top of the liquid (creaming). It may also sink to the bottom of the liquid (sedimentation). The van der Waals forces of attraction hold these flocs together. Van der Waals forces are generally the result of interactions with rotating or pulsating atom and molecule dipoles.

Two colloids' double layers overlap and interact when they are in close proximity to one another. Because of the overlapping, the double layer's charge-neutralizing action is still insufficient, and the colloidal particles appear to be equally charged. As a result, they repel one another. The particles' charges and the electrolyte content both affect this repelling force. The double layer repulsion and van der Waals attraction each has important role to the net interaction potential when charged colloidal particles approach one another. The thickness of double layer decreases with the rise of ion concentration in the medium, usually through addition of an external reagent, like salt [29]. This causes a reduction in the repulsion between the colloids due to which flocculation becomes possible.

1.5. Brief Introduction to Laponite® and bentonite :

Laponite® :

Laponite® is a 2:1 phyllosilicate mineral. It is synthesised by Rockwood Additives Ltd, such way that its particle size distribution is almost monodisperse. Though Laponite® has a structure similar to natural clay but it does not contain

any of the impurities seen in natural clays. The molecular formula of Laponite[®] is $\text{Na}^{+0.7}[\text{Si}_8\text{Mg}_{5.5}\text{Li}_{0.3}\text{O}_{20}(\text{OH})_4]^{-0.7}$. The size of a single Laponite[®] particle is much smaller than that of natural clay particles, it has almost 1 nm thickness and 25 nm diameter. The rim of the disc has a positive charge that depends on the pH, whereas the flat surface is negatively charged (Fig. 1.7). As the pH rises, the positive rim charge slowly decreases until it is neutralised at pH 11.5 [31]. We used Laponite[®] suspensions of concentration 6.25% (2.5 gm clay + 40 ml deionized water) to perform our experiments that form a film of thickness 0.576cm. In general, aqueous suspensions of Laponite[®] can exist in three different phases viz. isotropic liquid, isotropic gel and nematic gel, depending on the clay concentration. At the concentration of 6.25% the Laponite[®] suspension is found to occur in a nematic gel phase [55, 56] which displays birefringent properties. The suspension is thus referred to as Laponite[®] gel henceforth. The pH of 6.25 % aqueous Laponite[®] determined in our case to be 9.8. It implies that under our experimental conditions, the rims of Laponite[®] discs contain a positive charge. A single Laponite[®] crystal has a net negative charge that is approximately 700 times more than their electronic charge and is balanced by the cations (Na^+) in the interface region [32]. The negative charges of the discs in the dry powder state are counterbalanced by Na^+ ions that are present between the clay layers. The Na^+ ions create the double layer while the clay forms a colloidal dispersion in aqueous suspension.

Laponite[®] is insoluble in water but hydrates and swells to produce clear and colourless colloidal dispersions. Highly thixotropic gels can be formed at concentrations of 2% or higher in water (Fig. 1.7). The phase diagram of Laponite is given in figure 1.7(d). It is commonly used in personal care products, agriculture, polymer industry, and surface coating. We will discuss more about Laponite[®] in the following chapters.

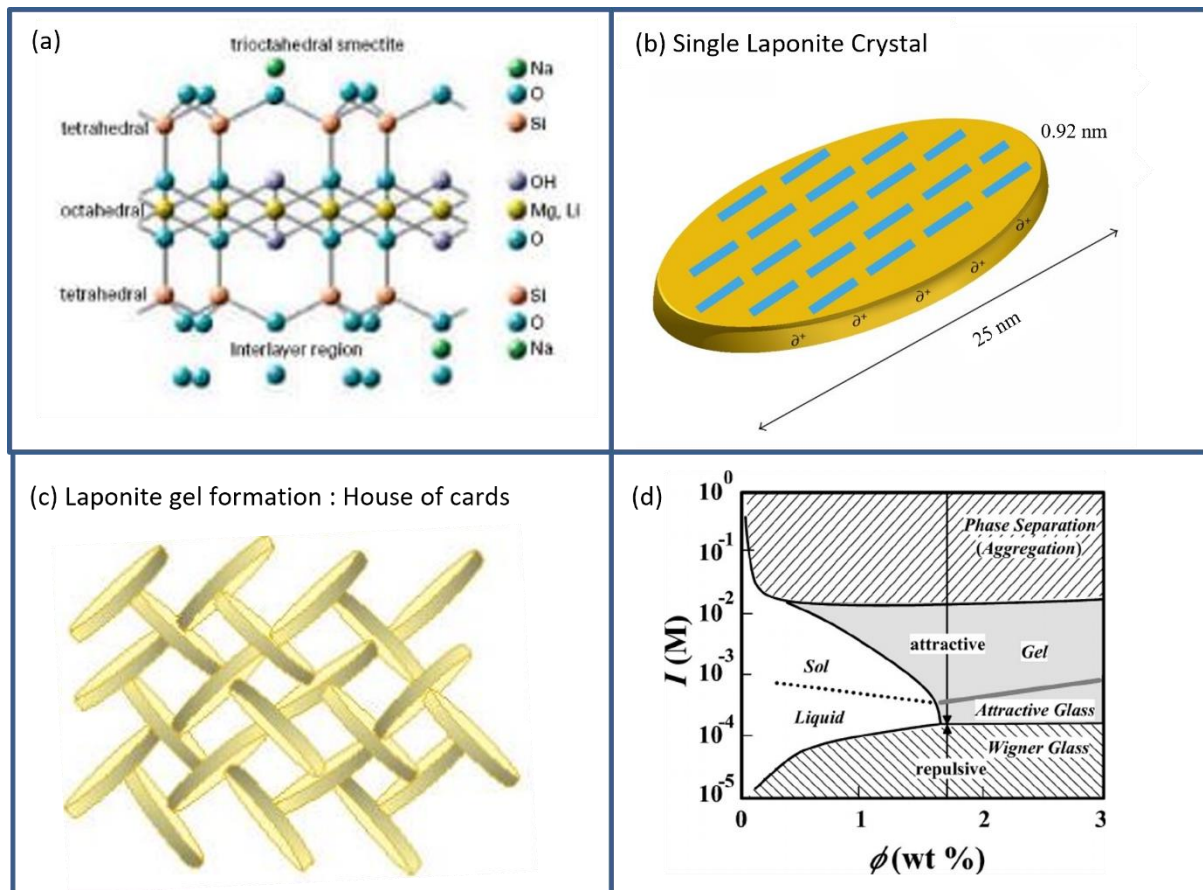
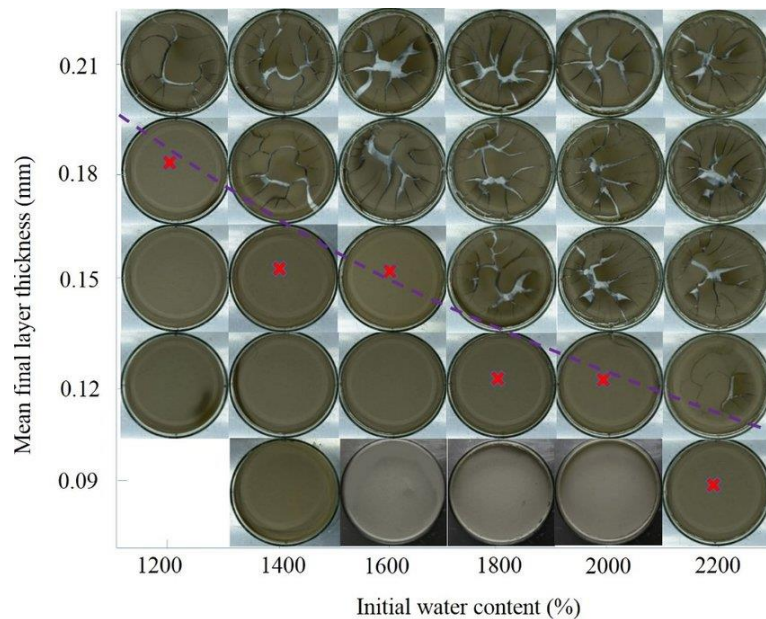


Figure 1.7. (a) Structural formula of Laponite[®] Clay, (b) Schematic diagram of a single Laponite[®] Crystal, (c) Formation of house of cards of Laponite[®] in gel phase. (d) Phase diagram of Laponite suspensions (Source: Tanaka, H., Meunier, J. and Bonn, D., 2004. Nonergodic states of charged colloidal suspensions: Repulsive and attractive glasses and gels. *Physical Review E*, 69(3), p.031404.)

Bentonite :

Bentonite is the commercial name for a broad range of natural clays that expand and swell due to their high water absorption capacity. Bentonite is mostly composed of montmorillonite, which is a clay mineral and belongs to the phyllosilicate class known as smectites. In addition to montmorillonite, bentonites may contain a number of other minerals. Numerous clay minerals,

including kaolin, mica, and illite, along with non-clay minerals, such as quartz, feldspar, calcite, and gypsum, may be in small amounts. The quality of bentonite, and hence its applications, is determined by whether it includes any of these additional minerals. It has the molecular formula of $(\text{Na,Ca})_{0.33}(\text{Al,Mg})_2\text{Si}_4\text{O}_{10}(\text{OH})_2n\text{H}_2\text{O}$ and is made up of plate-shaped particles with a typical diameter of about 1 micrometre. There are considerable concentrations of Na^+ , Ca^{2+} , and Li^+ ions between the layers. A single unit cell of bentonite is composed of one Al sheet sandwiched between two Si sheets, which is why it is known as a 2:1 layer clay. As a result, bentonite resembles the behaviour of negatively charged particles in the presence of water. The reason behind these negative charges have already described elaborately in earlier section. The Phase diagram and crack patterns of thin bentonite clay layers are given in figure 1.8.



*Figure 1.8. Sample in the blank (bottom-left of the figure) was not tested assuming that this one will be non-cracked sample. Red crosses represent to the critical thickness and the average dotted line drawn based on the critical thickness is defined as phase boundary. (Source: Mohammad, N., Meng, W., Zhang, Y., Liu, M., El-Zein, A. and Gan, Y., 2020. Desiccation crack formation and prevention in thin bentonite layers. *Environmental Geotechnics*, 9(8), pp.547-561.)*

1.5. Mechanism for Cracking :

1.5.1 Formation of Desiccation Cracks :

Desiccation could be regarded as a particularly severe sort of drying. Cracking could happen during drying. When water or another solvent is evaporated from a solid, semi-solid, or liquid material, the process is known as drying. 'Drying' is a mass transfer process. Evaporation and capillary action are the two most important controlling elements for drying and hence cracking.

Cracking by Evaporation :

Clay surfaces exposed to air dry faster than the clay surfaces not exposed to air. When clay or soil that has been saturated with liquid solvents, such as water, is exposed to dry air, the upper surface of the sample shrinks due to evaporation, which causes the sample to solidify. Tensile stress develops as a result of this type of process. Cracks can occasionally emerge due to this tensile stress caused by evaporation [33]. Temperature and humidity are the main variables that affect evaporation rate. It also depends on the solvent, as alcohol evaporates more quickly than water.

Cracking due to Capillary Action :

Capillarity is the effect by which liquid flows through narrow spaces without external forces, such as gravity. When the water layer covering the clay's surface evaporates, leaving only the particles and the waters trapped between the particles, intermolecular forces and the water's surface tension causes a concave

meniscus to develop in the gap between the particles [34, 35]. The term "capillary pressure" is used to describe the excess pressure above the concave meniscus and is expressed as (from Gauss-Laplace equation)

$$p_{cap} = -\gamma \left(\frac{1}{R_1} + \frac{1}{R_2} \right) \dots\dots(1h)$$

Where, p_{cap} = capillary pressure, γ = surface tension of water and R_1 , R_2 are the principal radii of curvature of water surface (Fig. 1.9d).

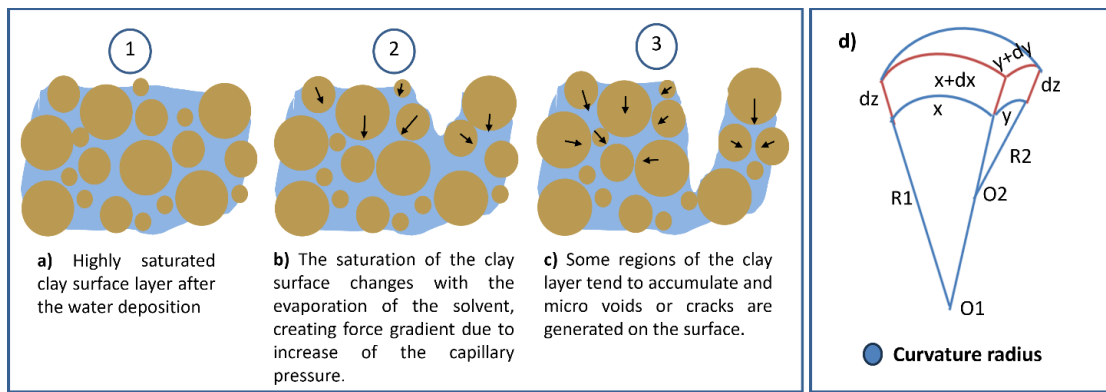


Figure.1.9.a)-c) Capillary action caused by drying the deposited fluid leads surface cracks to appear. d) Schematic image of radii of curvature of liquid surface.

Crack development begins if the elastic energy determined by the stress-strain equation for capillary pressure is greater than the surface energy. Actually, there is a connection between capillary actions and evaporation. Capillary action takes over when evaporation slows very significantly. The basic force behind desiccation fracture is provided by this capillary action. The Process of desiccation i.e., evaporation of fluid from the surface, exposing the solid to air with the formation of air gap that slowly penetrates into the interior layers is shown in figure 1.8(a-c).

1.5.2. Theory of Cracking: Griffith's Criterion:

In Griffith's opinion [36] a fracture in an elastically stressed body should be generated if, the potential energy that has developed inside it is higher than or equal to the energy required to produce the new crack surfaces. He took into consideration an elastic body with a single crack of a given length, l , and external loads acting at its boundaries (figure). Typically, the total energy U in the system that is involved in crack development can be subdivided into two terms: a mechanical term (U_M) and a surface term (U_S). Thus,

$$U = U_M + U_S \dots\dots (1i)$$

The mechanical energy U_M is again composed of two terms: U_E and U_L . Where U_E denotes the strain potential energy stored in the elastic material, and U_L is the potential energy owing to externally imposed loads. The work necessary to shift the loading points can be described as the negative of U_L . Therefore, we can write,

$$U = U_E + U_L + U_S \dots\dots (1j)$$

Assume for the moment that the system has a minor virtual fracture extension and is in thermodynamic equilibrium. To achieve thermodynamic equilibrium, the terms U_M and U_S must balance each other. The mechanical energy would reduce as the crack advanced because the system would restructure itself to a lower state of energy. On the other hand, the addition of new crack surface area would result in an increase in the surface energy term. As a result, the former term would be in favour of crack extension whereas the latter term would be against it. This defines how a body will fracture on the basis of energy conservation and is known as Griffith energy balance concept. This equilibrium has the following mathematical form:

$$\frac{dU}{dl} = 0 \dots\dots (1k)$$

The relationship between the energy U_L and U_E for the application of a constant load, or uniform tension is

$$U_L = -2U_E \dots\dots(1l)$$

Therefore,

$$U_M = -U_E \dots\dots(1m)$$

The negative sign suggests that the mechanical energy has decreased as a result of crack development. The energy U_E for unit width along the crack front can be expressed as

$$U_E = \pi L^2 \sigma_A^2 / E \dots\dots(1n)$$

considering a material with a Young's modulus of E and a uniform tensile stress σ_A in an infinitesimally small circular cavity of length $2a$.

Again,

$$U_S = 4l\gamma \dots\dots(1o)$$

where, γ is the free surface energy per unit area.

Therefore, the energy per unit length of the system is

$$U = -\frac{\pi l^2 \sigma_A^2}{E} + 4l\gamma \dots\dots(1p)$$

However, the energy balance criterion is a requirement for fracture but not an adequate condition. This means that even if the strain energy stored in the material is sufficient, cracking will occur only when the stress accumulated in the crack tip is enough to break the bonds within it. The critical crack length, or l_c , is the smallest length of crack that can exist for a given stress and below which a crack cannot grow on its own. This is given by,

$$l_c = 2\gamma E / \pi \sigma_A^2 \dots\dots(1q)$$

1.5.3. Modes of Fracture :

There are basically three different modes of fracture, depending on the loading type, and three different types of crack propagation. These are

- A. **Opening Mode (Mode I):** This type of mode is most frequently observed in cracks of extremely brittle substances. Here, cracks develop as a result of tensile stress. Both the fracture surface and the crack front that formed are perpendicular to the tensile stress direction. Brittle fractures are always tried to orient in a direction that reduces shear loading [37]. Figure 1.10(A) shows a 2D illustration of a Mode I crack on a material.
- B. **Sliding mode (Mode II):** Here, a shearing stress results in this mode of crack. In this case, the crack front is in normal direction and the fracture surface that resulted from the cracking is parallel to the direction of the shearing stress. The sliding manner of cracking is depicted in figure 1.10(B) with the arrow indicating the sliding direction. This type of fracture is often seen during frictional events and earthquakes along a predetermined fault, as well as in anisotropic materials.
- C. **Tearing Mode (Mode III):** Shearing stress again results in cracking in mode III crack, but unlike in Mode II, the generated crack front and fracture surface are both parallel to the direction of stress. This mode of cracking is also named as ‘Tearing Mode’ which is shown in the figure 1.10(C).

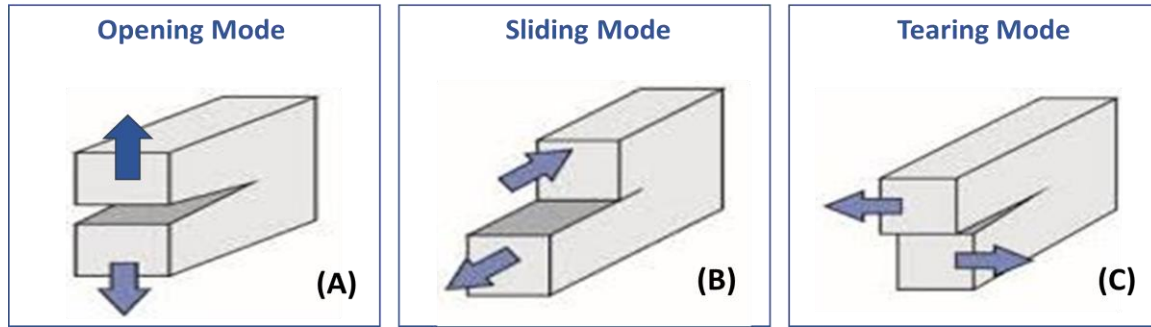


Figure. 1.10 (A) Mode I (opening mode), (B) Mode II (sliding mode) and (C) Mode III (tearing mode). The arrows indicate the directions of stresses.

In comparison to Mode II & Mode III fracture, Mode I fracture is the one that is most frequently observed in theoretical and experimental study. This is mostly due to the fact that the crack faces invariably push against one another (as opposed to Mode I, when the two fracture surfaces are forced apart), and the resulting force of friction between them is very challenging to measure precisely. These three modes of fractures typically happen when a material is loaded symmetrically. The fractures that are noticed, however, do not exclusively belong to any one mode because the stresses that are operating on a body in actuality are a combination of forces. These kinds of fractures are known as mixed mode fractures.

1.5.4. Critical Cracking Thickness :

It's not a certainty that fractures always appear just because clay has capillary pressure. The capillary pressure at which cracks form due to the elastic energy exceeding the surface energy is termed as "critical capillary pressure". When the water-air interface is inside the film, critical capillary pressure is determined by the particle size rather than thickness of the film [38, 39]. In the opposite scenario, where the water-air interface lies at the film's surface, the critical

cracking thickness is irrespective of particle size but dependent on the film thickness(h) as

$$p_{cap}^{crit} \sim \gamma G^{2/5} h^{-3/5} \dots\dots (1r)$$

using the Hertzian model [39]. The shear modulus in this case is G. The exponent of h is always negative. A thinner film is therefore more difficult to break than a thicker one. As a result, we can descend to a specific thickness below which no cracks manifest. The term "critical cracking thickness" (h_{cct}) refers to this film thickness [40].

1.5.5. Some Significant Features of Desiccation Cracks :

Crack patterns typically have a network-like structure that demonstrates their fractal nature [41,42]. A crack typically doesn't change after it forms; in other words, it isn't affected by cracks that emerge later. One crack's impact on another is not symmetrical. But the boundaries for the growth of mechanical stress and, consequently, for the emergence of new cracks, are defined by the existing fractures. The later cracks almost invariably intersect the former fractures at a straight angle, or nearly 90°, creating a "T" junction [43]. This is mostly due to the parallel alignment of the stress field at the medium's edges created by adjacent fractures and the fact that the rate of stress release is greatest when a crack propagates perpendicular to the largest stress field direction. The cracks were observed to meet at a 120° angle forming 'Y' junction when the mixture layer was thinner [44]. These are known as orthogonal and non-orthogonal crack patterns respectively. This could occur as a result of continually wetting and drying the dried layer of crack patterns with a "T" junction. Basically, mud cracks exhibit

this kind of behaviour. The ped size is considerably larger than that of the layer film thickness at the early stages of crack formation. Up till the ped size is equal to the layer thickness, cracks continue to form [45].

Usually, cracks start at the clay's upper surface and extend downward towards the bottom surface. It is quite uncommon for cracks to begin at the clay's bottom surface. Cracks should spread perpendicular to the axis along which stress is greatest in order to release the most stress throughout the cracking process. The direction of the stress that formed close to an edge is parallel to the edge. Therefore, cracks typically start at an edge that is perpendicular to it, or a crack can meet an existing fracture by twisting in its direction. Concave edges experience the highest stress, where the majority of cracks start to appear [46].

Additionally, Groisman et al. demonstrated that the absence of a polygonal crack network was a consequence of the influence of the change in layer thickness. Khatun et al. [47], who conducted research on suspensions of halloysite, bentonite, and Laponite[®] clay, also reported on this effect. The crack patterns clearly correlated with the clay film thickness. However, the nature of this cracking remained specific to the type of clay used.

One variety of soil is clay. The main distinction between soil and clay is that the former is a material made up of liquids, minerals, organic materials, and living things, while the latter is a kind of soil that becomes elastic when wet. According to C. S. Tang et al. [48], clayey soil cracking is temperature-dependent. It was allowed for the clay slurry to dry at three different temperatures. The experimental results demonstrated that the rate of soil water loss increased with increasing temperature. The water-air meniscus occurs near the soil's surface as it begins to dry, and capillary suction develops in the top layers. Because of this, each soil particle experiences tensile stress. Tensile stress rises with continued evaporation and eventually surpasses the soil's tensile strength. As a result, the soil cracks.

Euler number ($= N-H$), a topological quantity that can be used to describe the connectivity of fracture patterns, was first developed by Vogel et al. [49], N denotes the number of isolated objects, and H the number of isolated holes. By varying the resolution during the image processing, they were able to recognise cracks as objects and peds as holes, and they were able to observe the connectedness of fracture patterns.

1.6. Experimental Apparatus :

The clay used in the studies for this paper has particles with sizes on the order of nanometers. Hence it is crucial to have a deeper grasp of the micro-level features in addition to the macro-level observations in order to appreciate the intricate mechanisms involved in the cracking phenomena. In this work, I have obtained magnified images of the fractured film surfaces at different magnifications using FESEM and an optical microscope. Below is a brief explanation of these instruments.

Optical Microscope : An optical microscope produces a magnified image of any object using first an objective lens, that creates an inverted, real image, and then by an eye piece, that magnifies the image further and produces an erect, virtual one. The microscope has a resolution range of micrometre order, limited by the wavelength of light and numerical aperture of the objective lens. It allows for a closer look at the clay samples to check for surface irregularities and other topological features. In the present work, the Leica DM750 optical microscope has been used.

FESEM : The Field Emission Scanning Electron Microscope (FESEM) uses a beam of electrons that are emitted from a field emission source to scan and image topographical details of the sample surface. It has a magnification range of 20X–30,000X with a spatial resolution of 50 nm – 100 nm. The SEM service of the Physics Department of Jadavpur University, Configuration no. QUO-35357-0614 funded by FIST-2, DST Govt. of India, has been used for this thesis.

The FESEM is basically used to observe the microscopic structures of the dried clay films, to investigate the alignments of the clay platelets. In the present work the sample pieces are mostly thin, gel-like films and need to be handled with utmost caution, keeping in mind their delicate and fragile nature. The samples are carefully removed from the experimental Petri-dishes or containers before they are completely dried. If the film is allowed to dry completely it will harden and become brittle which breaks in the process of removal from its container. Hence the film for loading in SEM is taken out when it is still soft. Small portions of the film are lifted from the substrate with the help of a clean, flat spatula so as not to upset its structure. They are then carefully placed inside a clean and dry Petri-dish and kept covered. This is stored in desiccators. Before being loaded onto the SEM, the samples become completely dry. These are then mounted for conductive coating before being placed in the vacuum chamber for imaging.

1.7. List of References :

- [1] Goehring, L., Nakahara, A., Dutta, T., Kitsunozaki, S. and Tarafdar, S., 2015. *Desiccation cracks and their patterns: Formation and Modelling in Science and Nature*. John Wiley & Sons.
- [2] El-Sehily, B.M., 2016. Fracture mechanics in ancient Egypt. *Procedia Structural Integrity*, 2, pp.2921-2928.
- [3] Cotterell, B., 2002. The past, present, and future of fracture mechanics. *Engineering fracture mechanics*, 69(5), pp.533-553.
- [4] Leonardo da Vinci Codex Atlanticus 1504 Milano. 1894. In: Pinati, Milano, Biblioteca Ambrosiana.
- [5] Galilei, G., 1914. *Two new sciences* (p. 147). Dover.
- [6] Griffith, A.A., 1921. VI. The phenomena of rupture and flow in solids. *Philosophical transactions of the royal society of london. Series A, containing papers of a mathematical or physical character*, 221(582-593), pp.163-198.
- [7] Griffith, A., 1924. The theory of rupture. In *First Int. Cong. Appl. Mech* (pp. 55-63).
- [8] Orowan, E., 1933. Die Zugfestigkeit von Glimmer und das Problem der technischen Festigkeit. *Zeitschrift für Physik*, 82(3-4), pp.235-266.

-
- [9] Irwin, G.R., 1948. Fracture dynamics, *Fracturing of Metals*. American Society of Metals. *Cleveland, Ohio*, p.296.
- [10] Pauchard, L., Elias, F., Boltenhagen, P., Cebers, A. and Bacri, J.C., 2008. When a crack is oriented by a magnetic field. *Physical Review E*, 77(2), p.021402.
- [11] Nam, K.H., Park, I.H. and Ko, S.H., 2012. Patterning by controlled cracking. *Nature*, 485(7397), pp.221-224.
- [12] Bucklow, S., 1997. The description of craquelure patterns. *Studies in conservation*, 42(3), pp.129-140.
- [13] Wyvill, B., van Overveld, K. and Carpendale, S., 2004, June. Rendering cracks in batik. In *Proceedings of the 3rd international symposium on Non-photorealistic animation and rendering* (pp. 61-149).
- [14] Giorgiutti-Dauphiné, F. and Pauchard, L., 2016. Painting cracks: A way to investigate the pictorial matter. *Journal of Applied Physics*, 120(6), p.065107.
- [15] Daegling, D.J., Warren, M.W., Hotzman, J.L. and Self, C.J., 2008. Structural analysis of human rib fracture and implications for forensic interpretation. *Journal of forensic sciences*, 53(6), pp.1301-1307.
- [16] Ramasamy, A., Hill, A.M., Masouros, S., Gibb, I., Bull, A.M. and Clasper, J.C., 2011. Blast-related fracture patterns: a forensic biomechanical approach. *Journal of the Royal Society Interface*, 8(58), pp.689-698.
- [17] Brutin, D., Sobac, B., Loquet, B. and Sampaol, J., 2011. Pattern formation in drying drops of blood. *Journal of fluid mechanics*, 667, pp.85-95.

-
- [18] Kiruthika, S., Rao, K.D.M., Kumar, A., Gupta, R. and Kulkarni, G.U., 2014. Metal wire network based transparent conducting electrodes fabricated using interconnected crackled layer as template. *Materials Research Express*, 1(2), p.026301.
- [19] Kim, M., Ha, D. and Kim, T., 2015. Cracking-assisted photolithography for mixed-scale patterning and nanofluidic applications. *Nature communications*, 6(1), p.6247.
- [20] Kim, B.C., Matsuoka, T., Moraes, C., Huang, J., Thouless, M.D. and Takayama, S., 2013. Guided fracture of films on soft substrates to create micro/nano-feature arrays with controlled periodicity. *Scientific reports*, 3(1), p.3027.
- [21] Adelung, R., Aktas, O.C., Franc, J., Biswas, A., Kunz, R., Elbahri, M., Kanzow, J., Schürmann, U. and Faupel, F., 2004. Strain-controlled growth of nanowires within thin-film cracks. *Nature materials*, 3(6), pp.375-379.
- [22] Zhu, X., Mills, K.L., Peters, P.R., Bahng, J.H., Liu, E.H., Shim, J., Naruse, K., Csete, M.E., Thouless, M.D. and Takayama, S., 2005. Fabrication of reconfigurable protein matrices by cracking. *Nature materials*, 4(5), pp.403-406.
- [23] Milad, R.E. and Shackel, K.A., 1992. Water relations of fruit end cracking in French prune (*Prunus domestica* L. cv. French). *Journal of the American Society for Horticultural Science*, 117(5), pp.824-828.

-
- [24] Considine, J. and Brown, K., 1981. Physical aspects of fruit growth: theoretical analysis of distribution of surface growth forces in fruit in relation to cracking and splitting. *Plant Physiology*, 68(2), pp.371-376.
- [25] El-Maarry, M.R., Watters, W., McKeown, N.K., Carter, J., Dobrea, E.N., Bishop, J.L., Pommerol, A. and Thomas, N., 2014. Potential desiccation cracks on Mars: A synthesis from modeling, analogue-field studies, and global observations. *Icarus*, 241, pp.248-268.
- [26] Everett, D.H., 2007. *Basic principles of colloid science*. Royal society of chemistry.
- [27] Birdi, K.S., 2009. *Surface and colloid chemistry: principles and applications*. CRC press.
- [28] Van Olphen, H., 1977. An Introduction to Clay Colloid Chemistry.: John Wiley & Sons, New York. *An introduction to clay colloid chemistry. 2nd ed. John Wiley & Sons, New York*.
- [29] Van Olphen, H., 1964. An introduction to clay colloid chemistry. *Soil Science*, 97(4), p.290.
- [30] Messina, R., Holm, C. and Kremer, K., 2001. Strong electrostatic interactions in spherical colloidal systems. *Physical Review E*, 64(2), p.021405.
- [31] de Melo Marques, F.A., 2012. *Aging Investigations of Laponite Systems* (Doctoral dissertation, Thesis ID).

[32] Cummins, H.Z., 2007. Liquid, glass, gel: The phases of colloidal Laponite. *Journal of Non-Crystalline Solids*, 353(41-43), pp.3891-3905.

[33] Lee, W.P. and Routh, A.F., 2006. Temperature dependence of crack spacing in drying latex films. *Industrial & engineering chemistry research*, 45(21), pp.6996-7001.

[34] Slowik, V., Schmidt, M. and Villmann, B., 2010. Capillary shrinkage cracking—experiments and numerical simulation. *Fracture mechanics of concrete and concrete structures-assessment, durability, monitoring and retrofitting of concrete structures*. Seoul: Korea Concrete Institute.

[35] Routh, A.F. and Russel, W.B., 1999. A process model for latex film formation: Limiting regimes for individual driving forces. *Langmuir*, 15(22), pp.7762-7773.

[36] Griffith, A.A., 1921. VI. The phenomena of rupture and flow in solids. *Philosophical transactions of the royal society of london. Series A, containing papers of a mathematical or physical character*, 221(582-593), pp.163-198.

[37] Lawn, B., 1993. *Fracture of Brittle Solids* 2nd edn Cambridge Univ. Press, Cambridge.

[38] Mason, G. and Mellor, D.W., 1995. Simulation of drainage and imbibition in a random packing of equal spheres. *Journal of Colloid and interface Science*, 176(1), pp.214-225.

-
- [39] Man, W. and Russel, W.B., 2008. Direct measurements of critical stresses and cracking in thin films of colloid dispersions. *Physical Review Letters*, 100(19), p.198302.
- [40] Singh, K.B. and Tirumkudulu, M.S., 2007. Cracking in drying colloidal films. *Physical review letters*, 98(21), p.218302.
- [41] Baer, J.U., Kent, T.F. and Anderson, S.H., 2009. Image analysis and fractal geometry to characterize soil desiccation cracks. *Geoderma*, 154(1-2), pp.153-163.
- [42] Mal, D., Sinha, S., Mitra, S. and Tarafdar, S., 2005. Formation of crack networks in drying laponite films. *Physica A: Statistical Mechanics and Its Applications*, 346(1-2), pp.110-115.
- [43] Bohn, S., Pauchard, L. and Couder, Y., 2005. Hierarchical crack pattern as formed by successive domain divisions. *Physical Review E*, 71(4), p.046214.
- [44] Goehring, L., Conroy, R., Akhter, A., Clegg, W.J. and Routh, A.F., 2010. Evolution of mud-crack patterns during repeated drying cycles. *Soft Matter*, 6(15), pp.3562-3567.
- [45] Bohn, S., Platkiewicz, J., Andreotti, B., Adda-Bedia, M. and Couder, Y., 2005. Hierarchical crack pattern as formed by successive domain divisions. II. From disordered to deterministic behavior. *Physical Review E*, 71(4), p.046215.
- [46] Groisman, A. and Kaplan, E., 1994. An experimental study of cracking induced by desiccation. *Europhysics Letters*, 25(6), p.415.

-
- [47] Khatun, T., Dutta, T. and Tarafdar, S., 2015. Topology of desiccation crack patterns in clay and invariance of crack interface area with thickness. *The European Physical Journal E*, 38, pp.1-11.
- [48] Tang, C.S., Cui, Y.J., Shi, B., Tang, A.M. and Liu, C., 2011. Desiccation and cracking behaviour of clay layer from slurry state under wetting–drying cycles. *Geoderma*, 166(1), pp.111-118.
- [49] Vogel, H.J., Hoffmann, H. and Roth, K., 2005. Studies of crack dynamics in clay soil: I. Experimental methods, results, and morphological quantification. *Geoderma*, 125(3-4), pp.203-211.
- [50] Hunter, R.J., 1998. Recent developments in the electroacoustic characterisation of colloidal suspensions and emulsions. *Colloids and Surfaces A: Physicochemical and Engineering Aspects*, 141(1), pp.37-66.
- [51] Wilkinson, K.J. and Lead, J.R. eds., 2007. Environmental colloids and particles: behaviour, separation and characterisation. *John Wiley & Sons*.
- [52] Antonietti, M. and Göltner, C., 1997. Superstructures of functional colloids: chemistry on the nanometer scale. *Angewandte Chemie International Edition in English*, 36(9), pp.910-928.]
- [53] Pamme, N., 2007. Continuous flow separations in microfluidic devices. *Lab on a Chip*, 7(12), pp.1644-1659.
- [54] Soo-Jin Park, Min-Kang Seo, in *Interface Science and Technology*, 2011.

[55] Mourchid, A., Lecolier, E., Van Damme, H., & Levitz, P. (1998). On viscoelastic, birefringent, and swelling properties of Laponite clay suspensions: revisited phase diagram. *Langmuir*, 14(17), 4718-4723.

[56] Gabriel, J. C. P., Sanchez, C., & Davidson, P. (1996). Observation of nematic liquid-crystal textures in aqueous gels of smectite clays. *The Journal of physical chemistry*, 100(26), 11139-11143.

2

Effect of Uniform Electric Field in Laponite[®] Clay: Formation of Branched Crack Pattern

2.1. Introduction :

In many branches of science and engineering, the significance of the research of desiccation crack patterns and fracture growth is generally acknowledged [29-35]. It has been discovered that manipulating and modifying the cracks allows us to create a wide range of designer fractures that are suitable to nanofabrication [1] and the development of surfaces exhibiting distinctive characteristics. In an aqueous system where clay particles are charged [2], a reaction to an electric field is expected. Although the impact of electric fields on mechanical fracture in dielectric materials has been documented considerably earlier [3], the use of electric fields to regulate the cracking behaviour of clays is a relatively unexplored topic of study. Another such intriguing and distinctive crack topology, which was seen in drying films of Laponite[®] clay in the presence of direct electric fields in rectangular geometry is detailed in the sections that follow. The pattern has been examined, and the cause of the origin has also been analysed.

In section 2.2 of this chapter, we go over the earlier research that is relevant to our topic. The chemical formula, particle size, and a few other crucial details of the material used and the methods used to prepare the samples, conduct the experiments, are provided in section 2.3. In 2.4. sections we discuss the observation that has been seen in the experiments. Here, we also discuss an additional experiment that we conducted to confirm the primary aspect of the cracks. The results and analysis of the results will then be assessed in 2.5. In part 2.6, we attempt to apply theoretical knowledge to determine the origin of the distinct pattern developed in the examinations. Finally, we will analyse and draw conclusions from the entire study.

2.2. Overview of Previous Relevant Work :

Clay particles suspended in a liquid form charged solution that react to external electric fields. Such clay solutions exhibit distinctive fracture patterns that are considerably different from the pure desiccation cracks when they are allowed to desiccate in the existence of applied electric fields. Mal et al. [4, 5] made the initial report of Laponite[®] cracking in presence of an electric field. When Laponite[®] clay aqueous solutions were left to dry while being surrounded by a radial, static electric field then cracks appeared radially from the core electrode when it was kept positive, and they proceeded directly to the outer, negative electrode.

The cracks began at the peripheral, positive end and moved inside when the central electrode was kept negative. These cross-radial cracks, on the other side, prevent these cracks from spreading to the central negative electrode. Random cracks were observed to emerge when the sample was left to dry in the same configuration but without the application of an electric field. The strength of the field used was also observed to affect the radial pattern of the cracks. When the magnitude of the field strength was reduced, a change in the applied voltage resulted in small changes in the crack orientations. The interaction of the non-zero quadrupole moment of the Laponite[®] discs shaped particles with the applied field was considered to be the cause of the cracks' radial pattern.

Under an alternating electric field with a fixed frequency, Khatun et al. [6] reported crack patterns with a similar circular geometry. The cracks on the outer electrode began to develop while the voltage was quite low, but instead of spreading inward, the cracks curled to rejoin the border once more. When the voltage is larger, the cracks start at the core electrode and curve before they reach the outside electrode. The cracks were seen to become more curved as the field

strength rose. Additionally, it was found that as the field strength grew, the time it took for the first crack to appear decreased. When a rectangular geometry was applied to the clay sample, such patterns were not visible. It is obvious that the field shape has a significant impact on the fracture properties.

The existence of memory in Laponite[®] gel under a radial, static electric field was yet another intriguing work initiated by Khatun et al. [7] and reported elaborately by Hazra et al. [8]. However, compared to earlier circular systems, the system under issue here is considerably smaller. These systems, which have a volume of only a few microlitres, are referred as droplets. For both centre positive (CP) and centre negative (CN) arrangements, cracks formed in the same way as in the bigger systems when the electric field was kept on constantly. When the field was applied for a short moment τ ($\tau \leq$ the initial crack's appearance time), interesting outcomes were seen. After the field was turned off, cracks appeared considerably later and replicated the pattern of the ones caused by the field, in contrast to growing randomly as would occur in the absence of any external field. This demonstrated clearly the gel's tendency to "remember" the electrical impulses that were delivered to it. The field's strength along with the exposure period had a significant impact on the formation of cracks.

Further Sircar et al. [9] has demonstrated the impact of an alternating electric field on a Laponite[®] film that is desiccating. Both an experimental examination of the frequency fluctuation of the field in radial geometry and a simulation analysis of the effects of voltage variation using 'The Randomized Spring Network Model' on the patterns of cracks in drying clay have also been reported. The investigations under a radial AC field revealed that when

Laponite[®] films were allowed to dry out in the vicinity of an uneven field gradient, cracking typically began from the higher field end and moving with parallel direction to the applied field. After that, the cracks moved in the direction

of the lower field end and, depends on the frequency and field voltage applied, they twisted perpendicular to the field. While the field voltage significantly affects the appearance and quantity of fractures in a radial system, the field frequency controls the cracks' appearance time, curvature, and path lengths.

Moreover, there are a number of studies on clay that have been conducted in the presence of various external forces, including magnetic and mechanical fields as well as directional drying.

Experimental study on the effects of an electric field on colloidal particles was conducted by Fraden et al. [10]. By applying a high-frequency external electric field in the sample's plane, they were able to see how micron-diameter polystyrene spheres that were suspended in an aqueous solution and contained in a thin layer gathered together. The spheres operate as dielectric holes in water at high frequencies, causing the electric field to be distorted into what is basically a dipole pointing in the direction of the external electric field.

In an electric field, colloidal particles may react with the electrode. By utilising a variety of electrodes, Janca et al. [11] investigated the kinetics of transport phenomena and electrode reactions brought on by an electric field and resulting in the generation of density gradients in the suspensions of charged colloidal silica. The types of electrodes affect how quickly a steady-state density gradient approach.

Schneider [12] investigated the effects of mechanical stress and electric field on ferroelectric material fracture. Ferroelectric ceramics are very desirable materials for practical applications due to the strong electromechanical coupling effect. Linear strain may be produced by an electric field (for instance, one of 1 kV/mm) and vice versa (piezoelectric effect). Ferroelectric ceramics are fragile because they share many mechanical traits with glass. The evolution of fracture mechanical theories and experiments that permit the electric field to be included

in the explanation of the fracture process is brought on by the inherent interdependence of electro - mechanical impacts. For the production of cracks, the electrically stored energy density of dielectric and piezoelectric ceramics must be compared to the elastically stored energy density. The comparison demonstrates that the only dielectric and piezoelectric ceramics that have electrically stored energy greater than elastically stored energies will be able to significantly affect crack formation.

Nakahara and his colleagues explored the role of a mechanical field on the development of paste crack patterns [13, 14]. On the clay and granular material pastes, they applied perturbations such flow, vibration, translation, and rotation. The resultant crack patterns exhibit the "memory" effect, or the uniqueness of the perturbation type used. Lamellar cracks are created as a result of both flow and vibration disturbances, but there is a fundamental distinction. When there is vibration, cracks travel parallel to the direction of oscillation, the resulting "memory effect" is known as the "Type-I Nakahara effect". The "memory effect" that results when flow cracks are parallel to external force is known as the "Type-II Nakahara effect". Takeshi upgraded the "memory effect" (also known as the "Nakahara effect") theory from a two-dimensional to a three-dimensional case [15, 16]. This theory predicts residual pressure in the normal direction as well as residual tension in direction of external force, confirming the existence of anisotropy in the horizontal plane.

Zhu et al. [17] evaluated the electrical field generated during the shattering of Westerly granite cylinder samples that were both dry and water-saturated. Two electrical fields are detected in experiments with water-soaked granite samples: an electromagnetic wave from seismoelectric conversion and a low-frequency electrical potential from the piezoelectric effect, which is a key sign of rock breaking.

Suo [18] reported on the impact of electrical fields on mechanical fracture in dielectrics. A dielectric sample experiences a low, evenly distributed current density when a weak electric field is applied to it. When the current suddenly increases at a critical electric field, the dielectric degrades. Along small tubular channels, permanent damage is frequently found, with the majority of the sample remaining undamaged.

There could be cracking and mechanical deterioration when ferroelectric ceramics are exposed to a strong alternating electric field. Cao and Evans conducted this experiment in 1994 [19]. They explained how to identify crack extension from pre-existing flaws in a material exposed to a strong AC field. The extension of a crack before the electric breakdown is always 90° to the electric field. Initial crack extension is thought to happen in small fields ($E < E_c$, E = applied AC field and E_c = coercive field) due to the interaction between the electric field concentration at the open fracture and the intensity of the stress brought on by the residual stress from the indent. When a crack grows large at higher fields ($E > E_c$), it cycles between opening and closing. The dielectric permittivity of the cracked zone is influenced by the contacts along the fracture faces, which causes the field to be different from that of the intact region. A strain is caused by this variation. On each cycle, the consequent displacements lead the crack to expand. A unique mode of fatigue crack development is induced by the AC field.

It has been demonstrated that the impact of electric fields can be helpful for finding cracks. A quick and accurate non-destructive evaluation (NDE) method can be used to find cracks in ceramic materials, whether they are in the bulk or on the surface. Suzuki et al. [20] demonstrated that a new NDE technique may be able to quantitatively assess cracks on ceramic surfaces based on the high-frequency electromagnetic wave transmission properties of ceramics. The presence of cracks or other imperfections inside the ceramic material affects the

transmission of high-frequency electromagnetic signals. Consequently, the flaw is found.

In the parts that follow, a crack pattern that was noticed in drying films of Laponite[®] clay in a rectangular geometry under a direct electric field is explored. The pattern has been examined, and the source of this behaviour has also been researched.

2.3. Materials and Experimental Method :

This section addresses how crack patterns develop in Laponite[®] gel when a direct electric (DC) field is applied externally in a rectangular geometry.

The Laponite[®] slurry is made by mixing 25.3gm of \Laponite[®] to 405ml of deionized water and stirring magnetically for 15 to 20 seconds. Before the suspension begins to gel, it is immediately placed into a 60cm × 14cm rectangular Perspex box (Fig.2.1). The suspension initially seems turbid white, but with some time, it turns clear. The opposing walls (lengthwise) of the box are covered by using aluminium foil, serving like electrodes. Before turning on the DC power supply after the gel has been deposited, a waiting period of around five minutes is maintained. A range of 357V/m to 928V/m field is produced by varying the applied voltage starting at 50V to 130V. The electric field is activated for 24 hours. Initially, the film has a thickness or height of about 0.5 cm (Fig. 2.2a), but this changes when an electric field is introduced, as seen in fig. 2.2b. Using a Canon 750D camera, photographs taken at regular intervals of time (Fig. 2.3) are used to track the evolution of the fracture pattern for various V. Using the tools ImageJ and Mathcad PTC, measurements from the photos are taken and theoretical calculations are made.

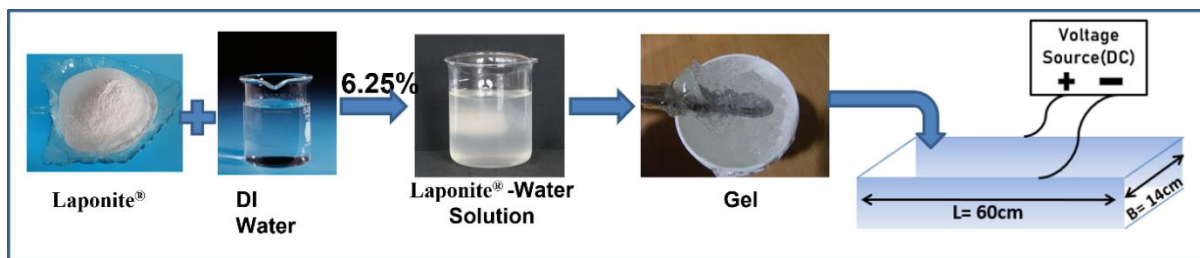


Figure. 2.1. Schematic diagram of preparation method of Laponite solution and the experimental setup.

To better comprehend the system and its topology, FESEM images of several areas of the film at each electrode as well as in the core portion is captured.

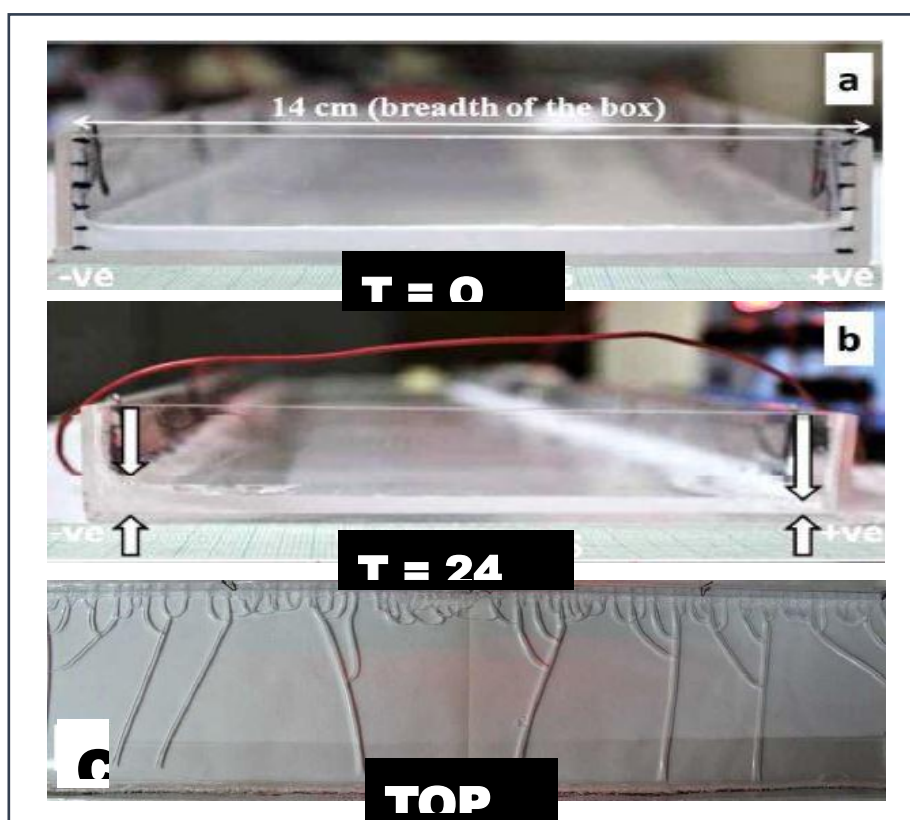


Figure 2.2. a) The side view of an aqueous Laponite[®] suspension that was placed into a rectangular setup before an electric field was applied. When no field is applied, the thickness

at the two electrodes is the same (~ 0.5 cm). The smallest division of the measurements on the box is 0.5 cm; b) the side view of the film after 24 hours of exposure to the electric field. The thickness at the negative electrode gets progressively thicker over time; c) the top view shows the crack pattern after 24 hours. At the positive end, which is wired into the positive side of the power supply (80V), closely spaced cracks develop, and as they move to the negative end, they merge.

2.4.Observations :

2.4.1. Experimental Findings :

It is observed that at the positive electrode, a significant number of cracks with little gaps first form. These cracks go ahead to the negative electrode, although few of them connect to adjacent cracks. As a result, after a distance, fewer, more widely spaced fractures are travelling in the direction towards negative electrode. A fraction of original crack number eventually reaches the opposite electrode as a result of this merging with neighbours, and thus the structure resembles a collection of trees with branches pointing in the direction of the positive electrode. The time evolution of the crack patterns created for $V = 80\text{V}$ is represented in Figures 2.3a, 2.3b, and 2.3c. The voltages V have significant impact on both the number of fractures at the beginning $N_{\text{cr}}(V)$, and merging of those fractures. On activation of the electric field, bubbles are seen to develop along the negative electrode's length. It should also be noted that water initially separates at the negative electrode before drying out over time. The layer of Laponite[®] gel has a homogeneous thickness after initial deposition, though at the contact of the gel with the vertical walls along both ends, capillary rise is visible. In contrast to the layer thickness close to positive electrode, the thickness at negative electrode increases with application of electric field over time. Figures 2.2a and 2.2b depict this. During the final drying stage, some fractures typically

form at the negative plate and link to the main cracks normally. These are solely the outcome of desiccation.



Figure 2.3. (a - c) illustrates how crack patterns developed over time with a voltage of 80 volts.

2.4.2. SEM-images of various parts :

Scanning electron microscopy (SEM) images for dried Laponite films have been acquired using the FESEM facility, configuration no. QUO-35357-0614 funded by FIST-2, DST Government of India, at the Physics Department, Jadavpur University. Figure 2.4 displays SEM pictures of the sample in three

different locations: (a) next to the positive electrode, (b) in the middle, and (c) close to the negative electrode. Focusing on the centre, Fig. 2.4b exhibits a smooth surface. On the

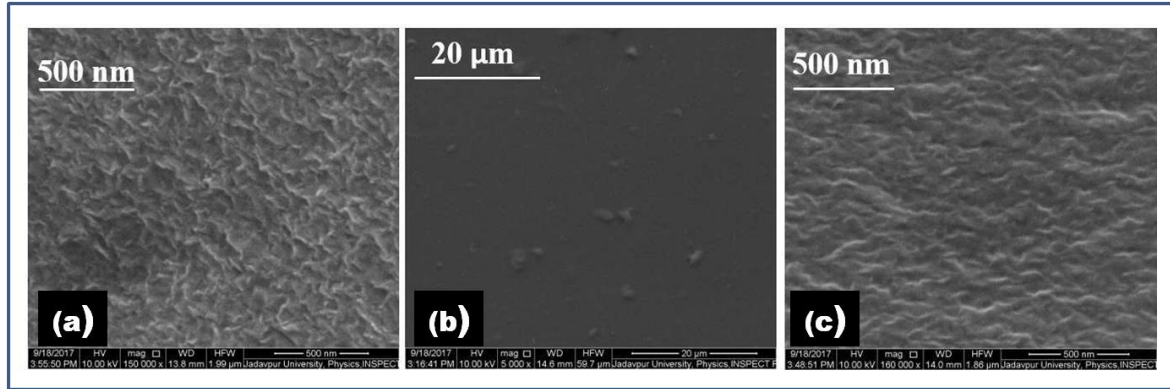


Figure 2.4. SEM pictures of the Laponite[®] layer taken at three different locations: a) close to the positive electrode; b) somewhere between two electrodes; and c) close to the negative electrode.

other hand, there is an uneven roughness in the areas close to both the electrodes. Although it looks to be quite rough, the surface close to the positive electrode (Fig. 2.4a) does not exhibit any anisotropy in a favoured direction. A visible texture is also present on the surface next to the negative electrode (Fig. 2.4c), but this texture is different from that in (Fig. 2.4a) and has a pattern anisotropy featuring striations in one direction.

2.4.3. An Additional Inspection :

An additional experiment is run to aid in the analysis. The negative end of sample layer thickens more than the positive end during drying in an electric field (Fig. 2.2b). Given that crack spacing is known to be significantly influenced by film thickness [5, 6], this may change the crack pattern. Thinner samples typically

have cracks that are more closely spaced, with the crack spacing usually following the layer thickness. Here, as shown in Fig. 2.5a, the bottom of the clay slurry-filled box is slanted from the beginning of the experiment at $\sim 5^\circ$ angle, causing the layer on one side to be significantly thicker than the layer on the other. The thick end electrode is now positively charged as a result of the voltage source being attached, as indicated (Fig. 2.5a).

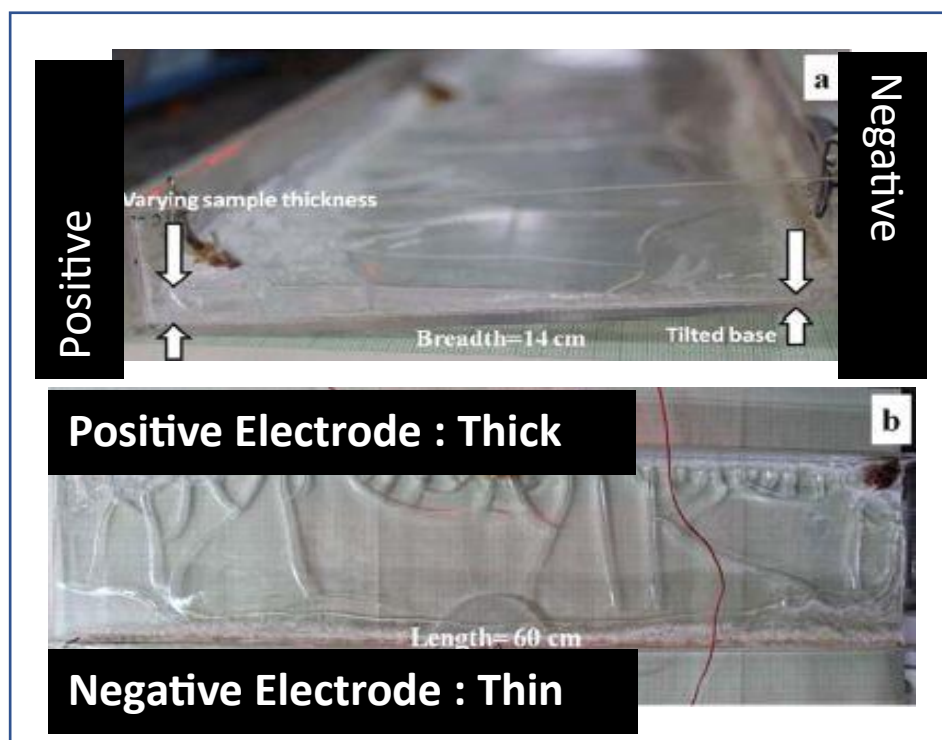


Figure 2.5. (a) The base of the clay-containing box is slanted, as indicated in the side view, and the thicker side is attached to the power supply's positive end (100V). (b) The top view pattern depicts the crack pattern that developed after couple of days. The positive end, which is thicker, has closely spaced cracks that progress to the negative end and combine.

2.5. Analysis and Results :

As was already noted, in order to exclude edge effects, the analysis of the crack patterns is conducted over the middle region of the rectangular system. To

do this, the rectangular box's ends are cropped by a length of $L_{\infty}/8$ (Fig. 2.5a, b). Desiccation cracks are not taken into account when analysing the impact of an electric field. Cracks that start to form at negative electrode much later after the electric field is turned on are the desiccation cracks. In the presence of an electric field, the patterns created by the cracks are entirely different from those formed in its absence. Pure desiccation cracks appear at random and do not follow any pattern. Furthermore, the time it takes in pure desiccation for the initial crack to form in the absence of an electric field is significantly longer.

The resulting fracture patterns for voltage(V) = 130V are shown in Fig. 2.6a.

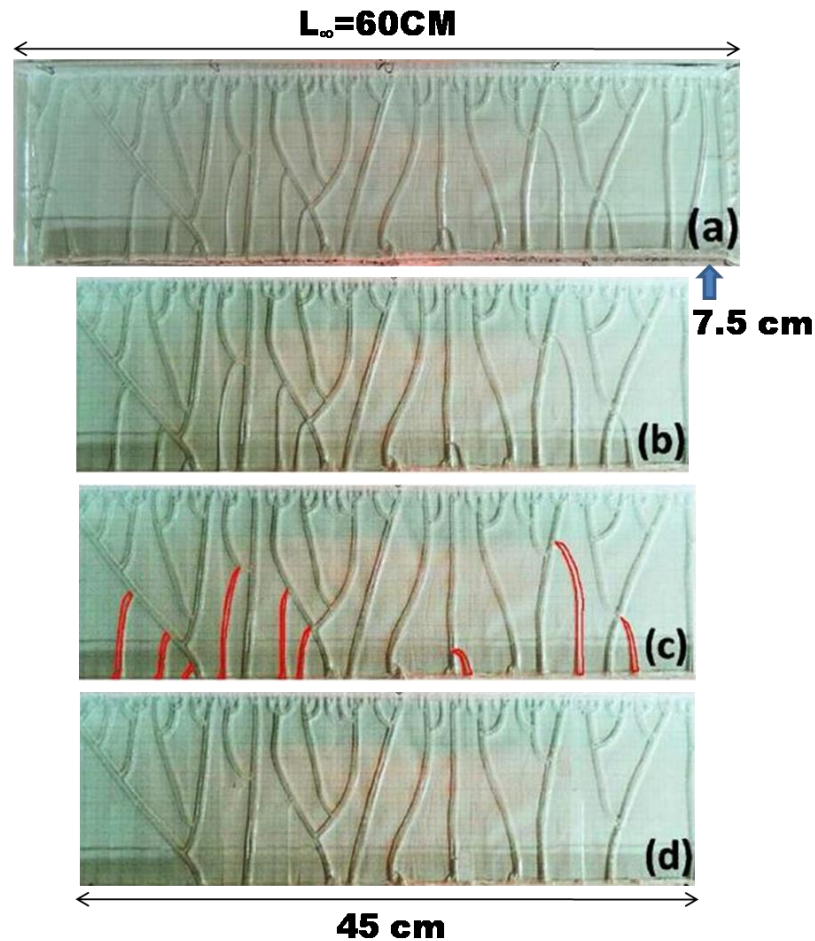


Figure 2.6. (a) Final crack pattern for voltage $V = 130V$ after 24 hours of application, (b) The length of each side is cut to determine the effect of parallel equipotential lines on the

sample; (c) In the final pattern, desiccation fractures are highlighted in red.; (d) To analyse cracks caused purely by the electric field, desiccation cracks are deleted.

In the original figures, the desiccation cracks that developed afterwards are highlighted in red (Fig. 2.6c). These desiccation fractures have been eliminated from the final tree patterns with the aid of ImageJ software. What is left is an examined typical pattern, as seen in fig. 2.6d. Figure 2.7 displays the final crack patterns for voltage ranges of 50V to 130V after removing a length $L_{\infty}/8$ from each edge and the desiccation cracks.

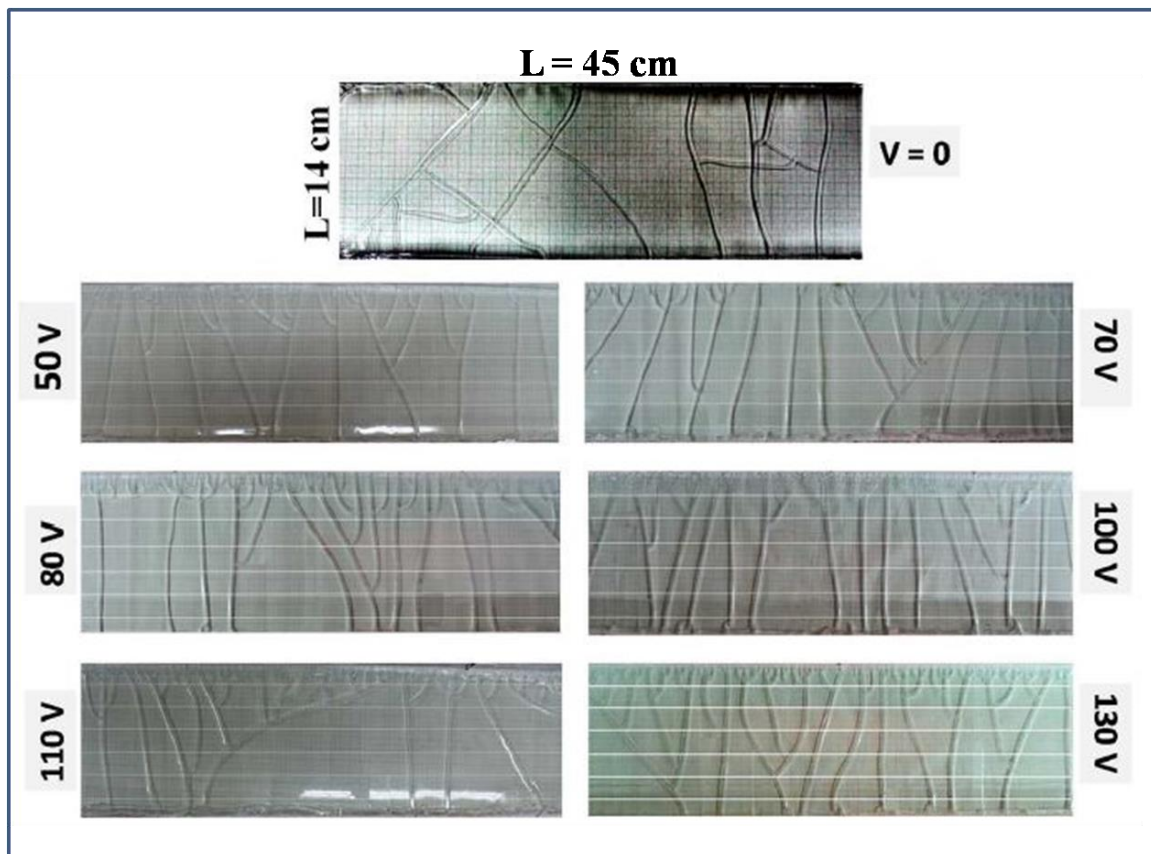


Figure 2.7. The picture at the top depicts desiccation cracks in the absence of any external field, in another way for $V = 0$. The remaining figures show the ultimate crack pattern for external fields 50V, 70V, 80V, 100V, 110V and 130V. The final patterns have been cleared of the desiccation cracks for study.

In order to crop the experimental patterns, approximately 7.5 cm of each end are removed. As one moves from the positive electrode to the negative electrode in the box (Fig. 2.6), the fracture density, or crack length/unit area, drops. The rectangular patterns are separated into seven lengthwise segments in fig. 2.7 in order to quantify this observation. For all the applied voltages, the crack length, $L_{cr}(S,V)$, and the number of cracks, $N_{cr}(S,V)$, are shown against the corresponding sections (Fig. 2.8a and Fig. 2.8b). The length and total number of cracks increase in all segments as V increases. It is clear that when you get further away from the positive electrode (d), the total crack length falls roughly exponentially. In fig. 2.8c, the total fracture length $L_{tot}(V)$ all through the system as a function of the applied voltage variations is depicted. Figure 2.8d shows the total number of cracks, $N_{tot}(V)$, that form at the positively charged electrode as a function of the applied voltage, V .

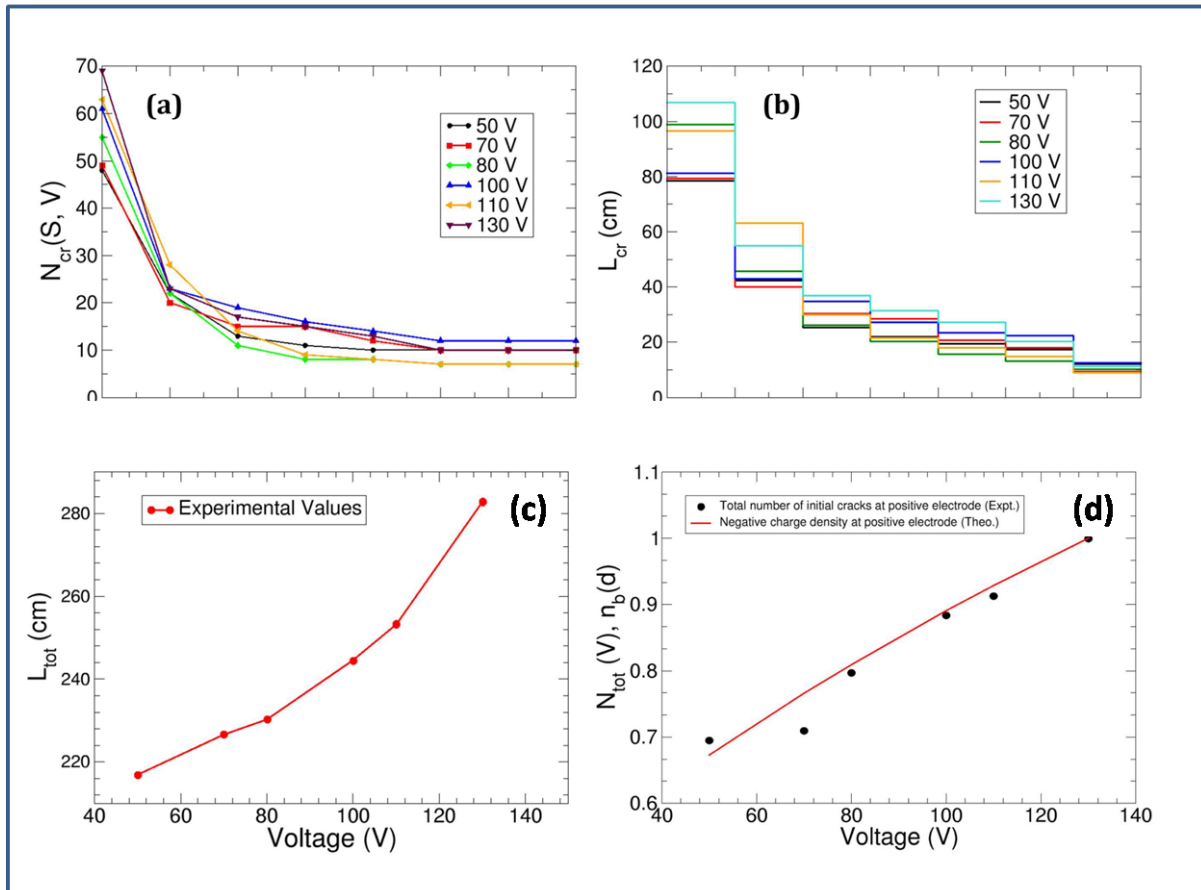


Figure 2.8. The variations of the total number of cracks $N_{cr}(S, V)$ and total crack length $L_{cr}(S, V)$ in each section (S) for various voltages (V) are shown in figures a) and b). For analysis, the total distance between the positive and negative electrodes has been split up into 7 sections (S). The length of each segment is 2 cm. c) The total crack length L_{tot} is plotted with the applied voltage (V); d) The total number of cracks $N_{tot}(V)$ that form at the positively charged electrode is plotted against the voltage V . When displayed against the experimental data, the red line reflects the negative charge density determined using theoretical considerations.

The additional experiment's findings (Figs. 2.5a and 2.5b) strongly demonstrate that the external electric field, rather than the changing sample thickness, is what causes this distinctive pattern. The similar pattern results from reversing the thickness gradient while maintaining the electric field's orientation.

2.6. Theory :

2.6.1. Origin of Tree-like crack pattern :

Laponite[®] platelets become negatively charged in an aqueous environment as the positive Na^+ ions dissolve and create a double layer with the clay particles which are negatively charged [21]. When the electric field is activated, the large Laponite[®] platelets have a very poor mobility and the clay slurry has gelled. Conversely, since the counter-ions are movable, they ought to move in the other direction, leaving the negatively charged, bare clay platelets closer to the positive electrode. Due of this mutual repulsion, the bare Laponite[®] platelets start to create cracks at positively charged plane.

The distribution of counterions and, subsequently, the charge density in the sample both are influenced by voltage., which rises toward the cathode. Near the

positive electrode, the sample's net charge density is negative, while the opposite is true farther away. The net charge density would naturally be 0 if there was no external field applied and the sample had an unlimited extent.

The energy provided by the electric field keeps the sample's non-uniform charge distribution. But the mutual repulsion between the clay platelet causes cracks to occur. Due to partial screening by the counter-ions, this repulsion decreases as d increases. As a result, the potential for crack formation is reduced. However, cracks that are moving away from the cathode typically continue. A dead end with high stress intensity would emerge from this. Therefore, merging nearby fractures would be the ideal method of decreasing the total crack length. As a result, many of the numerous primary fractures that originate from the positive electrode connect with one another to form a secondary set of cracks. Eventually, trees with higher-level branches will have evolved through merging repeatedly. The remaining cracks follow a more-or-less straight path right up to the cathode and they stop interacting and merging after a certain distance from the positive electrode, when they are too far away.

According to study [22], the energy needed to produce a fracture of length l is given by

$$E_T(l) = Glt \dots\dots(2a)$$

where t is the sample's thickness and G is the energy in J/m^2 needed to break the bonds in the material and form a new surface area $2lt$ that corresponds to the two walls of the crack.

In our experiment, the required energy is produced by the charge density $n(d)$ generated by the exposed Laponite® when applied to electric field. Since it is assumed that the sample layer thickness (t) is constant, the amount of total energy required is inversely related to the size(l) of the crack. This indicates that there is a growing correlation between the average co-ion density and the total length of cracks generated in each segment. By estimating the mobile

counter- ion density, which are rearranged by the applied field, it is possible to calculate the co-ion density as well, or the effective charge density which is the reason for cracking.

2.6.2. Role of Counter ion Charge density in crack formation :

The positive counter-ion density as a function of d from the positive electrode is symbolized by $n_+(d)$. The external field draws the positive counter-ions away from the positive electrode, where their density is at its lowest, towards the negative electrode, where it is at its highest. Though the inclination of the distribution against d curve is modified by thermal effect produced by the DC supply [36] and diffusion which balances out carrier concentrations in a device without applying any external force, such as those produced by generation and recombination.

The Laponite[®] layer in nematic gel phase is a slurry with a very high viscosity. As a result, along with the electric force and the thermal diffusion effect, the slurry's viscosity and other significant material parameters also have impacts. In addition, negative charges on the Laponite[®] discs, which may be thought of as immobile, tend to hold back the counter-ions as they are drawn away towards the negative electrode. The scenario is proposed to be represented by a straightforward empirical model. The displacement d from anode when there is a voltage of $+V$, is taken into consideration when calculating the quantity of positive counterions $n_+(d)$. L is defined to represent the distance between the two electrodes as measured by the extent of the Laponite[®] layer.

The gross potential at d is equal to the combined value of two factors.: (i) the external field contribution and (ii) the charged Laponite[®] layer contribution.

Considering a 1-dimensional portion along the rectangular system's length (L), $n_+(d, V)$ can be written as,

$$n_+(d, V) = n_0 \cdot \exp[A \cdot \psi_{\text{ext}}(d, V) - B \cdot \psi_{\text{Lap}}(\rho, d)] \dots\dots(2b)$$

Here, there are n_0 counter-ions altogether when there is no field. The external field is responsible for the term $A \cdot \psi_{\text{ext}}(d, V)$, whereas the Laponite® layer's symmetrical co-ion distribution is responsible for the term $B \cdot \psi_{\text{Lap}}(\rho, d)$.

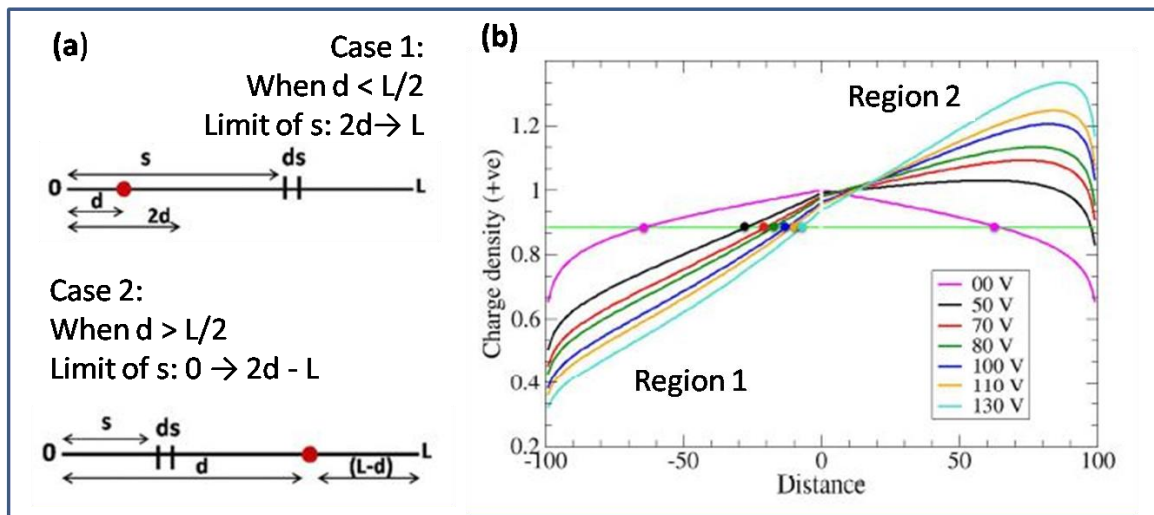


Figure 2.9. (a) An illustration that shows how to calculate the potential at a specific location on a sample where there is a charge. (b) Ion density vs the spacing between the positive and negative electrodes is displayed. 200 units are used to divide a distance of $L = 0.14$ m. The horizontal green line represents the charge density when the applied voltage $V = 0$ when the entire charge is assumed to be spread uniformly. The co-ion charge's influence is assumed to be present in the symmetrical magenta curve, which is for 0V. The estimated counter-ion charge density for applied voltages of 50V to 130V is represented by the asymmetric curves.

A semi-empirical technique is used since it is challenging to search for expressions and values because of the intricate mechanisms happening inside this system. Assuming an infinite system with no boundaries, A and B are considered as free parameters and changed to provide a realistic variation for $n_+(d)/n_0$, which is the percentage of the charge density at d compared to that in the absence of any

field. $\psi_{\text{ext}}(d, V)$ shows a linear relationship across the sample length between $d = 0$ to L .

This empirical relationship resembles the equation that describes the charge density of the electric double layer in terms of form [21].

$$n_+(d) = n_{+\infty} \exp\left(\frac{z_+ e \psi(d)}{k_B T}\right) \dots\dots(2c)$$

Where, $\psi(d)$ stands for the potential at d and $n_{+\infty}$ represents the charge density at zero potential. However, in contrast to those in equation the current experiment, the measurements are of a macroscopic scale.

To calculate the function $\psi_{\text{Lap}}(d)$, assume that the charge carried by the Laponite[®] layer of length L is constant over the sample and is considered to be ρ per unit length. Calculating the potential at a point P that is located in the sample at a distance d from the positive electrode requires taking into account a linear portion of the sample in between the opposite electrodes (Fig. 2.9a). Parallel straight lines to the larger dimension are considered to be equipotential because it is assumed that the sample is infinite lengthwise. The negative effect of the charge between distances 0 and d is cancelled by the charge on an equal portion from d to $2d$. Therefore, just this impact of the segment from $2d$ to L needs to be taken into account. The potential at d is then written as

$$\psi_{\text{Lap}}(d_{<}) \sim \int_{2d}^L \frac{\rho}{s-d} ds \dots\dots(2d)$$

Which gives

$$\psi_{\text{Lap}}(d_{<}) = b. \rho. \ln\left(\frac{L}{d} - 1\right) \dots\dots(2e)$$

In this case, b is equal to $1/(4\pi\epsilon_0)$. This formula is true for the sample's left half $0 < d < L/2$. A similar process can be used to integrate the right half, with integration limits of 0 to $(2d-L)$. Thus, for $(L/2) < d < L$, it gives,

$$\psi_{\text{Lap}}(d_{>}) = b \cdot \rho \cdot \ln \left(\frac{d}{L-d} \right) \dots\dots(2f)$$

The positive charge density is expressed as a function of the distance from the positive end, $d_{\text{pos}}(i)$, where i varies from -99 to -1 for the left half of the sample and from 1 to 99 for the right half, in order to simplify the computation. The sample's length L is divided into 200 equal parts. The external potential has a positive end and a negative end of $+\phi(V)$ and $-\phi(V)$, respectively. The complete charge density expressions can therefore be expressed as,

A) $-99 < d(i) < -1$ i.e., positive electrode \rightarrow centre of the sample

$$n_{+<}(i)/n_0 = \exp \left[\alpha \left(\phi(V) - \frac{2d(i)}{L} \right) - \beta \cdot \ln \left(\frac{L}{d(i)+L/2} - 1 \right) \right] \dots(2g)$$

Graphically shown in fig.2.8b (Region 1)

The square-bracketed first part is caused by the applied voltage $\phi(V)$, α accounts for the necessary constants. The influence of the co-ion charge is represented by the second part and β also contains the constant (ρ).

B) $1 < d(i) < 99$ i.e., centre of the sample \rightarrow negative electrode,

$$n_{+>}(i)/n_0 = \exp \left[\alpha \left(\phi(V) - \frac{2d(i)}{L} \right) - \beta \cdot \ln \left(\frac{d(i)+L/2}{L/2-d(i)} \right) \right] \dots\dots(2h)$$

as shown in fig. 2.8b (Region 2)

Equations (2g) and (2h) for $\phi(V)$ changing from 50V to 130V are used to compute the counter-ion charge density variation for the entire sample. The values of the best-fitting parameters are $\alpha = -0.005$ and $\beta = 0.08$. Fig. 4.9b displays the resulting plots.

Equation(2b) may now be used to determine $n_f(d) = n_+(d)/n_0$ over the sample width.

Two adjustable parameters, A and B, are made up of all free parameters and thermal effect variables. The part of the formula that becomes indeterminate at $d = L/2$ is omitted. The percentage of counter-ions that are still bound to the Laponite[®] discs is shown by the value of $n_f(d)$.

The percentage of negatively charged Laponite[®] discs that are left bare is $n_b(d) = (1 - n_f(d))$, which is the negative charge density. Since bare Laponite[®] discs oppose one another to generate cracks, the hypothesis states that $n_b(d)$ controls fracture formation at d .

When d rises, the possibility of developing new cracks drops. The cracks eventually converge with their neighbours to lower the total length of the cracks. Through the end of the sample, just the old cracks remain after the net charge reaches zero because co-ions and counter-ions' charges balance one another at that time. Because the cracks are so widely apart, merging will no longer result in a reduction of length of cracks due to their distance. This is put out as the origin of unique cracking pattern in rectangular geometry that resembles a forest or more accurately, a tree-like forest.

The study found that for external electric field $(V)=0$, the distribution of counter-ions is not uniform, but rather achieves a maximum in the middle part of the sample (i.e., at $d=0$). At $V=0$, the distribution is symmetrical as one would anticipate but it is not uniform. Counter-ions are pulled towards the sample's centre, with a maximum at $d=0$. The characteristic, though, results due to the

small sample size. Hence, the sample border is actually what is responsible for keeping the charged clay platelets confined.

As sample size grows, counter-ion distribution seems to be uniform, and the total charge density typically equals zero throughout the sample. Fig. 2.10a depicts how the size of the system affects the result. The distribution of the counter-ion charge, which is very non-uniform if the sample size is 200 (arbitrary units), but tends to become almost flat if it is 2000 (arbitrary units), with just a slight dip at the borders, as can be seen in the fig. 2.10a.

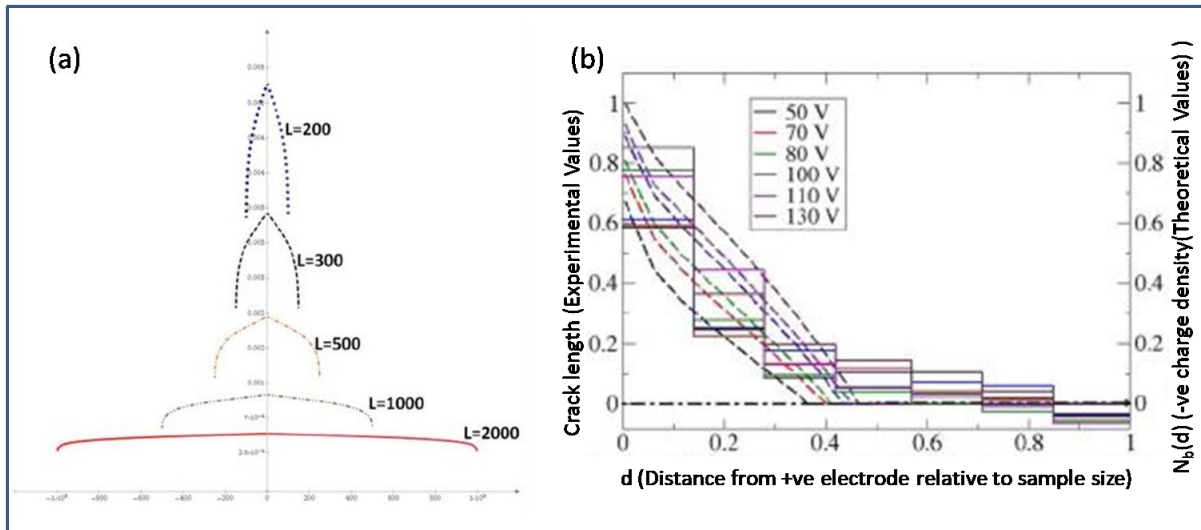


Figure 2.10. (a) The distribution of the counter-ion charge density per unit length for different sample sizes in the absence of an external electric field (L). As system size grows, the distribution flattens out and tends to become uniformly distributed for infinite systems. (b) The step graph displays the variation in crack length (experimental), segment by segment, for various voltages, whilst the broken lines display the variation in the theoretical density of the negative charge moving from the positive electrode to the negative electrode. Zero bare co-ion charge density is shown by the broken horizontal line with the arrow.

By integrating the region under this curve, one may get the overall charge of the counter ions. The value of the integral is 176.5 units. The total charge on the Laponite[®] discs, Q_{tot} , is equal to this total charge. Hence, the Laponite layer has a charge/length of 0.883 (in arbitrary units to facilitate analysis). A horizontal

line that depicts charge distribution that would be attained in an infinite sample with $V=0$ is shown in green in figure 2.10b. Using an external field of V ranging from 50V to 130V, the counter-ion charge distribution can be estimated using equation (2b), which shows a charge accumulation near the cathode and a charge reduction near the anode, keeping the total charge (Q_{tot}) equals to constant.

The positions where the co-ion and counter-ion charges balance out for each V are shown by the intersections of this series of curves with the green straight line in fig. 2.10b. The Laponite® discs have an uncompensated negative charge for $V > 0$ (at the left side of each of these intersection points), which causes the platelets to oppose one another and encourages the development of cracks. Each segment's susceptibility for fracture formation is influenced by its net negative charge. The charges on Laponite discs is balanced towards the right, preventing the possibility of new crack growth. Despite being in excess, counterions play no part in the formation of cracks. Thus, based on the study, for a given V , the first segment (left most), $S = 1$, has the highest crack density, and it gradually decreases and gets saturated at point of net zero charge. Thus, there is a connection in between external voltage V and the quantity of cracks formed at the positively charged electrode.

For each V , the number of cracks observed throughout the experiment at the positive electrode is noted (Fig. 2.8d), and the corresponding theoretical value of charge density is calculated. This is apparent that a fairly accurate reproduction of the type of variation with V has been made. The positive electrode is the furthest away from the compensation point for the greatest V , which is 130V, whereas the points for decreasing V gradually get closer. Theoretically, this indicates that for lower voltages, cracks will converge and join sooner (for smaller d). Existing fractures will continue to the cathode after the intersection places (Fig. 2.10b), continuing without further convergence. Examining the crack patterns in experiments (Fig. 2.7) reveal that in most studies, this is the situation.

The symmetric charge distribution curve (when $V=0$) intersects the horizontal green line twice (Fig. 2.9b). Therefore, small area with bare Laponite[®] particles are there close to each electrode, which encourages crack growth. According to experimental findings, without an external voltage, cracks indeed begin to form initially at both boundaries of the sample before the pattern finally appears arbitrary (upper most picture of fig. 2.7).

Graphs of $n_b(d)$, generated for different external voltages ranging $50V \rightarrow 130V$ for $d = 0 \rightarrow L$, are compared with the outcomes for total crack length recorded in the horizontal divisions along the lengths to make a quantitative comparison (Fig. 2.10b). In the lengthwise segments of the sample, the magnitude of the net charge on the Laponite particles obtained from fig. 2.9b for varied V (broken curves) is displayed superimposed on the calculated crack lengths (step-wise distribution). The estimated results accurately reflect the trend that was seen in the experiments.

The experimental finding of joining cracks, which results in a decrease of total crack length while increasing the number of segments, is thought to be caused by a drop in exposed co-ion charge away from the positive electrode increases. The arrowed, broken horizontal line is for exposed co-ion charge density of zero. There shouldn't be any more crack merging until the theoretically broken curves reach this line. The experimental data show some merging beyond this limit, albeit at a much slower rate than the swiftly descending steps to the left end of fig. 2.10b.

2.7. Discussion and Conclusion :

Experimentally, the cracking of rectangular Laponite[®] samples with length significantly more than breadth is investigated, where the area far from the short

edges is a component of area with infinity in length and a limited breadth. The positive electrode develops numerous cracks when exposed to an external electric field; the quantity depends on the external voltage, V . As they move closer to the negative electrode, the cracks gradually join with their neighbours to form a sequence of tree-like cracks. As is widely known [23], the Laponite® clay discharges positive counterions and changes its charge to a negative one when it is in an aqueous media.

The charged Laponite® particles try to repel the counter-ions as they are propelled towards the negative electrode by the external electric field. According to the present theory, this leads to an uneven distribution of charge (Fig. 2.9b). The density of negative charge on the Laponite® discs controls the propensity of cracking in the external field direction because the repulsion caused by negative charge is what causes crack growth. Given that the density of negative charge diminishes with distance from the positive electrode, no cracks started from the positive end can be sustained. and as a result, cracks merge together and shorten the length of the total crack.

The energy of the electric field, which preserves the sample's non-uniform charge distribution, can be used to drive the growth of cracks between clay platelets through mutual repulsion. Less energy is available for crack formation as the distance from the positive electrode increases because the counterions partially remove this repulsion. However, cracks that continue beyond the cathode typically don't end. A dead end with extreme stress intensity at the tip would arise from this. Therefore, merging nearby cracks would be the ideal method of minimising the total crack length. As a result, a significant portion of the numerous primary fractures that originate at the positive electrode join forces with their neighbours to form a secondary set of cracks. As the applied voltage increases the amount of required energy of the cracks to grow and go forth also

increases. Thus, naturally for higher voltages they join their adjacent cracks later than they would have join for lower voltages.

The sample is separated into numerous segments from the positive to the negative end to demonstrate the validity of this methodology. An average charge density is assumed for each segment, and this density can be associated to the total length of cracks formed in that segment, as shown in Fig. 2.10b. After the surplus charge is compensated, combining the current cracks, which are now widely spread apart, is not beneficial energetically. Thus, hereafter, Pre-existing cracks spread to the negative electrode.

The following hypothesis is supported by the SEM images. On a scale of 20m, the middle portion (segment S=4) seems smooth even when magnified (Fig. 2.4b) This suggests that the electric field has no impact in this situation and that the charge on Laponite® discs has already been entirely compensated, leaving no additional counter-ions. Indicators of interactions between charged species may be seen in the morphology at the positive end (Fig. 2.4a), which gives the structure uneven appearance. The pattern of the negative end (Fig. 2.4c) is also irregular, though significantly less compared to the positive one. The emerging water in this area, flows out of the negative end, which has a thicker sample, may be the reason of the directional striations seen there.

Although numerous articles have described the interactions between static and alternating electric fields and radial geometry [24-26], this is the first description and analysis of the intriguing anisotropic fracture patterns created in uniform static electric field. The thickness variation from the negative to the positive end that forms when the electric field is applied, has also been purposely reversed in a separate experiment. Even under these circumstances, the same fracture pattern is obtained, proving conclusively that the hierarchical pattern of tree like cracks formed is a product of the external electric field and not owing to

a variation in sample thickness. The possible explanation of sample thickening at negative electrode is as follows.

Clay like colloidal particles which dissociate in water form macro-ions with a negative surface charge and positively charged counter-ions. Counter-ions form a double layer on the surface of the clay platelet, screening the bare charge. Laponite forms a double layer in aqueous medium releasing Na^+ ions. The platelet size is about 25 nm. The net negative charge of a single Laponite disc is approximately 700e (Cummins, 2007). It is well known that (van Olphen, 1977) addition of a suitable salt (particularly those releasing multivalent cations) can lead to a strong accumulation of opposite charge on the surface, which actually reverses the net charge on the macro-ion. $\text{Al}(\text{OH})_3$ produces such an effect on clay (van Olphen, 1977). The counterintuitive accumulation of oppositely charged ions which is in excess of the negative surface charge is a result of strong ion-ion correlations which are neglected in the Debye-Huckel theory. Messina et al. (Messina et al., 2001) have proposed a theory which demonstrates this and shows that for large colloidal particles the minimum energy configuration has a double layer where the net opposite charge exceeds the charge on the colloid. In the presence of multivalent cations, in fact, overcharging is the rule rather than an exception (Messina et al., 2001). Another group (Diehl and Levin, 2006) shows that a minimum of 0.05 C/m^2 negative bare surface charge is likely to lead to overcharging by multivalent cations. For Laponite the bare surface charge density comes out as 0.3 to 0.5 C/m^2 , which is quite above the threshold value. We can conjecture that Al^{+3} ions enter the system from the anode and overcharge the Laponite discs exhibiting a negative electrophoretic effect. This conclusion fits in with our experimental results showing thickening at the negative electrode.

Recently, connected conducting networks for transparent electrodes have been created using templates created from crack patterns in colloids [27, 28]. The findings of this work, where a self-assembling pattern with a structure like tree is

formed, may be used to develop unique anisotropic electrical conductors for certain circuit needs.

A basic phenomenological model has been used to qualitatively explain and replicate the results. For a quantitative approach, a more exact self-consistent model is required in order to make further advancements possible. However, the strategy used here offers a good place to start.

2.8. List of References :

- [1] Nam, K.H., Park, I.H. and Ko, S.H., 2012. Patterning by controlled cracking. *Nature*, 485(7397), pp.221-224.
- [2] Van Olphen, H., 1977. An Introduction to Clay Colloid Chemistry.: John Wiley & Sons, New York. *An introduction to clay colloid chemistry. 2nd ed. John Wiley & Sons, New York.*
- [3] Ho, S. and Suo, Z., 1993. Tunneling cracks in constrained layers.
- [4] Mal, D., Sinha, S., Middya, T.R. and Tarafdar, S., 2007. Field induced radial crack patterns in drying laponite gel. *Physica A: Statistical Mechanics and its Applications*, 384(2), pp.182-186.
- [5] Mal, D., Sinha, S., Middya, T.R. and Tarafdar, S., 2008. Desiccation crack patterns in drying laponite gel formed in an electrostatic field. *Applied clay science*, 39(1-2), pp.106-111.
- [6] Khatun, T., Choudhury, M.D., Dutta, T. and Tarafdar, S., 2012. Electric-field-induced crack patterns: Experiments and simulation. *Physical Review E*, 86(1), p.016114.
- [7] Khatun, T., Dutta, T. and Tarafdar, S., 2013. Crack formation under an electric field in droplets of laponite gel: Memory effect and scaling relations. *Langmuir*, 29(50), pp.15535-15542.

-
- [8] Hazra, S., Dutta, T., Das, S. and Tarafdar, S., 2017. Memory of electric field in laponite and how it affects crack formation: modeling through generalized calculus. *Langmuir*, 33(34), pp.8468-8475.
- [9] Sircar, S., Tarafdar, S. and Dutta, T., 2018. Crack formation in desiccating Laponite® films under AC field: effect of varying frequency. *Applied Clay Science*, 156, pp.69-76.
- [10] Fraden, S., Hurd, A.J. and Meyer, R.B., 1989. Electric-field-induced association of colloidal particles. *Physical review letters*, 63(21), p.2373.
- [11] Janča, J., Checot, F., Gospodinova, N., Touzain, S. and Špírková, M., 2000. Transport phenomena and electrode reactions generated by an electric field in colloidal silica. *Journal of colloid and interface science*, 229(2), pp.423-430.
- [12] Schneider, G.A., 2007. Influence of electric field and mechanical stresses on the fracture of ferroelectrics. *Annu. Rev. Mater. Res.*, 37, pp.491-538.
- [13] Nakahara, A. and Matsuo, Y., 2006. Transition in the pattern of cracks resulting from memory effects in paste. *Physical Review E*, 74(4), p.045102.
- [14] Matsuo, Y. and Nakahara, A., 2012. Effect of interaction on the formation of memories in paste. *Journal of the Physical Society of Japan*, 81(2), p.024801.
- [15] Takeshi, O., 2008. Continuum theory of memory effect in crack patterns of drying pastes. *Physical Review E*, 77(6), p.061501.

-
- [16] Takeshi, O., 2009. Three-dimensional residual tension theory of Nakahara effect in pastes. *Journal of the Physical Society of Japan*, 78(10), pp.104801-104801.
- [17] Zhu, Z., Morgan, F.D., Marone, C.J. and Toksoz, M.N., 2001. *Experimental studies of electrical fields on a breaking rock sample*. Massachusetts Institute of Technology. Earth Resources Laboratory.
- [18] Suo, Z., 1993. Models for breakdown-resistant dielectric and ferroelectric ceramics. *Journal of the Mechanics and Physics of Solids*, 41(7), pp.1155-1176.
- [19] Cao, H. and Evans, A.G., 1994. Electric-field-induced fatigue crack growth in piezoelectrics. *Journal of the American Ceramic Society*, 77(7), pp.1783-1786.
- [20] Suzuki, M., Ogawa, K. and Shoji, T., 2006. Quantitative NDE of surface cracks in ceramic materials by means of a high-frequency electromagnetic wave. *Materials transactions*, 47(6), pp.1605-1610.
- [21] Masliyah, J.H. and Bhattacharjee, S., 2006. *Electrokinetic and colloid transport phenomena*. John Wiley & Sons.
- [22] Goehring, L., Nakahara, A., Dutta, T., Kitsunezaki, S. and Tarafdar, S., 2015. *Desiccation cracks and their patterns: Formation and Modelling in Science and Nature*. John Wiley & Sons.
- [23] Cummins, H.Z., 2007. Liquid, glass, gel: The phases of colloidal Laponite. *Journal of Non-Crystalline Solids*, 353(41-43), pp.3891-3905.

-
- [24] Khatun, T., Choudhury, M.D., Dutta, T. and Tarafdar, S., 2012. Electric-field-induced crack patterns: Experiments and simulation. *Physical Review E*, 86(1), p.016114.
- [25] Khatun, T., Dutta, T. and Tarafdar, S., 2013. Crack formation in Laponite gel under AC fields. *Applied clay science*, 86, pp.125-128.
- [26] Sircar, S., Tarafdar, S. and Dutta, T., 2018. Crack formation in desiccating Laponite® films under AC field: effect of varying frequency. *Applied Clay Science*, 156, pp.69-76.
- [27] Rao, K.D.M., Gupta, R. and Kulkarni, G.U., 2014. Fabrication of large area, high-performance, transparent conducting electrodes using a spontaneously formed crackle network as template. *Advanced Materials Interfaces*, 1(6), p.1400090.
- [28] Kumar, A. and Kulkarni, G.U., 2016. Evaluating conducting network based transparent electrodes from geometrical considerations. *Journal of Applied Physics*, 119(1), p.015102.
- [29] Giorgiutti-Dauphiné, F. and Pauchard, L., 2018. Drying drops: Drying drops containing solutes: From hydrodynamical to mechanical instabilities. *The European Physical Journal E*, 41, pp.1-15.
- [30] Zang, D., Tarafdar, S., Tarasevich, Y.Y., Choudhury, M.D. and Dutta, T., 2019. Evaporation of a Droplet: From physics to applications. *Physics Reports*, 804, pp.1-56.

[31] Goehring, L., Nakahara, A., Dutta, T., Kitsunezaki, S. and Tarafdar, S., 2015. *Desiccation cracks and their patterns: Formation and Modelling in Science and Nature*. John Wiley & Sons.

[32] Hull, D., 1999. *Fractography: observing, measuring and interpreting fracture surface topography*. Cambridge University Press.

[33] Lawn, B.R., 1983. Physics of fracture. *Journal of the American Ceramic Society*, 66(2), pp.83-91.

[34] Ritchie, R.O. and Liu, D., 2021. *Introduction to fracture mechanics*. Elsevier.

[35] Freund, L.B., 1998. *Dynamic fracture mechanics*. Cambridge university press.

[36] Zhang, J., Chi, M., Chen, Q., Sun, W. and Cao, J., 2020. Effect of temperature on space charge distribution in two layers of transformer oil and impregnated pressboard under DC voltage. *IEEE Access*, 8, pp.16647-16655.

3

Study of Tree-Like Crack Morphology : Existence of Fractal Laws

3.1. Introduction :

The morphologies of cracks created by nature are interesting and diverse. The kind of pattern that is created is a significant clue of the circumstances under which the fractures develop. The cracks typically create a network when they link to one another. These networks can be created either by the hierarchically arranged creation of successive fractures, where each new crack connects to the preceding ones to form a pattern, or by the simultaneous propagation of numerous cracks throughout the system's volume. The type of these crack networks is heavily influenced by the thickness of the drying layer. The process used to induce desiccation has a significant impact on the pattern as well. The section that follows provides a brief explanation of the many types of cracks, their patterns, growth, and origins.

3.2. Overview of previous related work :

Numerous fields, including engineering, physics, geology, and other disciplines, place a significant emphasis on the research of fracture formation and crack patterns [1–7]. Desiccation cracks on clays have recently received a lot of attention due to their potential for technological applications and the intriguing effects that external disturbances like mechanical, electrical, or magnetic fields have on them [3,8-10]. Cracks can be categorised based on their size, shape, direction, position, and severity. The most prevalent desiccation crack patterns, which create networks that are either totally or partially linked,

are found in naturally occurring muddy sediments. According to the angle at which the component cracks intersect, networks are divided into orthogonal (Figs.3.1(3a-3c)) and non-orthogonal (Fig.3.1(3e,3f)) networks. J. K. Kodikara [11] noticed such patterns. In dried-out mud pebble layers, joined non-orthogonal patterns are rather common [12]. Typically, orthogonal fractures are found in quickly desiccating mud, which is characterised by dispersed, partially or completely unjoined cracks without any obvious preferred orientation in the early phases of formation. Non-orthogonal cracks are occasionally seen when breaking mud in its initial phases. In some particular mud beds, radial (non-orthogonal) and concentric-radial (orthogonal) patterns are sometimes seen (Fig.3.1(3b & 3f)). While concentric radial cracks have only ever been spotted once in a deep, nearly circular depression that was partially filled with mud, radial cracks are especially created in thin, slowly drying, homogeneous mud layers that are visible in coastal wetlands and are occasionally seen in winter or spring.

Additionally, individual fractures have unique properties. They can be roughly categorised as straight (Fig. 3.1(2a)), curved (Fig. 3.1(2b)), or sinuous (Fig. 3.1(2c)) ones based on their general shapes. Straight cracks are those that have very little curvature, not necessarily those that are precisely straight in the geometric meaning of the word.

These are typically discovered in thick, somewhat homogenous mud layers. Contrarily, long, sharply curved or winding cracks are produced when thick, extensive layers of mud are swiftly dried; occasionally, a small number of straight cracks are also present. Desiccation cracks exhibit additional significant characteristics, such as vertical cracks that span the whole volume of the drying mud, in addition to such two-dimensional crack networks, which are primarily created by horizontal cracks on a desiccating layer. These lead to the development

of pillar-like structures. These pillars could then be divided into storeys by horizontal cracks.


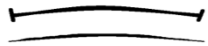






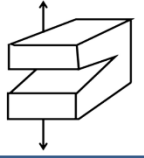
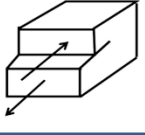
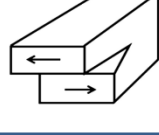
1.Size	A. Microcracks		B. Macrocracks	
2.Shape	A. Straight 		B. Curved 	C. Sinuous 
3.Direction	A. Orthogonal a)  b)  c) 			B. Non-Orthogonal e)  f) 
4.Position	A. Facial cracks		B. Sub-facial cracks	
5.Severity	A. Mode I 	B. Mode II 	C. Mode III 	

Figure 3.1. Crack classification based on morphologies.

Spiral cracks have a different intriguing fracture structure that was explored by N'eda et al. [13]. Aqueous solutions of various chemicals such as, $Ni_3(PO_4)_2$, $Fe_4[Fe(CN)_6]_3$, $Fe(OH)_3$, were used in experiments, and they were allowed to desiccate in circular petri-dishes. Prior to the formation of spiral cracks, which are regular in character, as well as other curved cracks in the shape of circles, ellipses, etc., the suspensions must first dry to create fragmented portions. The humidity gradient across the layer thickness causes the fragments

to have a propensity to curl up and separate from the substrate. Large tensile stresses are produced normal to the detached front in a radial direction as a result of the detachment. The portion that remains linked to the substrate continues to contract as a result of further desiccation, forcing the ring-shaped front to move inward. When the force at the front is greater than the material's strength, cracks are developed. The ring-shaped front was the preferred direction in which this crack developed. The expanding crack may have already gone through one full cycle while desiccation continued, and the ring front had to move even further inward as a result of this. The fracture was compelled to move even deeper inside. As a result, a crack in the shape of a spiral is created. Depending on the layer thickness and grain sizes of the drying samples, it is observed that the diameters of these formations ranged from 5 mm to several hundred microns. Analysis revealed that all of these spirals' shapes adhere to a logarithmic relationship,

$$r(\Theta) = r_0 e^{k\theta} \dots\dots(3a)$$

Where r and Θ are Polar coordinates. Θ can be any number between 0 and 2π . Both r_0 and k are constants, with k determining how tight the spiral is overall and r_0 being an apparent length scale that can be absorbed into the phase as $\Theta(0) = \ln(r_0)/k$ so that equation (3a) can be modified to

$$r(\Theta) = e^{(\theta-\theta_0)} \dots\dots(3b)$$

This demonstrates that the spirals are scale independent. Such logarithmic spirals are known as equiangular spirals, and they can be seen in plenty in nature.

Lazarus and Pauchard [14] also noticed spiral cracks in films of varying thickness made of aqueous dispersions of Latex particles that were allowed to dry at ambient temperature with controlled relative humidity on non-porous glass substrates. This study mainly looked at the impact of film thickness on the kinds of crack patterns that occurred. Above a specific film thickness, h_s , a broad

array of patterns was seen, but below a crucial thickness, h_C , the film was completely free of cracks. In this instance as well, a network of cracks first developed, delaminated from the substrate, and then spiral cracks started to appear. Delamination is a type of failure in which a material cracks into layers. Many materials can delaminate from the coated substrate, including laminate composites [34], concrete, and surface coatings like paints and films. In layered composites, the layers frequently separate because the adhesive between them fails first [35]. Delamination is caused by matrix cracking, bending cracks, and shear cracks. Delamination can have an impact on the composite laminate's compression strength and gradually lead to buckling failure in the composite. Additionally, it was observed that the film thickness, whose essential value is indicated by h_D , affects the delamination process. The diverse patterns of crack formation are classified into distinct regimes based on the final film thickness, h_f . In sequence of increasing film thickness, solitary junctions, sinuous fractures, partially linked networks, and fully connected networks occur when $h_f > h_C$. The network separates the film into polygonal cells. When $h_f > h_D$, delamination in these cells occurs. The thickness of the films was also observed to influence the delaminated front forms. Delamination only happens on the corners and edges of the broken cells at the thinnest limit ($h_f \leq 30\mu\text{m}$). The adherent regions of the cells assume increasingly complicated structures as the film thickens, eventually becoming circular at $h_f \geq 45\mu\text{m}$. The only time spiral and circular cracks emerge is when $h_f > h_s$. These cracks develop inside the cells' non-delaminated regions. The fractures begin at the edges of the adherent regions and spread to take the form of spiral or circular cracks. Conical spiral cracks were observed to emerge as a result of the spiral cracks' formation at an oblique angle to the substrate.

In drying colloidal solutions of (i) latex and (ii) nano latex particles placed on a glass plate, Pauchard et al. [15] also noted some intriguing morphologies. The suspensions were placed in a humidity-controlled atmosphere with a little

thickness gradient in the films, and they were then allowed to dry at room temperature. Evaporation led to the suspensions starting to gel. A front was formed at the intersection of the gelled and fluid regions of the film because the thinner parts of the film gel more quickly. The gel tries to shrink as it dries more, but is stopped from doing so by its attachment to the substrate. Due to the accumulation of stress, cracks start to appear. The latex samples generate a parallel array of periodic fractures that move in the same direction and at the same speed as the advancing gelation front. The film thickness and a pre-factor that depended on the physico-chemical characteristics of the material, gel adhesion, and desiccation conditions were determined to be the key determinants of the periodicity of the cracks.

However, for the nano-latex particles, cracks do not initially expand in a line with the drying or gelation front. The speed of the cracks is significantly higher than that of the drying front. The crack tips' velocity diminishes as they get closer to the drying front and come to a stop at the drying point. The cracks now turn back and move in the direction of the gel's driest areas. The speed quickens once more on the way back. A network of linear cracks that are closely spaced and contained within each arch develops within it. Multiple arches can occasionally emerge simultaneously at various frontal locations. The drying front is parallel to the straight line formed by the envelop of the arches. When the drying front reaches the thicker parts of the film, new cracks begin to emerge from the old ones and spread to create parallel arrays of cracks that are uniformly spaced. The variation in the ensuing crack morphologies is caused by very different nucleation processes. The presence of several nucleation sites in latex causes multiple cracks to form at once, allowing them to be ordered parallel to the gelation front. On the other side, the nucleation process takes longer and is more challenging for the nano-latex sample. Thus, the cracks begin some distance behind the drying front, but once they do, they move quickly and catch up to it.

This demonstrated that the energy requirements for the propagation and nucleation processes were different. The homogeneity of the samples was thought to be responsible for this behaviour. It was found that latex samples were less homogenous than nano-latex samples. This was deduced from the fact that the former's crack surfaces were more irregular than the latter's.

When an aqueous Laponite[®] paste is dried in a rectangular box and exposed to a DC electric field, a fascinating pattern of cracks forms that resembles a row of trees [16]. The number of trees and the number of branching levels on each tree depend on experimental factors like the size of the box and the strength of the applied electric field. The pattern is reflective of the structure of the Cayley tree or Bethe lattice. Examples of such fractal or scale-invariant hierarchical patterns include the development of river networks [17], blood vessel branching [18], and viscous fingering patterns [19], where a tree-like network is also observable.

3.3. Materials and Experimental Method :

In the current work, we study the development of crack patterns in samples with two different rectangular areas under the influence of an externally applied DC (direct current) electric field with voltage V varying from 50V to 130V and 75V to 195V, respectively, corresponding to a field of 357V/m to 928V/m. We use the synthetic clay Laponite[®] RD for this purpose. The smaller container is known as box 1, and the bigger container is known as box 2.

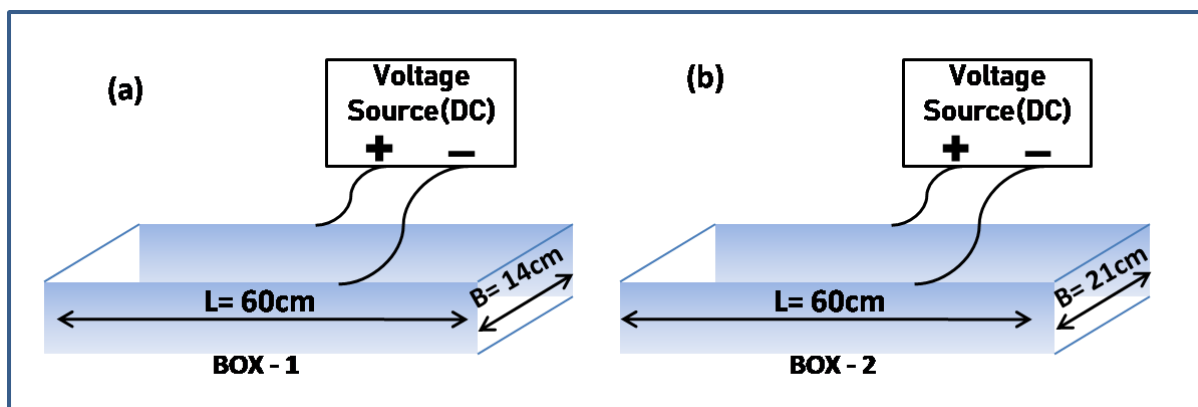


Figure 3.2. Diagram showing the two rectangular configuration used to apply the electric field.

In order to create the Laponite[®] gels, 25.30gm of Laponite[®] and 405ml of deionized water for box 1 and 38.06gm of Laponite[®] and 609ml of deionized water for box 2 are combined. The boxes are constructed from perspex sheet. Box 1 measures 60 cm by 14 cm, while Box 2 is 60 cm by 21 cm. Box 2 is the same length as box 1, but it is 1.5 times wider. An aluminium foil lining is applied to the opposing walls of the rectangular boxes along their length to create the electrode. The suspension initially seems turbid white, but after some time, it turns clear. The solution is then quickly put into the corresponding rectangular box after being thoroughly mixed with a magnetic stirrer for around 30–40 seconds. The films' heights or thicknesses are estimated to be 0.5 cm for both boxes. Before turning on the DC power supply after the solution has been deposited, we wait till it becomes transparent. To determine the ultimate crack pattern, the electric field is delivered to boxes 1 and 2 for 24 and 48 hours, respectively. The evolving crack morphology for varied voltages is watched over and photographed at periodic durations. The experimental set up is shown schematically in Figure 3.2.

3.4. Observation : Formation of Crack Patterns

Figure 3.3 depicts the crack pattern creation over time on the larger system (box 2) for $V = 165V$. The figure demonstrates how many closely spaced cracks initially form at the positive electrode. The fractures then continue in the direction of the negative electrode, merging with some of their neighbours before reaching the end. The early cracks finally make it to the negative electrode in lower number after going through this process of combining with neighbouring cracks multiple times. Because of this, the pattern resembles a row of trees branching in the direction of the positive electrode.



Figure 3.3.(a)–(c) depict the time evolution of the crack patterns created in box 2 at a voltage of 165V. The box is 60 cm in length and 21 cm in width, respectively.

The applied voltage V has a significant impact on both the initial number of cracks that form at the positive electrode and how quickly they merge.

Desiccation may cause some fractures to form from the negative electrode later on and meet the initial cracks naturally. Since these cracks are solely the effect of desiccation and not the electric field, we do not account for them in our analysis. Desiccation stress that builds up at the positive electrode as drying progresses is dissipated relatively early at the positive electrode by the creation of electric field driven cracks. So, realistically speaking, there are no desiccation cracks at the positive electrode.

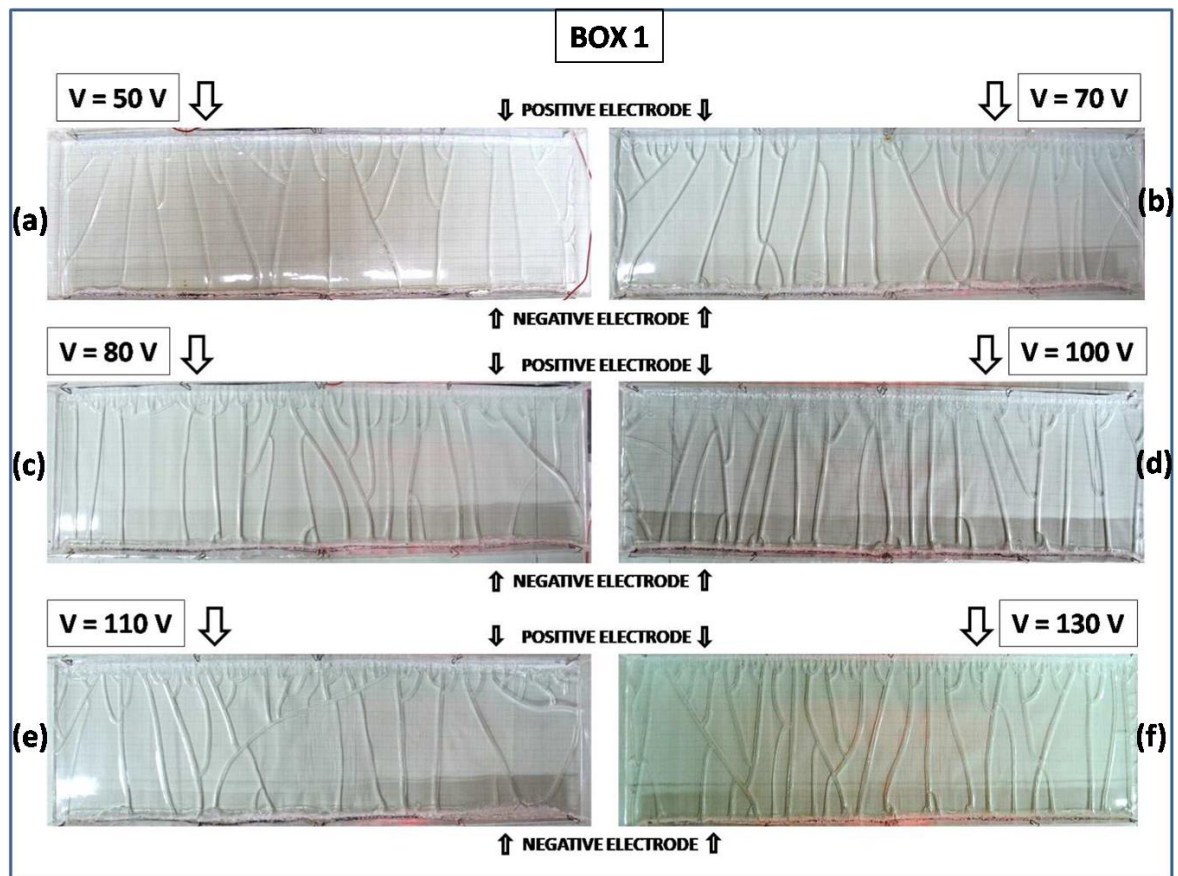


Figure 3.4. Final crack patterns for different voltages in box 1 are shown in (a-f). The box is 60 cm in length and 14 cm in width, respectively.

Bubbles start to develop along the negative electrode's length as soon as the electric field is turned on. Additionally, water initially pours out at the

negative electrode before drying over time. Although the Laponite[®] gel layer had a uniform thickness prior to applying the electric field, the negative electrode now has a thicker layer than the positive electrode. Where the gel reaches the vertical walls at both ends of the sample, there is a tiny elevation because of the capillary effect. Figures 3.4 and 3.5, which represent the ultimate fracture patterns for the two different box sizes and voltages, respectively.

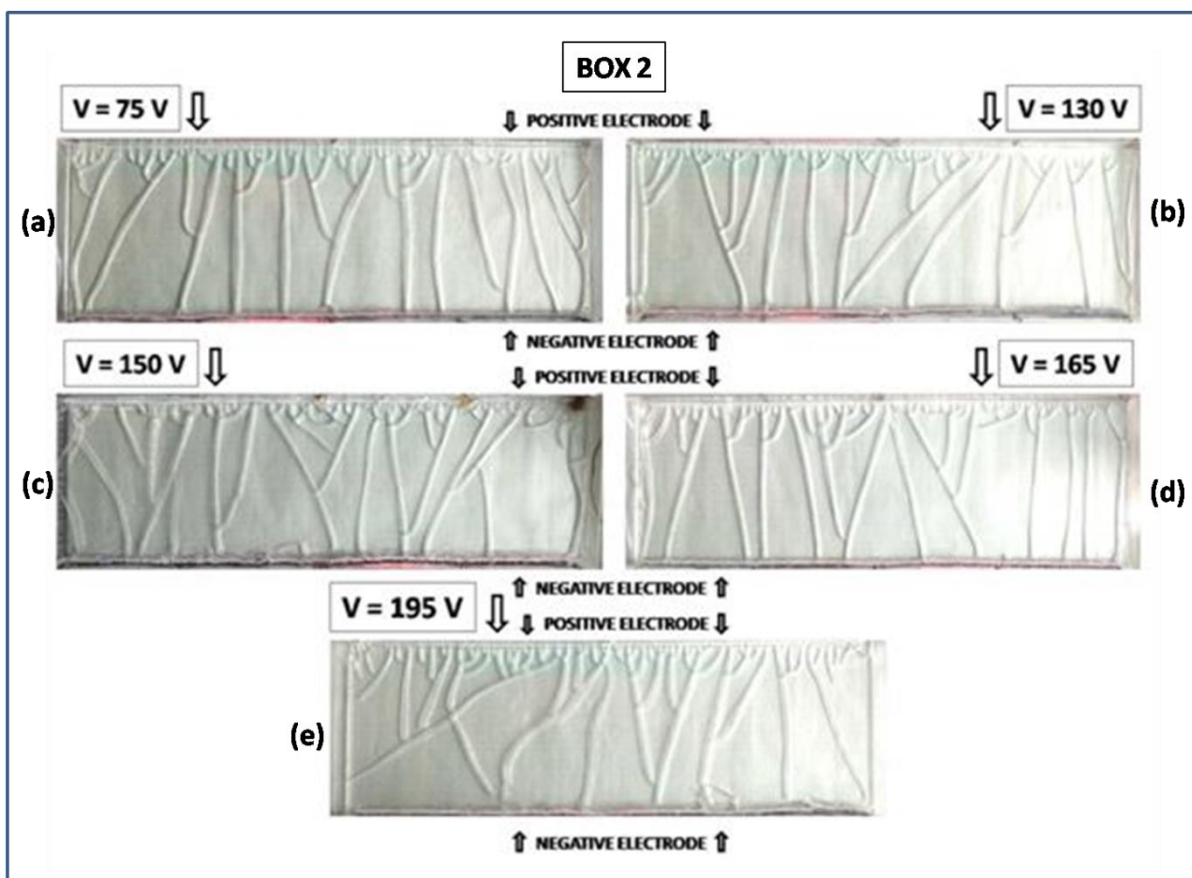


Figure 3.5. Final crack patterns for different voltages in box 2 are shown in (a-e). The box is 60 cm in length and 21 cm in width, respectively.

3.5. Analysis :

The size of a single Laponite[®] particle is substantially smaller than that of natural clay particles, measuring a diameter of 25nm and 1nm in height only. While its flat surface is negatively charged, the rim of the disc might have either a positive or negative charge [20]. With rising pH, the positive rim charge drops and is neutralised at pH ~11 [21]. The measured pH of the 6.25% aqueous Laponite[®] in our case is 9.8. This indicates that under the circumstances of our experiment, positive charge is present on the edge of Laponite[®] discs. The net negative charge of a single crystal of Laponite[®], which is roughly 700 times greater than the electron charge, is balanced by the interlayer cations Na⁺ [22]. Laponite[®] is almost mono-disperse and has a uniform distribution. The sample preparation procedure and environmental factors like temperature and humidity have a serious influence on the gel and as a result on the cracks behaviour also [22].

We make an effort to comprehend the reason behind the fracture patterns that resemble trees as an ongoing static electric field causes the clay layer to dry out. As the positive Na⁺ ions dissolve in water, Laponite[®] platelets become negatively charged and form a double layer [23]. When electric field is activated, the hefty Laponite[®] platelets having very poor mobility, start to form gel. However, the counterions are mobile and will presumably travel in the direction of the negatively charged electrode, leaving the exposed charged clay platelets closer to the positively charged electrode. Finally, at the anode, cracks emerge when the exposed Laponite[®] platelets repel one another.

The voltage affects the amount of counterions in the sample and thus the density of charge, which rises toward cathode. Near the positive electrode, the sample's net charge density is negative, while the opposite is true farther away. If the sample were infinitely large and no electric force was being applied, the overall charge density would definitely be zero. The energy provided by the electric field maintains the sample's non-uniform charge distribution. Due to this,

the clay platelets oppose one another and can form cracks in films as a result. Partial screening by the counterions, decreases this repulsion with increasing distance from the positive electrode, which reduces the energy accessible for crack formation. Moreover, cracks that are extending away from the cathode usually persist as otherwise, the tip would be a dead end with high levels of stress. Therefore, merging nearby fractures would be the optimal solution of minimizing the total crack length. As a result, a significant fraction of the numerous primary fractures that originate at positively charged electrode combine with their adjacent cracks and form a new set of cracks. After numerous repetitions of merging, a tree with higher-level branches may have generated. The surviving cracks continue in a more-or-less straight path right up to the cathode after a certain d because they are no longer close enough together to interact and merge.

3.5.1. Ped size distribution :

Each crack pattern in rectangular boxes, as shown in figs. 3.4 and 3.5, has the impression of a line of trees. Every tree resembles a section of the idealised Cayley tree depicted in figure 3.6. The Cayley tree is a perfect mathematical system that can act as a model for these kinds of actual physical circumstances. Let's have a brief idea about Cayley tree and Bethe Lattice.

A Cayley tree can be explained if each node in a branching network with coordination number Z is connected to Z other nodes without forming a loop (unless the node is on the edge). According to what is described in [24], the structure of the order q tree can be defined. Begin with the root vertex, 0; then, link q additional vertices with q additional edges. The $n = 1$ shell is created by the first group of q vertices. The solitary root vertex 0 in Fig. 3.6 represents the shell

with $n = 0$, which is not depicted. When it comes to the shells $n \geq 2$, every vertex of the shell $n = 1$ joins with $q-1$ new vertices. It should be noted that all other vertices have degree q , but the last shell's n vertices have degrees $q_n = 1$. The number of edges or branches connecting a vertex to another vertex determines its degree.

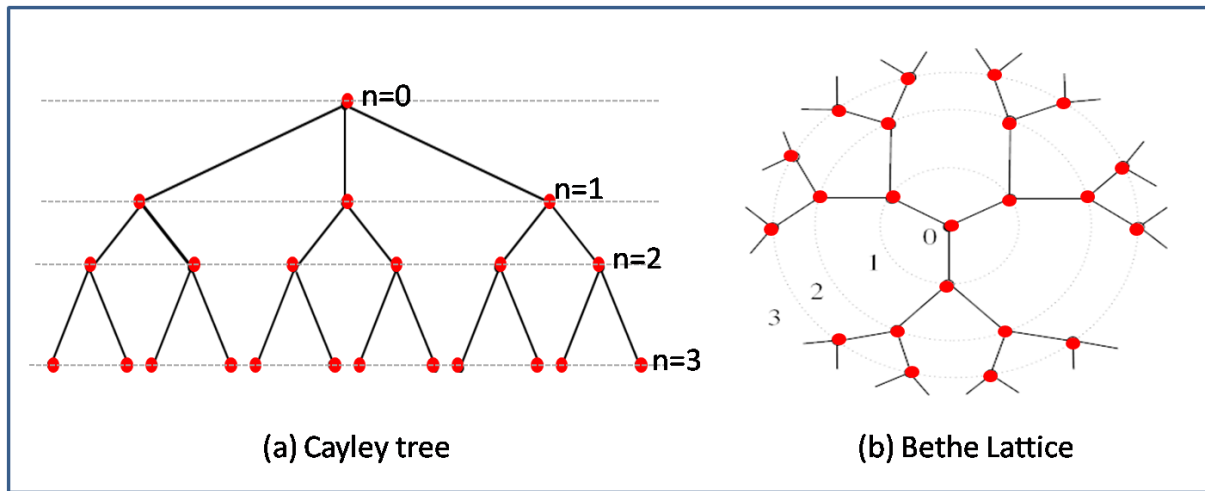


Figure 3.6. An illustration of a typical Cayley tree and Bethe Lattice with $q = 3$.

The "tree" parts move away from the centre toward its edge. There are six trees in the figure if the nodes numbered 2 are considered the starting point of a tree, i.e. the shell=1 in fig. 3.6. The trees in our rectangular crack system is also arranged in a straight line. The peds have polygonal shapes, with triangles making up the smallest. An ultrametric space is formed by the junction sites of the branches or nodes [25].

Infinite Cayley trees make up a Bethe lattice. There is no boundary and no centre vertex in the Bethe Lattice (BL) of degree q , in which every vertex has the same degree. Bethe lattice has same number of neighbors at each vertex. A huge but finite Cayley tree's interior section located far from the edge is initially taken

into consideration while creating a Bethe lattice. The Cayley tree boundary reaches infinity significantly more quickly than the edge of the inner section when the thermodynamic limit is defined by extending both the Cayley tree boundary and the interior section to infinity. Edge effects are thus formally removed for Bethe lattice calculations [26].

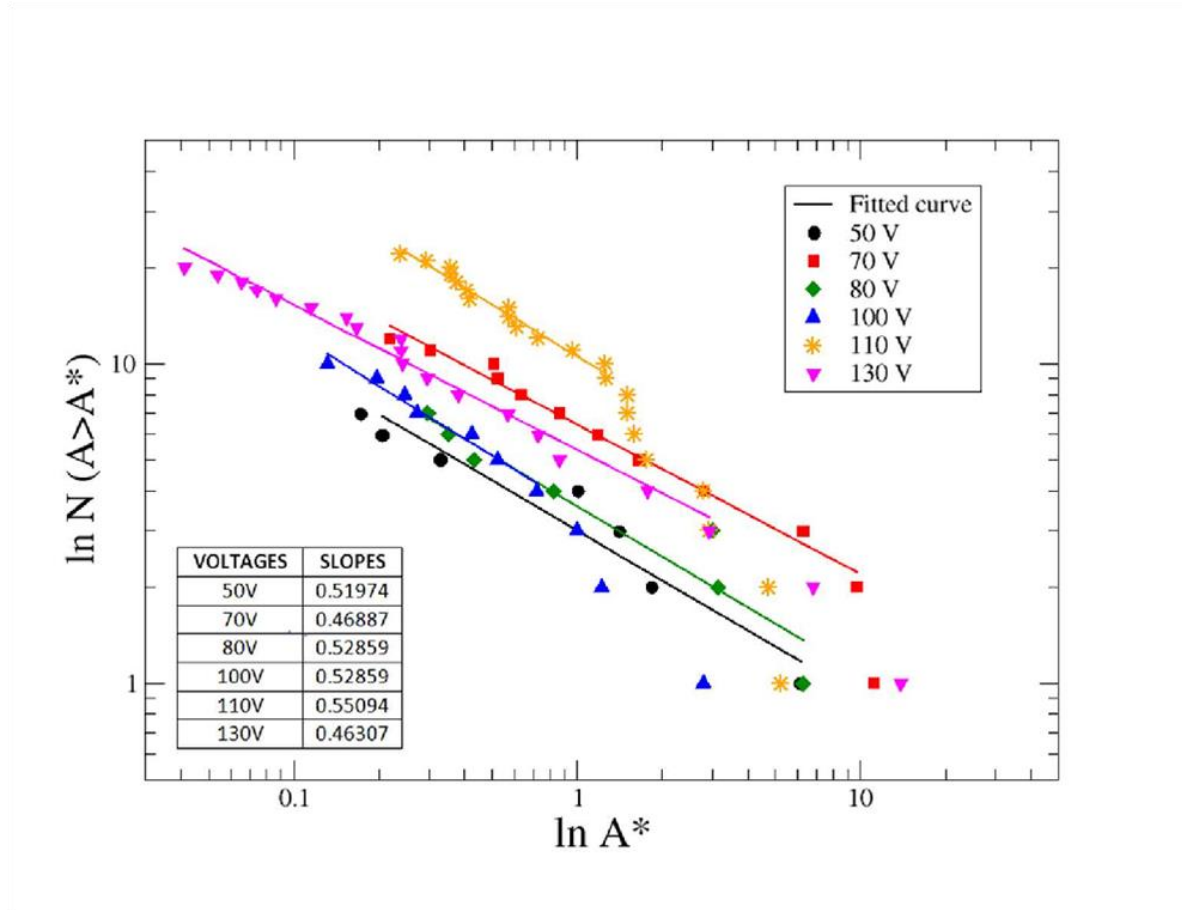


Figure 3.7. Findings for box 1. On a log-log plot, $N(A \geq A^*)$ is plotted against A^* for various voltages V , the cumulative size distribution, i.e. the number $N(A)$ with A exceeding A^* is recorded and plotted against A^* on a double logarithmic scale $N(A)$ stands for the number of peds of area A . Linear zones may be seen in the data for each V . According to the graph and the data box, the slopes of the linear regions are almost equal to 0.5 for all V .

The polygonal peds' areas are smaller close to the positive end and get bigger toward the negative. They are generally triangular closest to the positive end. We decide to analyse one or two of the biggest trees. All peds have their sizes

measured, and the cumulative size distribution—that is, the number $N(A)$ where A is greater than A^* (ped having minimum area) is noted and plotted against A^* on a double logarithmic scale. This is carried out for every voltage examined for the small and big systems in figs. 3.7 and 3.8, respectively.

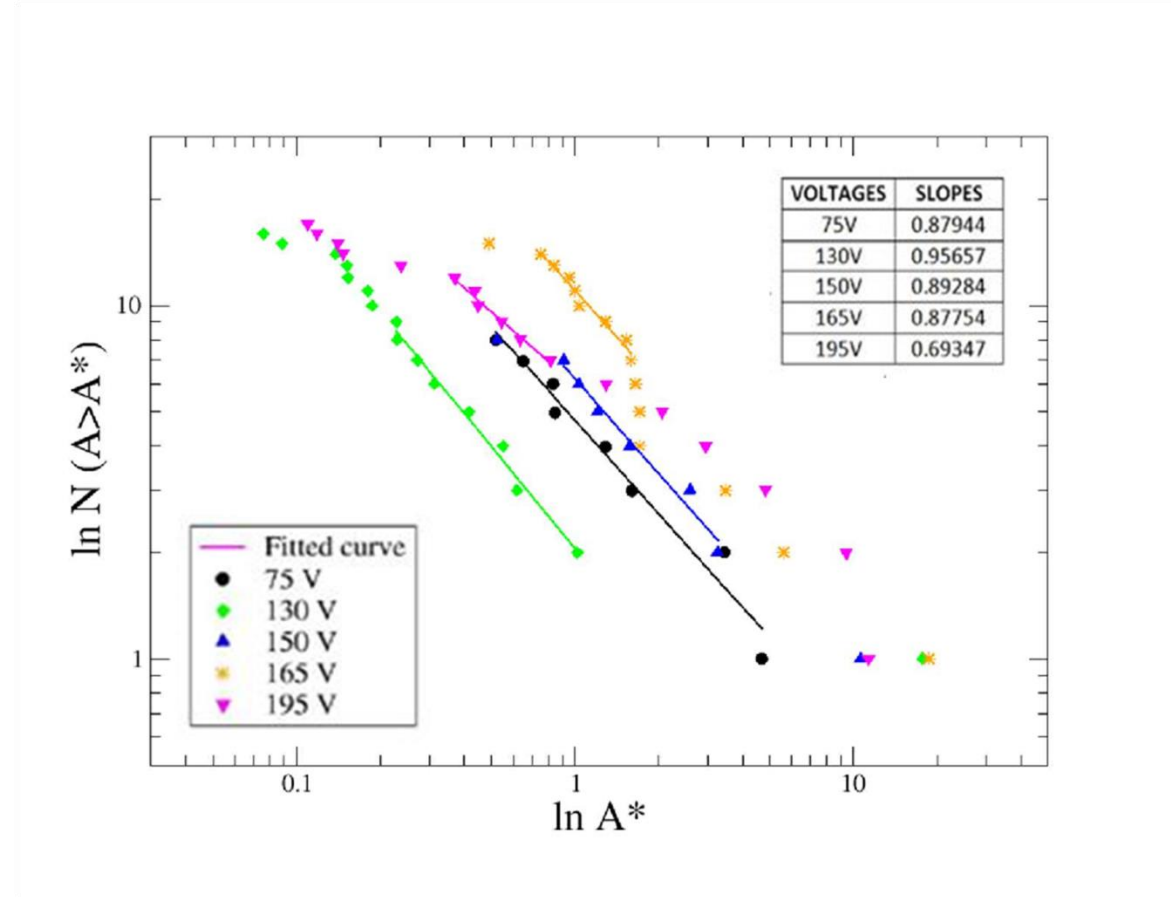


Figure 3.8. Findings for box 2. The number of peds in area A is denoted by $N(A)$, and $N(A \geq A^*)$ is displayed against A^* on a log-log plot for various voltages V . A linear zone may be seen in the data for each V . According to the graph and the data box, the slopes of the linear regions are almost equal to 0.9 for all V .

For small regions, the graphs display an initial linear zone that, as A expands, frequently deviates from linearity. For varying voltages, the slopes of the linear areas are very similar, falling between 0.47 and 0.55 for the smaller system (box 1) and 0.69 and 0.96 for the larger system (box 2). Figures 3.7 and 3.8 show the graphs and slopes. As a result, the pattern of fracture network

creation is consistent with the behaviour commonly found in other systems that adhere to the principle of minimum energy dissipation, such as river basins and viscous fingers [17,19]. It's also important to look into the system size dependence more thoroughly. To search for a system size-dependent exponent, a variety of system sizes must be explored. A power law can likely be used to approximate a more general law for short time intervals [27–31]. To completely comprehend the physics underlying these discoveries and the parallelism between this system and other scale invariant families exhibiting related characteristics, such as river basins and viscous fingers, more research is required.

It is impossible to combine the curves for various V into a single master curve since the data for boxes 1 and 2 in figures. 3.7 and 3.8 do not scale monotonically with voltage. The graph positions for varying V appear to oscillate somewhat, however the cause of this is not immediately clear. Another intriguing difference is that while the curves in the large box contain a few points on the low A side that may fit lines with slopes close to 0.5, the smaller box has a few data points towards higher A values that look to fall on a line of slope near to 0.9. Then, the result of both different sized systems would be in agreement.

3.5.2. Correlation of the dissipation of energy in the river network and the fracture system:

The scale-invariant or fractal hierarchical patterns are known to emerge in a variety of circumstances when the minimal energy dissipation principle is at play. A fundamental law of nature is the concept of minimum energy dissipation, which may be seen, for instance, in the development of river networks [17], blood vessel branching [18], and viscous fingering patterns [19], where a tree-like

network is also apparent. The tree pattern in many of these instances divides the background, or the underlying space, into segments of greatly variable sizes. These sections' areas have a unique property: on a double-logarithmic plot, the number $N(A \geq A^*)$ of sections with areas greater than A^* gives a straight line, indicating a power-law connection with an exponent.

$$N(A \geq A^*) \sim [A^*]^{-\beta} \dots\dots(3c),$$

Where β is typically around 0.5 in value [17]. This characteristic has been extensively researched in the area distribution of river basins in vast river networks. In the current study, we have compared the distribution of ped sizes to that of river basins using clay pieces bound by cracks (referred to as "peds" in geological terminology).

As we have noted, there are striking similarities between the distribution of ped sizes in the fracture network and the distribution of river-basin sizes. They share a similar backstory. There is a distinct externally imposed gradient in both cases which causes the average sizes of the cells (basin or ped) to vary from larger towards smaller as a boundary of the system is approached. For the river system, this is due to the average slope of the terrain towards the coast, and for the fracture network, due to the external electric field.

Sun et al. [17] demonstrate that this leads to a power-law relationship for mass discharge in the cumulative area of the river basins with river-basin area, with an exponent close to 0.45 for the river-basin system. A variety of empirical data are used to determine the exponent's value. The exponent for energy dissipation is close to 0.90.

An analogous principle works for the fracture system too. The stress accumulated near a crack of length 'a' is confined to an area of approximate extent $\sim a^2$ [18]. So, assuming the linear size of the peds at different location as the crack

length ' λ ', we can assume the ped area to be $\sim \lambda^2$ and apply an argument parallel to the river-basin case. The exponents in Fig. 3.7 for the smaller system have a fairly constant slope of 0.5 for all applied voltages. Although a set of power-law connections with approximately constant slopes is once again produced for the bigger system, the values of the slopes are somewhat higher (see Fig. 3.8). It should be noticed that although our larger system is wider, it is not longer. Our study is predicated on the supposition that the length is sufficiently long, allowing us to ignore the $L/4$ part of the length at each end and presuming the absence of end effects. The field strength depends on the system width. The applied voltage/m is taken into account when comparing the findings to ensure that the field intensities in boxes 1 and 2 are equivalent. However, since the sample's fundamental properties, such as the size of its Laponite[®] aggregates, are unaffected, the energy dissipation exponent may naturally rely on the size of the system. This could account for the discrepancy in the exponents measured for systems of different sizes. In other words, the gradient of the power-law might be sample size dependent.

3.6. Discussion and Conclusion:

In the current study, we demonstrate crack patterns that developed in aqueous Laponite[®] gel when exposed to a constant static electric field in a rectangular box. The crack pattern reveals an extremely intriguing structure that resembles a tree and extends from the positive to the negative electrode. However, the levels of branching have been seen to have dependence on the size of the boxes, precisely on the exposed area of the applied electric field. At the positive electrode, a significant number of cracks first develop and gradually merge with one another to generate fractal formations that resemble trees. These structures are similar to the Cayley tree or the Bethe lattice. The "trees" separate the system

into peds of varied sizes, with a large number of smaller ones on the positively charged end, progressively getting bigger, and getting fewer in number, towards the negatively charged end. A power-law relationship can be found by plotting the cumulative distribution of the number of peds surpassing a particular area's size against that area. This suggests that the pattern is fractal and scale-invariant. The exponent of the power-law has a value that is essentially constant for a given system size for various applied voltages.

To conclude, the results of our research on the development of branched cracks in Laponite[®] pastes dried in a DC electric field are intriguing and resemble the distributions of river basins and viscous fingers in a Hele-Shaw cell [32]. This circumstance offers another illustration of how uniform energy input leads to power-law spatial distribution of energy storage and fractal energy dissipation in an extended dissipative system [33]. Here, energy is introduced as electrical energy that is stored as elastic strain in the system and released as fracture, or cracks of different sizes.

In our previous work, we have reported desiccation crack formation on a layer of aqueous Laponite[®] gel, exposed to a uniform static electric field varying from 357 to 928 V m⁻¹. The cracks formed exhibit an interesting tree-like pattern. A large number of cracks (~70) appear initially at the positive end of the sample. Several neighbouring cracks merge with each other, while proceeding towards the negative end leading to a smaller number of cracks. This process is repeated a few times before the hierarchical pattern thus formed reaches the negative end of the sample. The number of cracks is finally reduced to ~10. The initial number of cracks increases with increasing field strength. The disc-like Laponite[®] clay particles behave as negatively charged in an aqueous medium, because of the diffusion of positive counterions into the solvent, which form a double layer. The external field causes gradual build-up of density of positive counterions towards the negative electrode. The bare Laponite[®] discs which are negatively charged

repel each other to create the cracks at the positive end. We developed a simple model to calculate the charge distribution of counterions along the sample. We offered an explanation for the structure of the anisotropic tree-like crack patterns observed on the basis of this model. The crack pattern shows a very interesting tree-like geometry extending from the positive to the negative electrode. These structures are reminiscent of the Bethe lattice or Cayley tree. The “trees” divide the system into peds of varying size, with numerous smaller ones on the positively charged end, gradually increasing in size, and decreasing in number towards the negative end. In this chapter we have shown, If the cumulative distribution of the number of peds exceeding a certain area in size, is plotted against that area, a power-law relation is obtained. This implies a scale-invariant fractal character of the pattern. For a given system size, the exponent of the power-law has a nearly constant value for different applied voltages. We presented an experimental study demonstrating this behaviour and discuss how it compares with similar distributions of river-basin areas and viscous fingers in a Hele-Shaw cell.

3.7. List of References :

- [1] Giorgiutti-Dauphiné, F. and Pauchard, L., 2018. Drying drops. *The European Physical Journal E*, 41(3), pp.1-15.
- [2] Zang, D., Tarafdar, S., Tarasevich, Y.Y., Choudhury, M.D. and Dutta, T., 2019. Evaporation of a Droplet: From physics to applications. *Physics Reports*, 804, pp.1-56.
- [3] Goehring, L., Nakahara, A., Dutta, T., Kitsunozaki, S. and Tarafdar, S., 2015. *Desiccation cracks and their patterns: Formation and Modelling in Science and Nature*. John Wiley & Sons.
- [4] Hull, D., 1999. *Fractography: observing, measuring and interpreting fracture surface topography*. Cambridge University Press.
- [5] Lawn, B.R., 1993. Fracture of brittle solids. *Cambridge solid state science series*.
- [6] Anderson, T.L., 2017. *Fracture mechanics: fundamentals and applications*. CRC press.

[7] Freund, L.B., 1990. Dynamic fracture mechanics cambridge university press. *New York*.

[8] Nam, K.H., Park, I.H. and Ko, S.H., 2012. Patterning by controlled cracking. *Nature*, 485(7397), pp.221-224.

[9] Pauchard, L., Elias, F., Boltenhagen, P., Cebers, A. and Bacri, J.C., 2008. When a crack is oriented by a magnetic field. *Physical Review E*, 77(2), p.021402.

[10] Khatun, T., Choudhury, M.D., Dutta, T. and Tarafdar, S., 2012. Electric-field-induced crack patterns: Experiments and simulation. *Physical Review E*, 86(1), p.016114.

[11] Kodikara, J.K., Barbour, S.L. and Fredlund, D.G., 2020. Desiccation cracking of soil layers. In *Unsaturated soils for Asia* (pp. 693-698). CRC Press.

[12] Allen, J.R.L., 1987. Desiccation of mud in the temperate intertidal zone: studies from the Severn Estuary and eastern England. *Philosophical Transactions of the Royal Society of London. B, Biological Sciences*, 315(1171), pp.127-156.

[13] Neda, Z., Jozsa, L. and Ravasz, M., 2002. Spiral cracks in drying precipitates. *Physical review letters*, 88(9), p.095502.

-
- [14] Lazarus, V. and Pauchard, L., 2011. From craquelures to spiral crack patterns: influence of layer thickness on the crack patterns induced by desiccation. *Soft Matter*, 7(6), pp.2552-2559.
- [15] Pauchard, L., Adda-Bedia, M., Allain, C. and Couder, Y., 2003. Morphologies resulting from the directional propagation of fractures. *Physical Review E*, 67(2), p.027103.
- [16] Ghosh, A., Sircar, S., Khatun, T., Dutta, T. and Tarafdar, S., 2018. Tree-like crack patterns in clay dried in a uniform DC electric field. *Materials Research Express*, 6(2), p.026305.
- [17] Sun, T., Meakin, P. and Jøssang, T., 1994. Minimum energy dissipation model for river basin geometry. *Physical Review E*, 49(6), p.4865.
- [18] Murray, C.D., 1926. The physiological principle of minimum work: I. The vascular system and the cost of blood volume. *Proceedings of the National Academy of Sciences*, 12(3), pp.207-214..
- [19] Roy, S. and Tarafdar, S., 1996. Patterns in the variable Hele-Shaw cell for different viscosity ratios: Similarity to river network geometry. *Physical Review E*, 54(6), p.6495.
- [20] Van Olphen, H., 1977. An Introduction to Clay Colloid Chemistry.: John Wiley & Sons, New York. *An introduction to clay colloid chemistry. 2nd ed. John Wiley & Sons, New York.*

-
- [21] Angelini, R., Zulian, L., Fluerasu, A., Madsen, A., Ruocco, G. and Ruzicka, B., 2013. Dichotomic aging behaviour in a colloidal glass. *Soft Matter*, 9(46), pp.10955-10959.
- [22] Cummins, H.Z., 2007. Liquid, glass, gel: The phases of colloidal Laponite. *Journal of Non-Crystalline Solids*, 353(41-43), pp.3891-3905.
- [23] Masliyah, J.H. and Bhattacharjee, S., 2006. *Electrokinetic and colloid transport phenomena*. John Wiley & Sons.
- [24] Ostilli, M., 2012. Cayley Trees and Bethe Lattices: A concise analysis for mathematicians and physicists. *Physica A: Statistical Mechanics and its Applications*, 391(12), pp.3417-3423.
- [25] Janahmadov, A.K. and Javadov, M.Y., 2016. *Synergetics and fractals in tribology*. Switzerland: Springer International Publishing.
- [26] Brookings, T., Carlson, J.M. and Doyle, J., 2005. Three mechanisms for power laws on the Cayley tree. *Physical Review E*, 72(5), p.056120.
- [27] Corral, Á. and González, Á., 2019. Power law size distributions in geoscience revisited. *Earth and Space Science*, 6(5), pp.673-697.
- [28] Guerriero, V., 2012. Power law distribution: Method of multi-scale inferential statistics. *Journal of Modern Mathematics Frontier*, 1(1), pp.21-28.

[29] Van Der Hofstad, R., 2016. *Random graphs and complex networks* (Vol. 43). Cambridge university press.

[30] Stegehuis, C., van der Hofstad, R., Janssen, A.J.E.M. and van Leeuwaarden, J.S., 2017. Clustering spectrum of scale-free networks. *Physical Review E*, 96(4), p.042309.

[31] Boguna, M., Krioukov, D. and Claffy, K.C., 2009. Navigability of complex networks. *Nature Physics*, 5(1), pp.74-80.

[32] Choudhury, M.D., Chandra, S., Nag, S., Das, S. and Tarafdar, S., 2011, September. Spreading of Non-Newtonian and Newtonian Fluids on a Solid Substrate under Pressure. *Journal of Physics: Conference Series* (Vol. 319, No. 1, p. 012006). IOP Publishing.

[33] Mandelbrot, B.B., 1974. Intermittent turbulence in self-similar cascades: divergence of high moments and dimension of the carrier. *Journal of fluid Mechanics*, 62(2), pp.331-358.

4

Experimental Findings of Crack -Prevention Strategy Using Clay-clay Composites

4.1. Introduction :

An important area of material science is the study of crack formation and possible prevention or remedial measures. Cracks are generally an issue. Colloidal paints or coatings frequently dry with a tendency to crack and the production of cracks in these circumstances is unacceptable in industrial applications. In addition to their primary function as a tool for experimentation, clay mixtures are also useful in architecture, pottery, sculpture, cosmetics, and other fields. The prevention of cracks is crucial in these applications also. Thus, it is important to understand the causes of fracture in such materials, which was one of the main driving factors behind the study of cracking in clayey substances. In this chapter, experimental findings are presented that illustrate how a proper combination of the montmorillonite clays, Laponite® and bentonite, can nearly totally prevent crack formation in a film. Additionally, the impact of different film thicknesses on crack prevention has been studied.

4.2. Overview of previous related work :

Cracks are undesirable in most cases like in industrial fields, in pottery or in buildings. Being an inherent property of materials, the cracks are difficult to avoid completely, though they can be controlled or minimized. In reality, it's exceedingly rare to discover systems that are completely devoid of cracks. In building structures for example, a fracture will affect the aesthetics of the structure, ruin the wall's structural integrity, affect shape protection, and lessen the concrete's durability. One of the main aims of study in this fields is to choose

the right solutions to address the concrete cracking issue which requires a thorough understanding of the origins and effects of cracking [1,2].

Colloidal paints and varnishes commonly crack as they dry. They are used in industrial applications as a coating on papers for ink-jet printing and for modern high-performance ceramics, such as turbine blades in jet engines. So, the generation of cracks in these conditions is unsatisfactory. Desiccation cracks are also a significant obstacle to the development of photonic devices [3,4]. It affects the size of the devices.

Pottery is a delicate material that is prone to cracking by nature. The main factor contributing to cracking is uneven drying, which results in certain portions of the pottery shrinking more than others. The key to avoiding these issues is setting up the drying environment systematically and making the required precautions to ensure that the total piece dries at a uniform rate. Several works are concerned with ways to prevent cracks [5-7].

This chapter presents a case study of experimental evidence that a suitable combination of the montmorillonite clays Laponite® and bentonite can almost suppress crack formation in a film. Additionally, the impact of different film thicknesses on crack prevention has been studied.

Clay is a porous material whose mechanical and hydraulic property can be changed by cracks. These have numerous applications in geotechnical engineering and may result in harm to structures built on the ground [8, 9]. Recent developments in material technology have encouraged the creation of numerous preparation methods and novel composite applications, such as polymer-nano clay composites [10], which have solved the problem of desiccation fractures. Due to their exceptional qualities, including improved density, strength, relatively large surface areas, high elastic modulus, flame retardancy, and thermomechanical/optoelectronic/magnetic capabilities [11,12], these

composites show promise as advanced materials. The morphology of the clay phase in the polymer governs the characteristics of clay-polymer composites [13-15]. Long chain polymer molecules improve the bonding between clay particles and are in charge of efficiently transferring stress to the clay layers.

Clay mixtures, such as lateritic soil and coastal clay, are inherently soft due to their high water concentration and the abundance of swelling clay minerals like montmorillonite and illite. When compacted and applied as landfill liners, these clay composites' mechanical qualities are essential because they keep toxic and other waste items separate from their surroundings and prohibit them from migrating into ground water [16-23]. Compacted clay soils provide a number of benefits, such as low hydraulic conductivity, but they also have a significant potential for shrinkage and expansion, which can lead to instability issues [24,25]. When the amount of smectite (bentonite) is greater, clay has a higher potential for swelling [26-29]. When smectite is compacted, the swelling pressure in the concentrate zone increases and cracks are more likely to form due to the opposing compaction force. The mechanical characteristics of Geosynthetic Clay Liners (GCL) based on bentonite have been extensively researched during the past three decades in geo environmental applications [30]. The GCLs are made up of two geotextiles stitched or chemically adhered together with a layer of bentonite sandwiched between them. Bentonite acts as a hydraulic barrier due to its extremely low hydraulic conductivity. These GCLs are more capable of self-healing because of the smectite's swell potential in bentonite [31, 32].

As the detailed discussion about the two main clays of these experiments Laponite® and Bentonite has been discussed in Chapter 1(Introduction), we skip to the methods of sample preparation and analytical procedures that are covered in the following sections. The presentation and discussion of the findings will come afterward, and then the conclusions.

4.3. Materials and Method of Experiment :

Bentonite (Aluminum Silicate Hydrate) powder from CDH[®] and Laponite[®] powder from Rockwood Additives were combined while maintaining the overall clay combination concentration at 6.25% by weight. Table(I) provides more information on the mixing ratios of Laponite[®] and bentonite. 14 different mixes of Laponite[®] and bentonite were taken into consideration for the initial round of trials. For each combination, 40 ml of the suspension was added to the petri dish and left to dry.

First, the necessary amount of bentonite powder was measured and pre-soaked in 40 ml of deionized water for almost a day. To get the necessary uniform suspension of bentonite clay, the swelled suspension was then cooled to a temperature of 20°C and stirred on a magnetic stirrer for roughly 5 minutes. After that, while the newly created bentonite colloidal suspension was still being mixed on the magnetic stirrer, the necessary amount of Laponite[®] powder was weighed out and added.

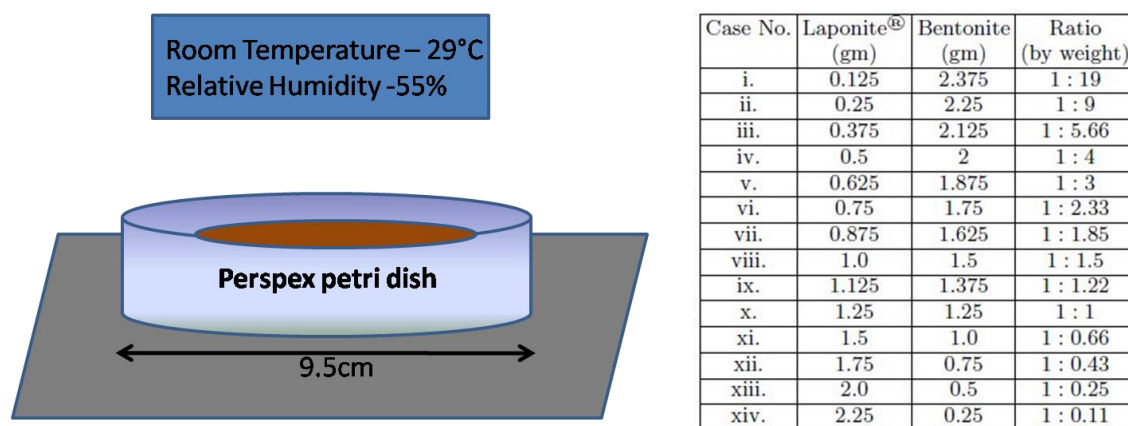


Figure 4.1. (a) Schematic diagram of experimental setup and (b) Table for mixing details of Laponite[®] and bentonite clay in 40 ml deionised water.

To create a homogeneous mixture, the composite clay suspension was stirred on the magnetic stirrer for an additional 30 seconds. The suspension was then immediately transferred onto 9.5 cm diameter polypropylene petri dishes, and was left to dry under natural room settings with an average relative humidity and temperature of 55% and 29°C, respectively. There was no aging of Laponite® [33] because the colloidal solution was placed into the petri dish right away after it was prepared.

In addition to the "regular film" produced with a 40 ml suspension, the impact of film thickness on crack prevention utilizing a Laponite® -bentonite composite was tested for two more cases. These were

- (i) lowering the film thickness in half from the original study and
- (ii) raising it to 1.5 times its original value.

The final concentration of total clay material in suspension was kept constant in both instances at 6:25%.

In case (i) the thickness of the film was increased by using a higher volume of suspension, 60 ml, while in case (ii), the thickness was decreased by using 20 ml as comparative to 40 ml.

Using a Canon 750D camera, the final fracture patterns were captured on camera. The presence of some noise in the data was reduced by repeated trials because crack formation is fundamentally a disordered event and is extremely susceptible to any type of disturbance. Every case examined was repeated seven times to ensure a relatively adequate data statistic. For analysis, the average of the three most reliable data sets was taken into account.

In order to calculate the evaporation rates in each case study, a defined volume of the material was allowed to dry in ambient room conditions. A 4-digit weighing machine was used to calculate the weight of the drying suspension.

When there was no further change in the weight for 24 hours, the film was taken to have attained a final dry state.

To determine the microstructure at various locations on the surface of the films for each combination of Laponite[®]: bentonite (L: B) (by weight), scanning electron microscopy (SEM) pictures were inspected. Multiple magnifications of the SEM images were recorded. A SEM of only Laponite[®] film and only bentonite film at the corresponding concentration were also obtained at each magnification in order to allow comparison.

4.4. Observation :

4.4.1. Effect of Addition of Laponite[®] into Bentonite Clay :

Each sub-figure of Fig. 4.2 has a different clay composition and a different Laponite[®]: bentonite ratio, which corresponds to the case numbers in Table (I). When the quantity of Laponite[®] in the composition was low (Figs. 4.2 a-d), the film cracked substantially. With increasing Laponite[®] concentration, the number of cracks continued to decline until they completely disappeared in the ratio L: B ~ 1:1 (Figs. 4.2 i-k). However, as the Laponite[®] percentage was further raised, the film once more developed cracks, although less in numbers (Figs. 4.2 l-n).

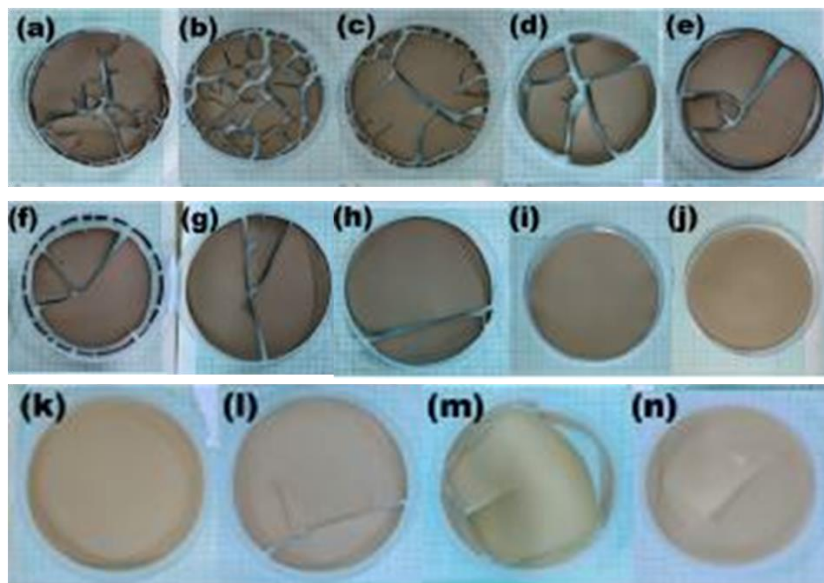


Figure 4.2. Crack pattern on dry films having composition of Laponite®: bentonite by weight ratio (Table in fig.1(b)): (a) 1:19; (b) 1:9; (c) 1:5.66; (d) 1:4; (e) 1:3; (f) 1:2.33; (g) 1:1.85; (h) 1:1.5; (i) 1:1.22; (j) 1:1; (k) 1:0.66; (l) 1:0.43; (m) 1:0.25; (n) 1:0.11. The pictures were taken after 24 hours from the deposition when the final dry state was achieved and there was no further change in their weights.

Three Laponite®: bentonite suspensions (1: 3, 1: 1, and 3: 1) were examined for their evaporation rates. The relative humidity and temperature remained at the same levels. The results (Fig. 4.3) demonstrated that, up to 150 minutes, the evaporation rates for the ratios L: B = 1: 3 and L: B = 1: 1 were nearly equal. The rate of water loss for L: B = 1: 3 grows substantially more than the rest for times > 150 minutes. However, it was noticed that a higher percentage of Laponite® in the composite, L: B = 3: 1, led to enhanced water retention at all times as seen in Fig. 4.3.

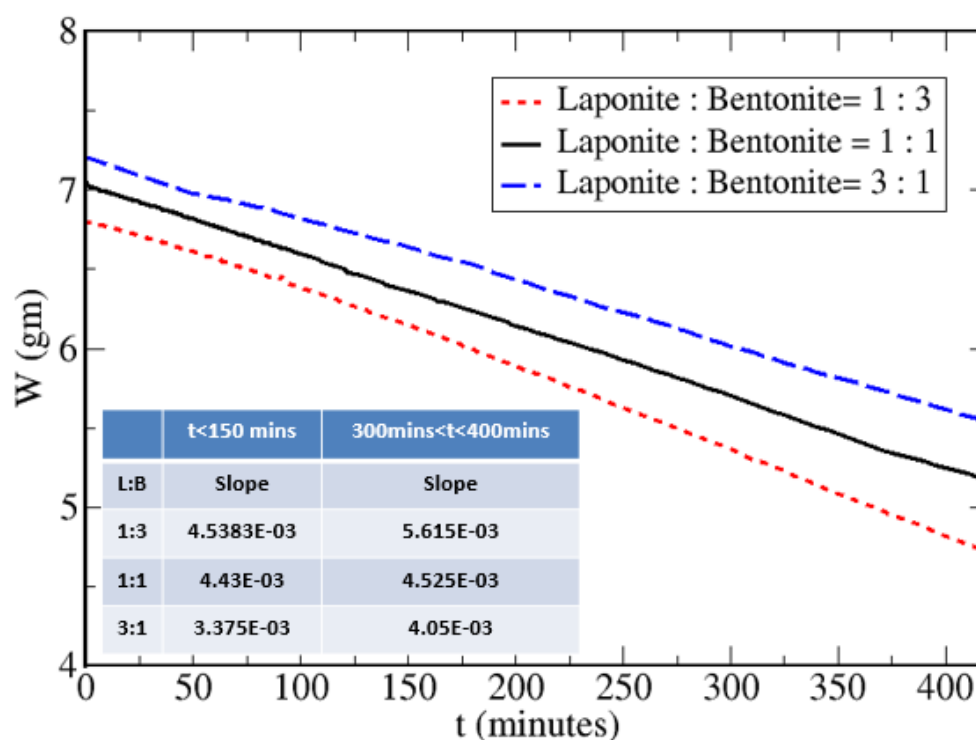


Figure 4.3. Evaporation rates of clay-clay suspensions of composition L : B = 1 : 3, L : B = 1 : 1 and L : B = 3 : 1. The table inside displays the slope of evaporation rates at different time zones for the three ratios.

4.4.2. Comparison of film thickness :

The impact of film thickness on the Laponite[®]-bentonite composite's crack pattern was also investigated (Fig. 4.4). As previously noted, the film thickness was altered by altering the total volume of suspension poured into the petri dish while the total clay concentration was kept constant at 6:25%.

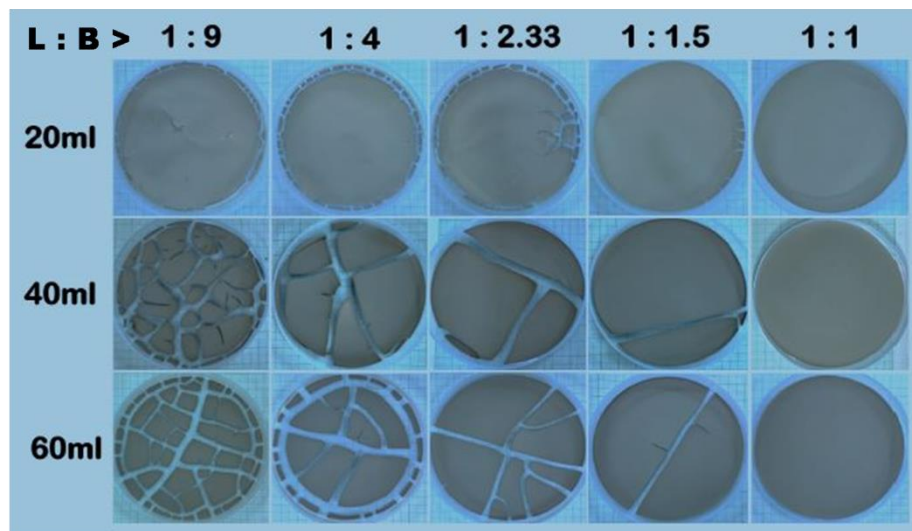


Figure 4.4. Comparison between crack patterns on films of varying thicknesses for the Laponite[®]-bentonite composite. Film thickness was varied by adjusting total volume of the clay-clay suspension: 20 ml, 40 ml and 60 ml. The L : B ratio for each column of the figure matrix is indicated at the top of the column.

The first row shows patterns on reduced film thickness that were altered by employing 20 ml of colloidal suspension in comparison to the reference experiments performed with 40 ml of suspension.

Nearly all of the compositions exhibited no cracks dividing the film body; however, for L:B ratios between 1:9 and 1:2:33, a peripheral ring crack was seen near to the boundary. There were no cracks for L: B = 1:1. It's likely that the film thickness is below the threshold thickness required for this material to generate

cracks [34]. The crack patterns for the 40 ml and 60 ml composite suspensions were comparable, with the exception that the film from the 40 ml suspension tended to peel off the petri dish for all L: B ratios. The broken films were firmly attached to the substrate in the third row of Fig. 4.4, in contrast.

4.5. Result Analysis :

4.5.1. Image Processing and Quantitative Analysis:

In order to analyse the statistics of different aspects of the crack patterns ImageJ software was used to do digital image processing on the final crack pattern on the films for each case. Fig. 4.5 shows the flow chart for the procedure.

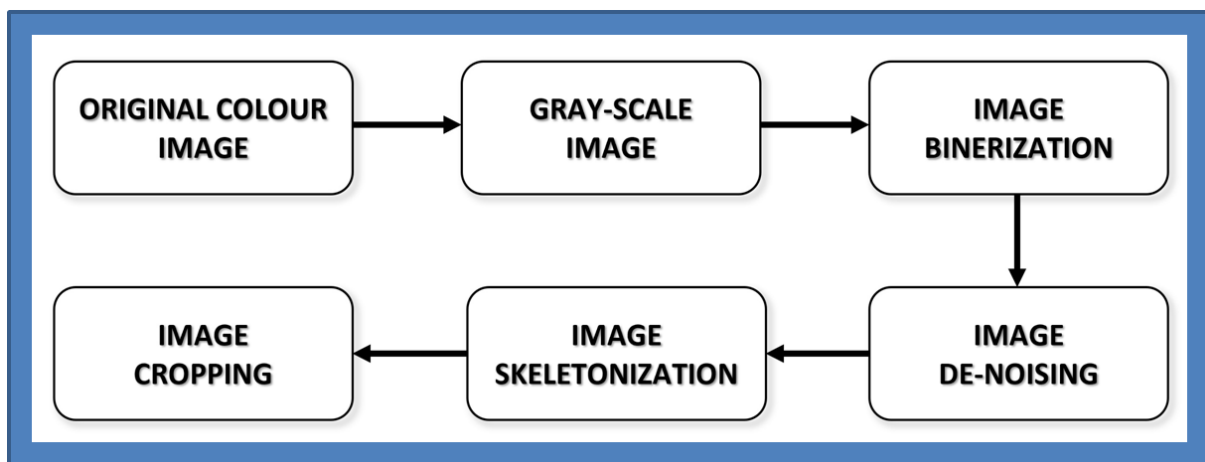


Figure 4.5. Flow chart of image processing procedure of crack image.

A faithful binary image representation must be produced from the original image, which demands precise grey-scale thresholding. The centre area of the patterns, with a diameter of 7.5 cm, was chosen after further cropping the binary

picture of the crack patterns to eliminate the edge effects. The binary file of this cropped image was used for all quantitative analysis.

The following quantitative parameters were identified and calculated for quantitative analysis:

1. *Crack intensity factor (CIF)* : CIF stands for the proportion of the crack's area to the sample's overall area. The greater the degree of superficial cracking, the higher the value of CIF.
2. *Number of nodes (N_n) and Number of cracks (N_c)* : A "node" is where more than one cracks converge. The 'skeleton' of a crack is the location of points halfway to the crack width. A crack is thought to exist along the skeleton line connecting two adjacent nodes. N_n and N_c can generally reflect the severity of the cracked sample surface.
3. *Total length of cracks (L_{tot})* : By measuring the distance between nodes, or junctions, on the skeleton, the fracture length was calculated. The L_{tot} is equal to the sum of all such crack lengths inside the image's cropped area.
4. *Number of peds (N_p) and Total area of peds (A_{tot})* : The independent closed area that is divided by a crack is referred to as the ped. The total ped area is calculated as the combined area of all the peds visible in the cropped image.

Graphical representations of statistics of various fracture pattern characteristics on films made of various Laponite[®] -bentonite ratios are provided in Fig. 4.6.

The film split into numerous fragments that resembled desiccation fractures in bentonite when the weight of Laponite[®] in the composite was very low (0.125 gm) [35]. Maximum cracks were seen when Laponite[®] weight was increased to 0.25 gm. The CIF reached its peak at this point (Fig. 4.6a), and it then rapidly

decreased as the amount of Laponite[®] in the composite increased. In the range of (L : B) = 1 : 1 to L : B = 1 : 1:5, the CIF was zero.

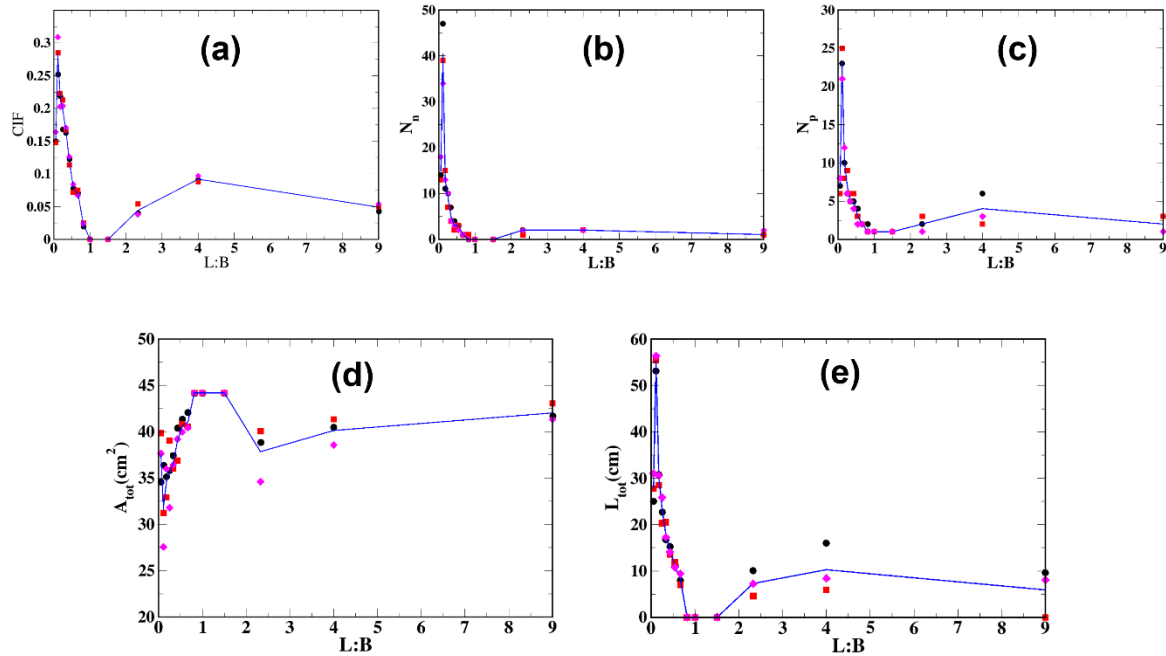


Figure 4.6. Crack pattern analysis on dry films having composition of Laponite[®]: bentonite in different weight ratios. (a) Variation of Crack Intensity Factor (CIF) versus composition; (b) Variation in number of crack-peds (N_p) versus composition; (c) Variation of number of crack nodes (N_n) with composition; (d) Variation of total ped area (A_{tot}) with composition. (e) Variation of crack length with composition. The different solid symbols for each graph represent the repeated sets of experiments and the solid line is representative of their mean values.

The layered structure of these clays' aids in water retention in the linked pore space. Clay expands and eventually breaks to alleviate the pressure. A reliable method of stress transfer between the layered structure of the clay composite that prevents cracking must exist at ratios of $L:B \geq 1:1:5$. However, the CIF showed a slight but noticeable increase with additional increases in Laponite[®] concentration. With an increase in Laponite[®] content in the composite, the similar trend of fracture pattern was seen in a reduction in the total number of crack peds (Fig. 4.6b). Since the CIF and crack ped trends were comparable, it followed that

adding more Laponite[®] to the composite would similarly reduce the number of crack nodes (Fig. 4.6c). The cracks got straighter and wider with fewer branches as the Laponite[®] content increased. When cracks were completely absent, the total ped area nearly matched the size of the system (Fig. 4.6d). The analysis of total crack length fluctuation with clay composition (Fig. 4,6e) further showed that cracks vanished in this clay-clay composite at a crucial ratio of L: B \approx 1: 1.

4.5.2. Role of film thickness :

Since there was essentially no difference in the crack pattern of films with reduced thickness for all ratios investigated (first row in the figure matrix of Fig. 4.4), statistical analysis of these films is not provided here. Analysis of crack data and comparison of the thicknesses of the regular (40 ml of suspension) and larger (60 ml of suspension) films employed in our studies allowed us to assess the impact of film thickness on crack pattern and prevention (Fig. 4.4).

According to what was predicted [36], the variation of CIF with composition of L: B (Fig. 4.7a) revealed a greater CIF for a thicker film up to a L: B 1: 0:56. Beyond this, though, the thicker film's CIF was lower than that of the ordinary film. The pattern was less branching with thicker films (Figs. 4.7b and c). Total ped area variation with composition for the two film thicknesses

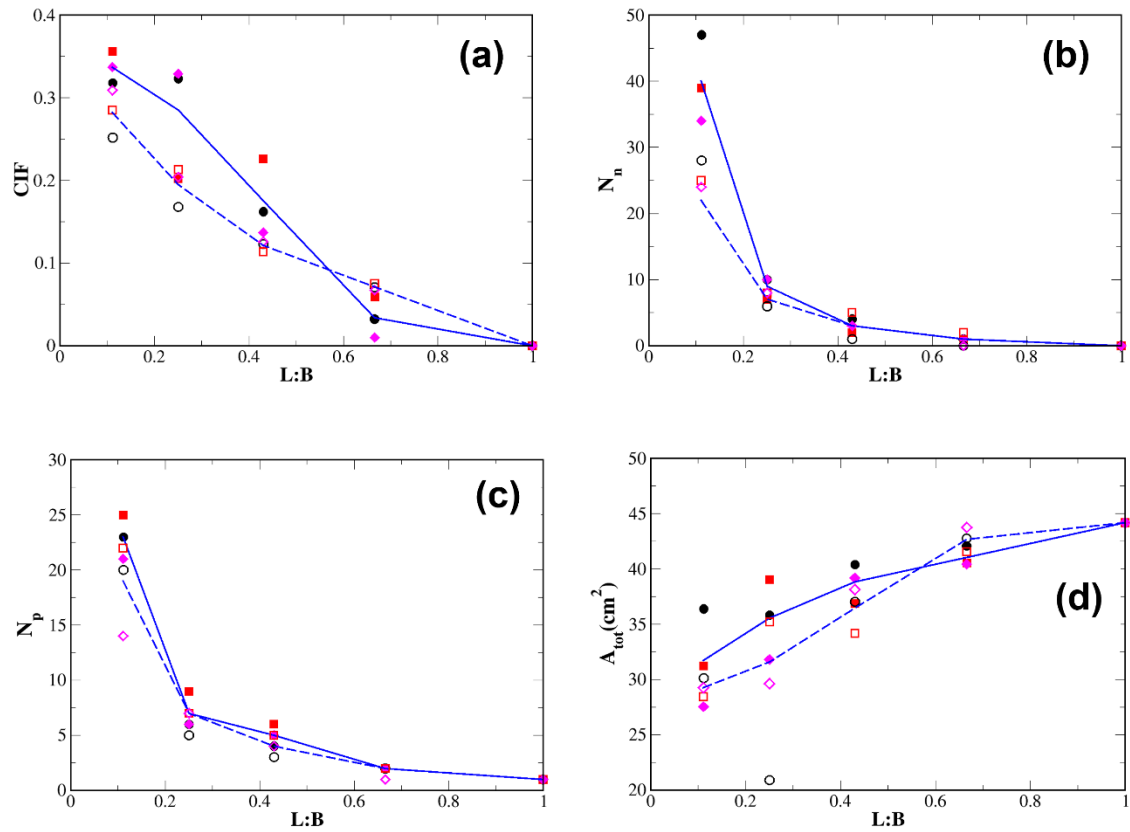


Figure 4.7. Comparison between crack pattern on films of varying thickness for the Laponite®-bentonite composite prepared from 40 ml and 60 ml clay-clay suspension for: (a) Variation of CIF with $L : B$; (b) Variation of N_n with $L : B$; (c) Variation of N_p with $L : B$; (d) Variation of A_{tot} with $L : B$. The hollow symbols denote the data for the experiments performed with 40 ml of suspension whereas the solid symbols denote the same for 60 ml suspension.

was shown in Figure 4.7d, and it was consistent with the behaviour shown there (Fig. 4.4).

A graphic illustrating the variance in the incidence of different degrees of nodes for the various ratios of $L : B$ is shown in order to better understand the branching nature of the two different-volume films (Fig. 4.8a and b). Fig. 4.8c shows the data for the same, where f_n is the percentage of all nodes that belong to a certain degree for a specific volume of the suspension, i.e.

$$f_n = \frac{\text{Frequency of occurrence}}{\text{Total number of nodes}}$$

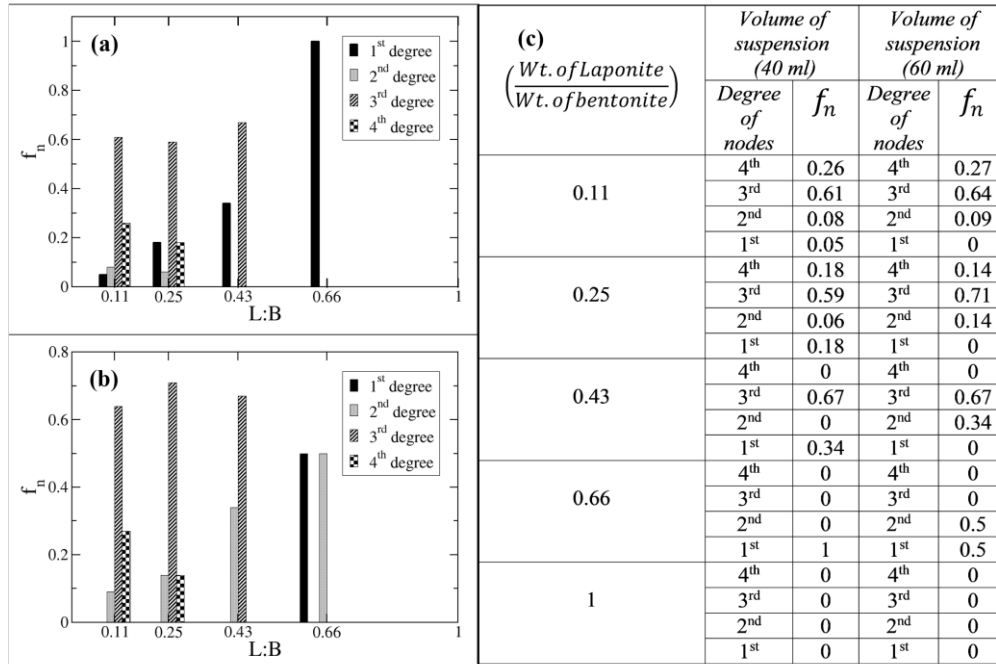


Figure 4.8. (a), (b): plot of the distribution of fraction of occurrence of nodes of a certain degree for 40 ml and 60 ml suspension, respectively; (c) data set tabulated for the two volumes of suspension.

4.5.3. Analysis of SEM images :

According to numerous experimental findings, the film exhibited cracks for L: B ratios except for L: B = 1: 1 where cracks were prevented. Scanning electron microscopy was used on various portions of a film for three different compositions: (i) L: B = 1: 3, (ii) L: B = 1: 1, and (iii) L: B = 3: 1 in order to get some insight into the mechanism responsible for crack avoidance in the Laponite[®]-bentonite composite film (Figs. 4.9, 4.10 and 4.11). For comparison, SEM photos of Laponite[®] film and pure bentonite at the same magnification are shown. The SEM pictures of pure Laponite[®] and bentonite revealed aggregates of exfoliated montmorillonite platelets in water while preparing the sample.

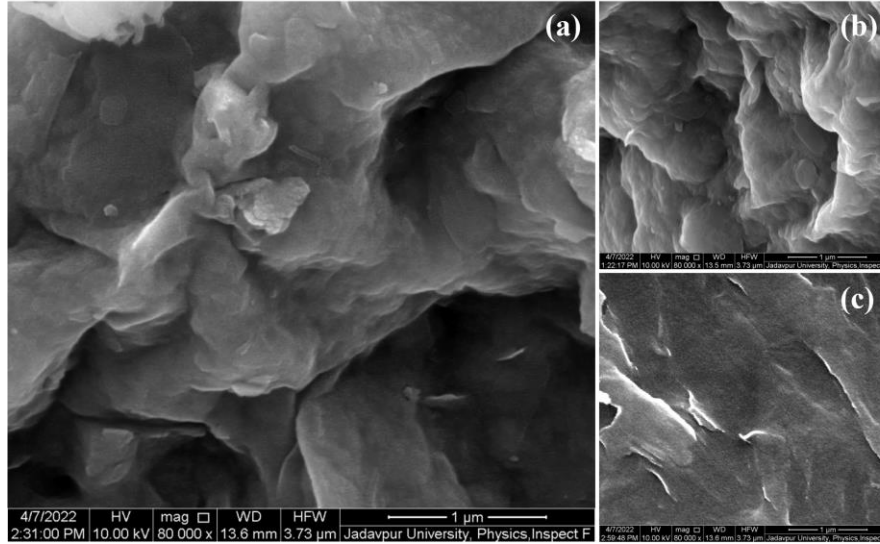


Figure 4.9. (a) SEM images of clay film of 6:25% for $L : B = 1 : 3$; (b) and (c) show SEM images of Laponite[®] and bentonite respectively, at the same magnification.

According to the SEM results for the proportion $L : B = 1 : 3$ (Fig. 4.9), the composite structure was extremely comparable to that of pure bentonite. As the original spacing between the bentonite platelets was less noticeable (Fig. 4.9a), it depicts the intercalation of Laponite[®] platelets (Fig. 9b) between the bentonite platelets (Fig. 4.9c). In contrast to either of the pure clays, which both exhibit stacks of lamellae (Fig. 4.10b, 4.10c), the SEM for $L : B = 3 : 1$ revealed an uneven structure (Fig. 4.10a). The increased concentration of Laponite[®] caused it to aggregate into flocs on the bentonite platelets.

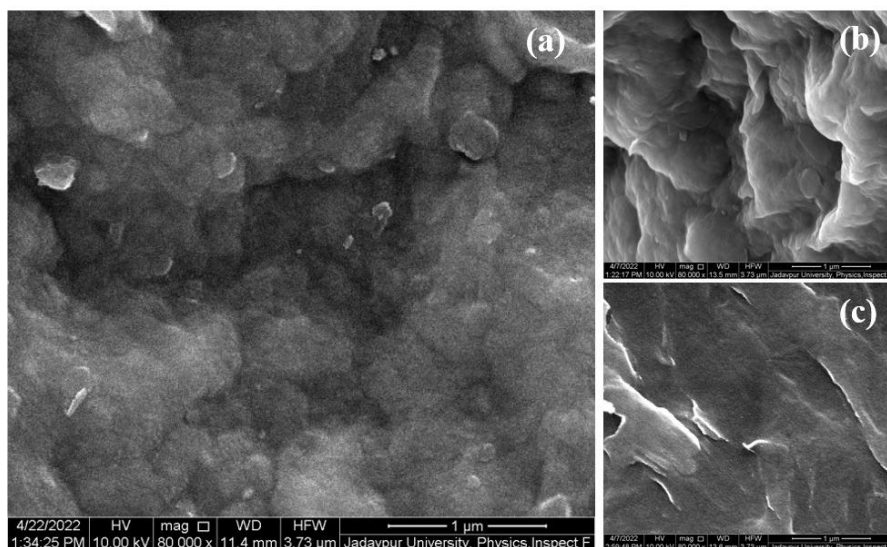


Figure 4.10. (a) SEM images of clay film of 6:25% for $L : B = 3 : 1$; (b) and (c) show SEM images of Laponite[®] and bentonite at the same magnification, respectively.

The $L:B = 1:1$ composite's SEM picture differed noticeably from the 1:3 and 3:1 composites (Fig. 4.11a). Two platelet-like structures in the composite texture fit into each other as if they were being stitched together effortlessly. At higher magnification, the film structure revealed elongated aggregates that were divided by microcracks (Fig. 4.11d). The individual clay particles are disc-shaped, have surface charges that are both positive around the rim and negative on their faces. To estimate the EDL, the positive ions are held fixed to the surface by the individual charged particles. However, the presence of electrostatic interactions between clay particles in solution is present in all composite compositions the presence of electrostatic interactions between clay particles in solution is present in all composite compositions.

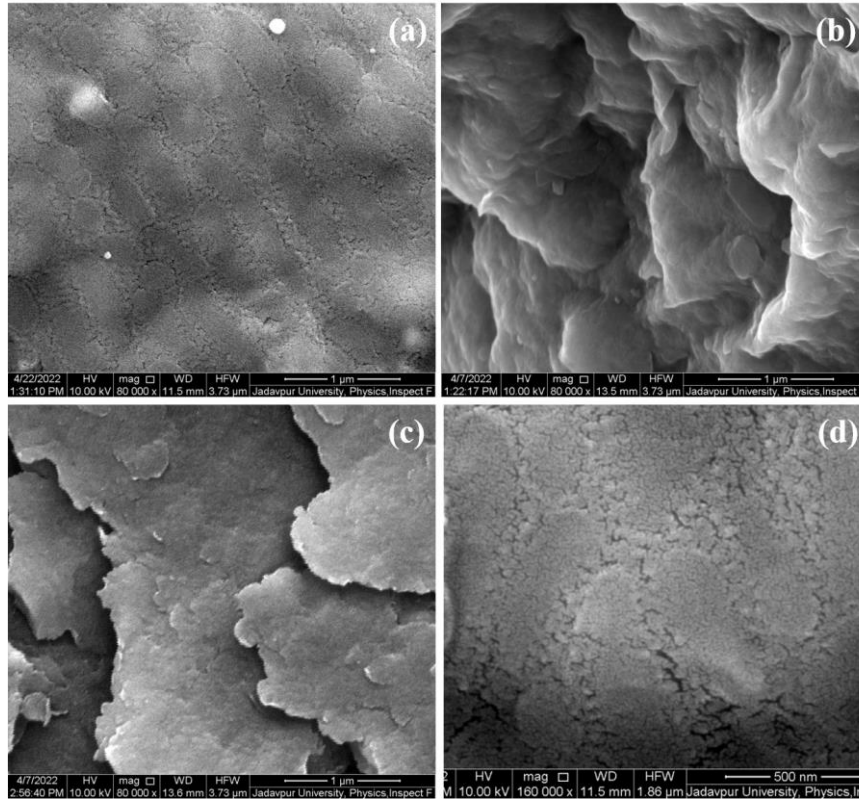


Figure 4.11. (a) SEM images of clay film of 6:25% for $L : B = 1 : 1$; (b) and (c) are the SEM images of Laponite[®] and bentonite, respectively, at the same magnification; (d) SEM images of clay film of 6:25% for $L : B = 1 : 1$ at $\times 2$ magnification

The number of ions released in solution depending on the fraction of clay particles in the water might have impact on the effective potential of the particles. Electrostatic response to field can be used to describe how clay particles and their aggregates align in the directions of external electric or magnetic fields. However, in the absence of a field, the almost flawlessly fitted mosaic with the ratio $L : B = 1 : 1$ warrant further investigation. The best explanation for why the clay aggregates are oriented in a specific direction is a combination of electrostatic forces between the particles and the shear force that was applied to them during the mixing of the two clay suspensions. The absence of rough edges on aggregates suggests that the smaller and more uniformly sized Laponite[®] platelets have been almost perfectly inserted into the bentonite gaps.

The water retention capacity was higher for compositions that contained more Laponite[®], but when the evaporation rate for the L: B = 1:1 was checked and compared with the evaporation rates of composites other than the critical value of 1:1, the evaporation rates were found to be very similar for all compositions. Therefore, the ability to hold onto water cannot be the only factor in crack prevention. In contrast to the platelet structure found in exfoliated bentonite or Laponite[®] in water, a smooth structure with zero breakage was found when SEM pictures of the composite for L: B = 1:1 were analysed. Only at a size of 500 nm there were tiny nano-cracks between the composite clay aggregates observable. The clay-clay composite film displayed the stacked platelet structure of montmorillonite or an uneven bumpy structure depending on whether the quantity of bentonite was more or less than Laponite[®].

A pH metre was used to measure the pH of aqueous solutions of Laponite[®] and bentonite, and it showed a pH of 9.8. At this pH, the particles organise themselves into aggregates with the T-structure found in House-of-Cards-style systems. When bentonite particles become exfoliated in suspension, it is proposed that Laponite[®] particles, which are orders of magnitude smaller than bentonite particles, can act as nano-fillers for the bentonite particles. The critical ratio of 1:1 result in a compact clay composite structure, as shown in the schematic Fig. (4.12b), where just enough Laponite[®] is present to fill the d-space between the bentonite platelets. Due to their high aspect ratio and molecular connection, the individual silicate layers of clay particles have outstanding stiffness and strength in two dimensions. It has been determined that a reinforcing action caused by stress transfer to the rigid individual silicate nanosheets is responsible for the increase in stiffness of the Laponite[®] -bentonite nanocomposite in an exfoliated condition. A large portion of the interconnected pore spaces that contribute to clay swelling, water retention, and

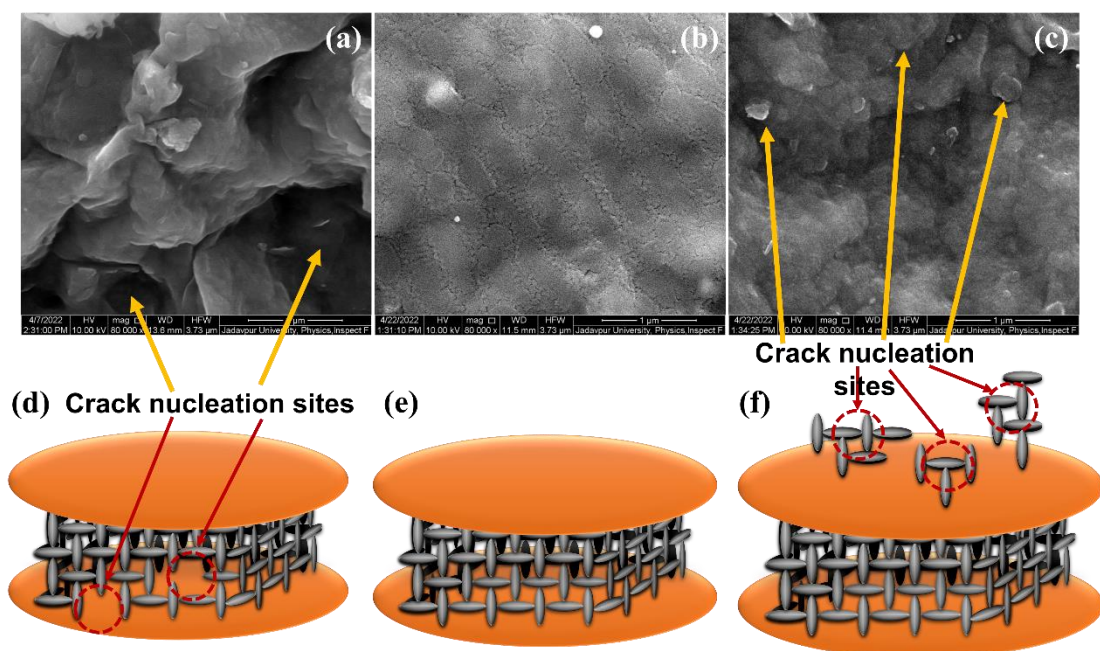


Figure 4.12. SEM pictures of Laponite: bentonite films at the appropriate ratios of $L: B = 1:3$, $L: B = 1:1$, and $L: B = 3:1$ are compared, and a corresponding schematic is used to give an explanation; Figure(a) and (d): Schematic of Laponite® discs with Laponite®-bentonite particle arrangement at ratio $L: B = 1: 3$ compared to SEM of film with the same composition. The crack nucleation sites in the figure are caused by the incomplete packing of Laponite® in the d-space of bentonite platelets; arrows point to the holes in the area between the bentonite particles in the SEM image (a); Figure(b) and (e): Schematic of Laponite® discs with Laponite®-bentonite particle arrangement at ratio $L: B = 1: 1$ compared to SEM of film with the same composition A complete lack of crack nucleation sites is caused by the nearly flawless packing of Laponite® in the house-of-card structure between bentonite platelets, as shown in the film SEM in (b); Figure(c) and (f): Schematic of Laponite® discs with Laponite®-bentonite particle arrangement at ratio $L: B = 1: 1$ compared to SEM of film with the same composition The schematic illustrates how Laponite® aggregates or forms flocs on top of the bentonite platelets when there is an excess of Laponite® particles relative to bentonite. These flocs serve as crack nucleation sites. The flocs seen on the bentonite faces in the SEM are indicated by the arrows.

finally stress release through crack development are closed by the compact layered structure. The homogeneous compressible isotropic nanocomposite formed by the $L: B = 1: 1$ composite has a higher shear strength and makes it easier to prevent cracks at the critical composition.

For example, in Fig. (4.12a), with a ratio of $L: B = 1: 3$, there is not enough Laponite® to completely fill the d-plane gap between the bentonite platelets. Shear stress transmission is less effective than it is when the critical ratio of $L: B$

= 1: 1 exists. The gaps serve as nucleation sites for cracks. In Fig. (4.12c), Laponite[®] particles, which are substantially more abundant than bentonite particles, are forced to form aggregates as flocs on the bentonite particles at ratios of L: B = 3: 1, in contrast. Both the SEM images and the schematic show that these flocs serve as crack nucleation sites.

4.6. Conclusions and Discussions :

Clay is a porous material whose mechanical and hydromechanical properties can be altered by cracks. Desiccation cracks develop as a result of water evaporating from the spaces between particle aggregates [37]. An overview of the mechanical and electrostatic forces that affect particle aggregates in aqueous solution is necessary since, in this situation, the porous aggregate is a composite of two clays. These forces influence the applications for such composites.

The electrical properties of the electric double layer (EDL), which surrounds the clay particles in an aqueous clay suspension, are governed by the isomorphous substitutions unique to the type of clay. An important factor that governs the dispersion of clay particle colloids in suspension is their surface potential [38].

The electrokinetic potential is influenced by the charges in the EDL [39-41], clay mineralogy, temperature, and pore fluid chemistry [42]. The negative zeta potential of anionic polyacrylamide dispersions can be significantly reduced by high molecular weight and charge density variations [43], which has a significant impact on the stability of clay dispersions. For the design of surface-mediated devices like EDL capacitors, the interfacial potential for suspension stability [44], aggregate stability [45-47], adsorption kinetics [48], electrochemistry [49], and ion exchange [50] are particularly crucial. As the

electrostatic repulsion between the clay particles is impacted, Xu et al. [51] suggested that the dielectric saturation should be taken into account to evaluate the number of tiny particles released by montmorillonite aggregates in suspensions of electrolytes. The surface electrical conductivity of a clay particle depends on its mineralogy and the concentration of electrolytes in its pore water. Properties like the effective electrical conductivity of aqueous clay can display anisotropy depending on the texture and orientation of the particle [52]. In their modification of Hashin and Shtrikman's [53] earlier model, Ellis et al. [54] suggested a geometric component to take the aspect ratio of the soil particles into account while studying soil electrical conductivity. By treating the clay particle and its related EDL as a single unit of effective clay particle, Hasan et al [55] and Hasan et al [56] reported the effect of clay mineralogy and its interaction with soil water in the research of electrical conductivity of aqueous clay mixtures. It has been suggested that the electrostatic repulsion between clay particles affects the aggregate stability of clays [57, 58] and that the electrostatic repulsion pressure between clay particles is estimated [59, 60]. The assumption that the ratio between the radius of curvature of the particle surface and thickness of the double layer is substantially bigger than 1 led to an estimation of the stability of montmorillonite particles.

This chapter has presented research on the cracking behaviour of composite materials made of bentonite and Laponite[®] in various ratios, both elements belong to montmorillonite group clays. It is well known that the material is prone to many and distinctive cracks brought on by desiccation of aqueous Laponite[®] or aqueous bentonite films alone. However, it is discovered that the fracture density changes depending on the ratio of each clay present in the composite when an aqueous composite of these two clays is dried, reaching a point where cracks are completely suppressed at a critical ratio of the two clays.

Repeated sets of studies on drying films of Laponite[®]-bentonite suspensions of varied proportions have revealed that desiccation fractures are almost completely inhibited for a film composition of L: B~1:1. Desiccation fractures formed in the drying clay-clay film when the bentonite proportion was larger or less than Laponite[®]. When the L:B ~ 1:1 crucial ratio was maintained, varying the film thickness also kept all apparent cracks completely absent. In contrast to the platelet structure seen in exfoliated bentonite or Laponite[®] in water, SEM pictures of the composite for L:B = 1:1 showed a smooth structure with almost no fracturing.

Since Laponite[®] particles are many times smaller than bentonite particles, it is hypothesized that they serve as nano-fillers for the bentonite particles. Laponite[®] packs precisely into the d-space of the bentonite platelets at the key ratio of 1:1. As drying gets underway, the tightly packed layered structure makes it easier for stress to be transferred between clay particles, successfully preventing crack formation at the critical composition.

In addition to many other uses in the future, using a clay-clay composite in a carefully chosen ratio may be a cheap and efficient way to prevent cracks in the crucial field of land-filler manufacture.

4.7. List of References :

- [1] Pise, N., Meshram, T., Doijad, Y., Gathe, R., Bobade, A., Kutemate, A., Patil, S., Raut, P. and Gudadhe, A., 2021. A Brief Study on Causes of Cracks, Prevention and Pattern of Cracks on Concrete. *Int. J. Sci. Res. Sci. Eng. Technol.*, 8, pp.439-443.
- [2] Das, B., Umnag, K. and Murthy, G., 2021. Study on Causes of Cracks and Its Preventive Measures in Concrete Structures of CCEM Building, Raipur. *International Journal of Architecture and Planning*, 1(1), pp.30-36.
- [3] Juillerat, F., Bowen, P. and Hofmann, H., 2006. Formation and drying of colloidal crystals using nanosized silica particles. *Langmuir*, 22(5), pp.2249-2257.
- [4] Zhang, J., Sun, Z. and Yang, B., 2009. Self-assembly of photonic crystals from polymer colloids. *Current Opinion in Colloid & Interface Science*, 14(2), pp.103-114.
- [5] Routh, A.F., 2013. Drying of thin colloidal films. *Reports on Progress in Physics*, 76(4), p.046603.
- [6] Tite, M.S., Kilikoglou, V. and Vekinis, G., 2001. Strength, toughness and thermal shock resistance of ancient ceramics, and their influence on technological choice. *Archaeometry*, 43(3), pp.301-324.
- [7] Hutchinson, J.W. and Suo, Z., 1991. Mixed mode cracking in layered materials. *Advances in applied mechanics*, 29, pp.63-191.

-
- [8] Tang, C.S., Shi, B., Liu, C., Gao, L. and Inyang, H.I., 2011. Experimental investigation of the desiccation cracking behavior of soil layers during drying. *Journal of Materials in Civil Engineering*, 23(6), pp.873-878.
- [9] Lozada, C., Caicedo, B. and Thorel, L., 2015. Effects of cracks and desiccation on the bearing capacity of soil deposits. *Géotechnique letters*, 5(3), pp.112-117.
- [10] Guo, F., Aryana, S., Han, Y. and Jiao, Y., 2018. A review of the synthesis and applications of polymer–nanoclay composites. *Applied Sciences*, 8(9), p.1696.
- [11] Utracki, L.A., 2004. *Clay-containing polymeric nanocomposites* (Vol. 1). iSmithers Rapra Publishing.
- [12] Roh, S.C., Kwan, H.J. and Kim, C.K., 2012. Nanocomposites of novolac type phenolic resins and organoclays: the effects of the resin molecular weight and the amine salt structure on the morphology and the mechanical properties of the composites. *Macromolecular Research*, 20(5), pp.496-502.
- [13] Park, J.H. and Jana, S.C., 2003. Mechanism of exfoliation of nano clay particles in epoxy– clay nanocomposites. *Macromolecules*, 36(8), pp.2758-2768.
- [14] Liu, T., Tjiu, W.C., Tong, Y., He, C., Goh, S.S. and Chung, T.S., 2004. Morphology and fracture behavior of intercalated epoxy/clay nanocomposites. *Journal of Applied Polymer Science*, 94(3), pp.1236-1244.
- [15] Wang, K., Chen, L., Wu, J., Toh, M.L., He, C. and Yee, A.F., 2005. Epoxy nanocomposites with highly exfoliated clay: mechanical properties and fracture mechanisms. *Macromolecules*, 38(3), pp.788-800.

-
- [16] Bjerrum, L., 1973. Geotechnical problems involved in foundations of structures in the North Sea. *Geotechnique*, 23(3), pp.319-358.
- [17] Anderson, S.A. and Hee, B.H., 1995. Hydraulic conductivity of compacted lateritic soil with bentonite admixture. *Environmental & Engineering Geoscience*, 1(3), pp.299-312.
- [18] Li, L.Y. and Li, F., 2001. Heavy metal sorption and hydraulic conductivity studies using three types of bentonite admixes. *Journal of Environmental Engineering*, 127(5), pp.420-429.
- [19] Rajasekaran, G., Murali, K., Nagan, S., Amoudhavally, V. and Santhaswaruban, V., 2005. Contaminant transport modeling in marine clays. *Ocean engineering*, 32(2), pp.175-194.
- [20] Du, Y.J. and Hayashi, S., 2006. A study on sorption properties of Cd²⁺ on Ariake clay for evaluating its potential use as a landfill barrier material. *Applied Clay Science*, 32(1-2), pp.14-24.
- [21] Covelo, E.F., Vega, F.A. and Andrade, M.L., 2007. Competitive sorption and desorption of heavy metals by individual soil components. *Journal of Hazardous Materials*, 140(1-2), pp.308-315.
- [22] Chalermyanont, T., Arrykul, S. and Charoenthaisong, N., 2009. Potential use of lateritic and marine clay soils as landfill liners to retain heavy metals. *Waste Management*, 29(1), pp.117-127.

-
- [23] Hamdi, N. and Srasra, E., 2013. Hydraulic conductivity study of compacted clay soils used as landfill liners for an acidic waste. *Waste Management*, 33(1), pp.60-66.
- [24] Di Maio, C., Santoli, L. and Schiavone, P., 2004. Volume change behaviour of clays: the influence of mineral composition, pore fluid composition and stress state. *Mechanics of materials*, 36(5-6), pp.435-451.
- [25] Booker, J.R., Quigley, R.M. and Rowe, R.K., 1997. *Clayey barrier systems for waste disposal facilities*. CRC Press.
- [26] Tabani, M. and Rolland, S., 2001. Hydromechanical behaviour of a compacted bentonite-silt mixture. *Clay Science for Engineering*. In: Fukue, Adachi (eds). *Balkema*, pp.245-250.
- [27] Muntohar, A.S., 2003. Swelling and compressibility characteristics of soil-bentonite mixtures. *Civil Engineering Dimension*, 5(2), pp.93-98.
- [28] Komine, H. and Ogata, N., 1994. Experimental study on swelling characteristics of compacted bentonite. *Canadian geotechnical journal*, 31(4), pp.478-490.
- [29] EL, S. and EA, R., 1981. SOME FACTORS AFFECTING SWELLING OF CLAYEY SOILS.
- [30] Kong, D.J., Wu, H.N., Chai, J.C. and Arulrajah, A., 2017. State-of-the-art review of geosynthetic clay liners. *Sustainability*, 9(11), p.2110.

-
- [31] Sivakumar Babu, G.L., Sporer, H., Zanzinger, H. and Gartung, E., 2001. Self-healing properties of geosynthetic clay liners. *Geosynthetics International*, 8(5), pp.461-470.
- [32] Parastar, F., Hejazi, S.M., Sheikhzadeh, M. and Alirezazadeh, A., 2017. A parametric study on hydraulic conductivity and self-healing properties of geotextile clay liners used in landfills. *Journal of environmental management*, 202, pp.29-37.
- [33] Saha, D., Bandyopadhyay, R. and Joshi, Y.M., 2015. Dynamic light scattering study and DLVO analysis of physicochemical interactions in colloidal suspensions of charged disks. *Langmuir*, 31(10), pp.3012-3020.
- [34] Khatun, T., Dutta, T. and Tarafdar, S., 2015. Topology of desiccation crack patterns in clay and invariance of crack interface area with thickness. *The European Physical Journal E*, 38(8), pp.1-11.
- [35] Shokri, N., Zhou, P. and Keshmiri, A., 2015. Patterns of desiccation cracks in saline bentonite layers. *Transport in porous media*, 110(2), pp.333-344.
- [36] Groisman, A. and Kaplan, E., 1994. An experimental study of cracking induced by desiccation. *EPL (Europhysics Letters)*, 25(6), p.415.
- [37] Goehring, L., Nakahara, A., Dutta, T., Kitsunzaki, S. and Tarafdar, S., 2015. *Desiccation cracks and their patterns: Formation and Modelling in Science and Nature*. John Wiley & Sons.

-
- [38] Liu, X., Tian, R., Du, W., Li, R., Ding, W. and Li, H., 2019. A theory to determine the surface potentials of clay particles in electrolyte solutions. *Applied Clay Science*, 169, pp.112-119.
- [39] Somasundaran, P. and Krishnakumar, S., 1997. Adsorption of surfactants and polymers at the solid-liquid interface. *Colloids and Surfaces A: physicochemical and engineering aspects*, 123, pp.491-513.
- [40] Ghosal, S., 2002. Band broadening in a microcapillary with a stepwise change in the ζ -potential. *Analytical chemistry*, 74(16), pp.4198-4203.
- [41] Jalil, A.H. and Pyell, U., 2018. Quantification of zeta-potential and electrokinetic surface charge density for colloidal silica nanoparticles dependent on type and concentration of the counterion: probing the outer Helmholtz plane. *The Journal of Physical Chemistry C*, 122(8), pp.4437-4453.
- [42] Cherian, C., Kollannur, N.J., Bandipally, S. and Arnepalli, D.N., 2018. Calcium adsorption on clays: effects of mineralogy, pore fluid chemistry and temperature. *Applied Clay Science*, 160, pp.282-289.
- [43] Shaikh, S.M., Nasser, M.S., Magzoub, M., Benamor, A., Hussein, I.A., El-Naas, M.H. and Qiblawey, H., 2018. Effect of electrolytes on electrokinetics and flocculation behavior of bentonite-polyacrylamide dispersions. *Applied Clay Science*, 158, pp.46-54.
- [44] Herman, D. and Walz, J.Y., 2013. Stabilization of weakly charged microparticles using highly charged nanoparticles. *Langmuir*, 29(20), pp.5982-5994.

[45] Norrish, K., 1954. The swelling of montmorillonite. *Discussions of the Faraday society*, 18, pp.120-134.

[46] Li, S., Li, H., Xu, C.Y., Huang, X.R., Xie, D.T. and Ni, J.P., 2013. Particle interaction forces induce soil particle transport during rainfall. *Soil Science Society of America Journal*, 77(5), pp.1563-1571.

[47] Hu, F., Xu, C., Li, H., Li, S., Yu, Z., Li, Y. and He, X., 2015. Particles interaction forces and their effects on soil aggregates breakdown. *Soil and Tillage Research*, 147, pp.1-9.

[48] Savaji, K.V., Niitsoo, O. and Couzis, A., 2014. Influence of particle/solid surface zeta potential on particle adsorption kinetics. *Journal of colloid and interface science*, 431, pp.165-175.

[49] Bae, J.H., Han, J.H. and Chung, T.D., 2012. Electrochemistry at nanoporous interfaces: new opportunity for electrocatalysis. *Physical Chemistry Chemical Physics*, 14(2), pp.448-463.

[50] Liu, X., Li, H., Du, W., Tian, R., Li, R. and Jiang, X., 2013. Hofmeister effects on cation exchange equilibrium: quantification of ion exchange selectivity. *The Journal of Physical Chemistry C*, 117(12), pp.6245-6251.

[51] Xu, C.Y., Yu, Z.H. and Li, H., 2015. The coupling effects of electric field and clay mineralogy on clay aggregate stability. *Journal of Soils and Sediments*, 15(5), pp.1159-1168.

[52] Mojid, M.A., Rose, D.A. and Wyseure, G.C.L., 2007. A model incorporating the diffuse double layer to predict the electrical conductivity of bulk soil. *European journal of soil science*, 58(3), pp.560-572.

-
- [53] Hashin, Z. and Shtrikman, S., 1962. A variational approach to the theory of the effective magnetic permeability of multiphase materials. *Journal of applied Physics*, 33(10), pp.3125-3131.
- [54] Ellis, M.H., Sinha, M.C., Minshull, T.A., Sothcott, J. and Best, A.I., 2010. An anisotropic model for the electrical resistivity of two-phase geologic materials. *Geophysics*, 75(6), pp.E161-E170.
- [55] Hasan, M.F., Abuel-Naga, H., Broadbridge, P. and Leong, E.C., 2018. Series-parallel structure-oriented electrical conductivity model of saturated clays. *Applied Clay Science*, 162, pp.239-251.
- [56] Hasan, M.F., Abuel-Naga, H. and Leong, E.C., 2021. A modified series-parallel electrical resistivity model of saturated sand/clay mixture. *Engineering Geology*, 290, p.106193.
- [57] Luo, Y., Gao, X., Tian, R. and Li, H., 2018. Approach to estimation of hamaker constant as taking hofmeister effects into account. *The Journal of Physical Chemistry C*, 122(17), pp.9432-9440.
- [58] Liu, X., Tian, R., Du, W., Li, R., Ding, W. and Li, H., 2019. A theory to determine the surface potentials of clay particles in electrolyte solutions. *Applied Clay Science*, 169, pp.112-119.
- [59] Langmuir, I., 1938. The role of attractive and repulsive forces in the formation of tactoids, thixotropic gels, protein crystals and coacervates. *The Journal of Chemical Physics*, 6(12), pp.873-896.

[60] Hou, J., Li, H., Zhu, H. and Wu, L., 2009. Determination of clay surface potential: a more reliable approach. *Soil Science Society of America Journal*, 73(5), pp.1658-1663.

5

Discussion and Future Plans

Due to the numerous practical, commercial, and industrial uses of various aspects of crack formation, study of crack patterns is a significant area of research in contemporary material science. We have studied how crack patterns develop in clay suspension under various conditions. The clays involved in our experiment are Laponite[®], a synthetic clay, and bentonite, which is normally montmorillonite. Laponite[®] is synthetically produced and used in the creation of a variety of commercial and research-focused goods, including household cleaners, surface coatings, and personal care products that are waterborne. It increases the product's stability and syneresis control and gives thixotropic shear sensitive viscosity (expulsion of the liquid from gel). In order to provide electrically conductive, antistatic, and barrier coatings, it is also useful as a film developer. Bentonite is a clay that swells and has the capacity to absorb enormous amounts of water, increasing its volume up to an eight-fold factor. Because of this, bentonite beds are unsuited in building and paving streets. However, the swelling feature is advantageously exploited as a binder, purifier, absorbent and carrier for fertilisers or pesticides in drilling mud and groundwater sealants. Bentonite is also utilised in environmental protection for soil conditioning and improvement as well as water clarifying due to its ion exchange, flocculation, and sedimentation capabilities. It is also widely used in the food industry (wine, edible oils and fats), pharmaceuticals, cosmetics, and spa mud therapies, as a detergent ingredient, as a thickening and/or suspending agent in paints & varnishes and in many other industries. Due to this wide range of application of these clays, the study on their crack profile and also how to control it, is an important topic of research.

We have studied the experimental cracking of a rectangular Laponite[®] sample whose length (L) is substantially greater than its breadth (B), and where

the area far from the short edges can be thought of as a component of a system with an infinite length and finite breadth. The number of cracks that form on the positive electrode when exposed to an external electric field depends on the voltage V that is delivered externally. As they go towards the negative electrode, the cracks gradually join with their neighbours to form a sequence of tree-shaped cracks. On the basis of the co-ion and counter-ion charge distribution in the presence of the electric field, the nature of the branching pattern could be described. Our theory is supported by the SEM photos as well. Recently, connected conducting networks for transparent electrodes have been created using templates created from crack patterns in colloids. Utilizing the findings of the current work, which generates a self-assembled pattern with a tree-like structure, it may be able to develop novel uses of conductors with anisotropic electrical properties for particular requirements in circuits.

In the next study, we show the crack patterns that emerged in aqueous Laponite[®] gel after being placed in various-sized rectangular boxes and exposed to a static electric field that was constant. A very unusual structure that resembles a tree and spans from the positive to the negative electrode is shown by the crack pattern. But it has been shown that the levels of branching rely on the size of the boxes, i.e., on the exposed area of the applied electric field. The Cayley tree and the Bethe lattice are comparable to these structures. The "trees" divide the system into peds of different sizes, with a lot of smaller ones on the positively charged end and gradually bigger ones and fewer in number on the negatively charged end. Plotting the cumulative distribution of the number of peds exceeding a specific region's size versus that area will reveal a power-law relationship which indicates the pattern is fractal and scale-invariant. With respect to a specific system size and a range of applied voltages, the exponent of

the power-law has a value that is basically constant. Another example of how uniform energy input results in power-law spatial distribution of energy storage and fractal energy dissipation in an extended dissipative system is provided by this situation.

In the following chapter, we reported research on the cracking behaviour of composite materials consisting of bentonite and Laponite® in various ratios, both of which are montmorillonite group clays. Desiccation cracks are virtually eliminated with a film composition of L: B~1:1 according to numerous tests on drying films of Laponite®-bentonite suspensions of various proportions. Desiccation fractures developed in the clay-clay film after drying. If one component is greater than the other. This is shown for various film thicknesses. Images taken using a scanning electron microscope (SEM) of the films at various compositions show that at this specific ratio, the considerably smaller Laponite® particles pack into the spaces between the bentonite platelets flawlessly, resulting in a smooth, defect-free film. A clay-clay composite in a properly considered ratio may be a low-cost and effective approach to prevent cracks in the vital area of land-filler production, in addition to many other uses in the future.

The field of fracture dynamics is a vast field and the works presented here do not even scratch the surface. There is broad scope for further investigation into the subject. The list below includes some of these active investigations as well as a rough outline of future work.

- A deeper knowledge of the crack-healing function of soil composites in aqueous solutions.

- The effect of varying pH of the solution on the crack patterns in composite soil systems.

-
- Simulation model investigations of the tree-like cracks as seen in experiments.
 - Study of crack patterns of Laponite[®] gel in rectangular system under the effect of AC (Alternating Current) field.
 - Study of crack patterns of Bentonite solution(aqueous) under DC and AC field.
 - Effects of temperature and humidity variations on clay cracking.